ABSTRACT

Khaled M. Gharaibeh Design Methodology for Multichannel Communication Systems. (Under the direction of Professor Michael B. Steer).

A methodology for understanding and modeling the interaction of multiple CDMA signals in a nonlinear multichannel environment is introduced and verified. The analysis is based on understanding the statistical properties of input signals and developing a modeling technique that enables distortion to be estimated. This is coupled with the introduction of a new behavioral modeling technique that captures the black box characteristics of multichannel amplifiers. In addition, a performance analysis that relates nonlinear distortion to probability of bit error (BER) is introduced. The analysis presented here provides an insight into communication system design by relating distortion to system performance. The methodology is verified using simulations and measurements performed on a nonlinear power amplifier. A nonlinear model was extracted and used in developing the statistical model by which distortion is estimated. The resulting estimates of distortion were verified using measurements of distortion performed on the amplifier using the IS-95 CDMA system standard.

Design Methodology for Multichannel Communication Systems

by

Khaled M Gharaibeh

A dissertation submitted to the Graduate Faculty of
North Carolina State University
in partial satisfaction of the
requirements for the Degree of
Doctor of Philosophy

Department of Electrical and Computer Engineering

Raleigh

2004

Approved By:

Dr. K. Townsend	Dr. Jean Pier Fouque
Dr. Michael B Steer Chair of Advisory Committee	Dr. Gianluca Lazzi

I dedicate this work to my mother and father who dedicated their lives to my happiness ...

Biography

Mr Khaled M. Gharaibeh received his B.S. and M.S. in Electrical Engineering in 1995 and 1998 respectively, both from Jordan University of Science and Technology, Irbid, Jordan. From 1996–2000, he was a Senior Engineer at Jordan Telecom, Amman, Jordan. Since May 2000, he has been a PhD student and research assistant in the Electrical and Computer Engineering Department of North Carolina State University. His research interests are in statistical modeling of nonlinear RF circuits for CDMA system applications. He is a student member of the Institute of Electrical and Electronic Engineering (*IEEE*) and a member of the honor society Eta Kappa Nu.

Acknowledgements

I would like to express my thanks and gratitude to my advisor Dr. Michael Steer for his technical and moral support during my Ph.D. I would also like to express my sincere appreciation to Dr. Jean Pier Fouque, Dr. Keith Townsend and Dr. Gianluca Lazzi for serving on my Ph.D. committee and for their help. I would also like to thank Dr. Kevin Gard for his help in developing the MATLAB code. Very big thanks go to my graduate student and post-doctoral colleagues for their cooperation and their sense of humor. I would also like to thank Ajith Kamath and Pallav Sudrashan, from Dr. Brian Hughes' group for the useful discussions about communication theory. Finally, I would like to thank my family in Jordan for their support, encouragement and motivation.

"If I have seen further it is by standing on the shoulders of Giants" —Isaac Newton

Contents

List of Figures

List of Tables

List of Abbreviations

CDMA	Code Division Multiple Access
LAN	Local Area Network
CDMA	Code Division Multiple Access
LAN	Local Area Network
dB	decibel
RF	Radio Frequency
PA	Power Amplifier
SCPA	Single Channel Power Amplifier
MCPA	Multi Channel Power Amplifier
GPS	Generalized Power Series
MHz	MegaHertz
GHz	Gigahertz
AM-AM	Amplitude Modulation-Amplitude Modulation conversion
AM-PM	Amplitude Modulation-Phase Modulation conversion
IMD	Intermodulation Distortion
IMR	Intermodulation Ratio
IIP3	Input third order Intercept Point
OIP3	Output third order Intercept Point
ACPR	Adjacent Channel Power Ratio
BER	Bit Error Rate
SR	Spectral Regrowth
GaAs	Gallium Arsenide
MESFET	Metal Semiconductor Field Effect Transistor
VNA	Vector Network Analyzer
VSA	Vector Signal Generator
VSA	Vector Signal Analyzer
PSD	Power Spectral Density
CDMA	Code Division Multiple Access
GSM	Global System for Mobile
DS-SS	Direct Sequence Spread Spectrum
PAR	Peak-to-Average Ratio
AOM	Arithmetic Operator Method
WSS	Wide Sense Stationary
DUT	Device Under Test
OSC	Oscillator
I-O	Input-Output
AMPS	Advanced Mobile Phone Service
L-N	Linear-Nonlinear
N-L	Nonlinear-Linear
F-N	Filter-Nonlinearity
N-F	Nonlinearity-Filter

Chapter 1

Introduction

Current mobile communication architectures have been designed to address audio and data transmission using narrowband channels at fairly low microwave frequencies. However, future mobile communications are expected to provide a wide variety of services that range from regular audio to high-speed local area networks (LAN) through wideband access channels. On the other hand, multifunctional systems are expected to accommodate multiple radio signals from different sources with different power levels, modulation formats, and carrier frequencies. In response to all these scenarios, there is a need to develop an RF front-end architecture that meets the above requirements in terms of performance, power consumption and size. The first step towards achieving this goal is to develop a behavioral modeling methodology to model the performance of the proposed system. In addition to optimizing system design, the role of modeling and simulation in modern communication systems is to allow concepts to be explored even before enabling technologies have been brought to maturity (see Fig. 1.1).

A fundamental design concern for system designers of multichannel and wideband communication and Radar systems is modeling distortion introduced by the nonlinear behavior of the devices incorporated in the design. Unlike single channel systems, multichannel and multi-band systems suffer from the interaction of multiple channels with nonlinearities. Therefore, traditional figures of merit of nonlinearity are not adequate and do not provide enough insight on system performance. The development of a behavioral modeling technique for such scenarios must, therefore, be based on the thorough understanding of the

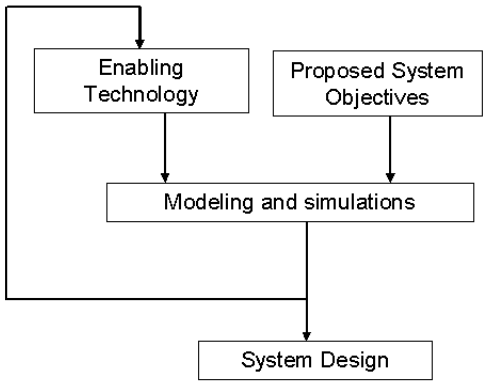

Figure 1.1: Simulation strategy of modern communication systems

signal properties in terms of signal generation, modulation and coding in addition to the inherent nonlinearity of the system. Unlike circuit level modeling, behavioral modeling enables the integration of various system parameters to be viewed in a more comprehensive way. This, in addition to the simplicity of extracting system parameters when the system is overwhelmingly complex.

In this chapter the motivation to this study is be presented where the problem of the interaction of multiple channels through the nonlinear behavior will be defined and clarified through examples. A summary of the original contributions and an overview of the thesis will also be presented.

1.1 Motivation

The new trend in mobile communication system design is to eliminate redundant RF signal paths to achieve lower sizes and cost. This leads to the utilization of multichannel radio architectures where multiple RF transmitters are replaced by a single multichannel system. These architectures are expected to reduce the size and cost of base stations in addition to a dramatic reduction in power consumption.

In the traditional multichannel configuration, shown in Fig. 1.2(a) [1], the individual channels are applied to a narrowband single channel power amplifier (SCPA) and then

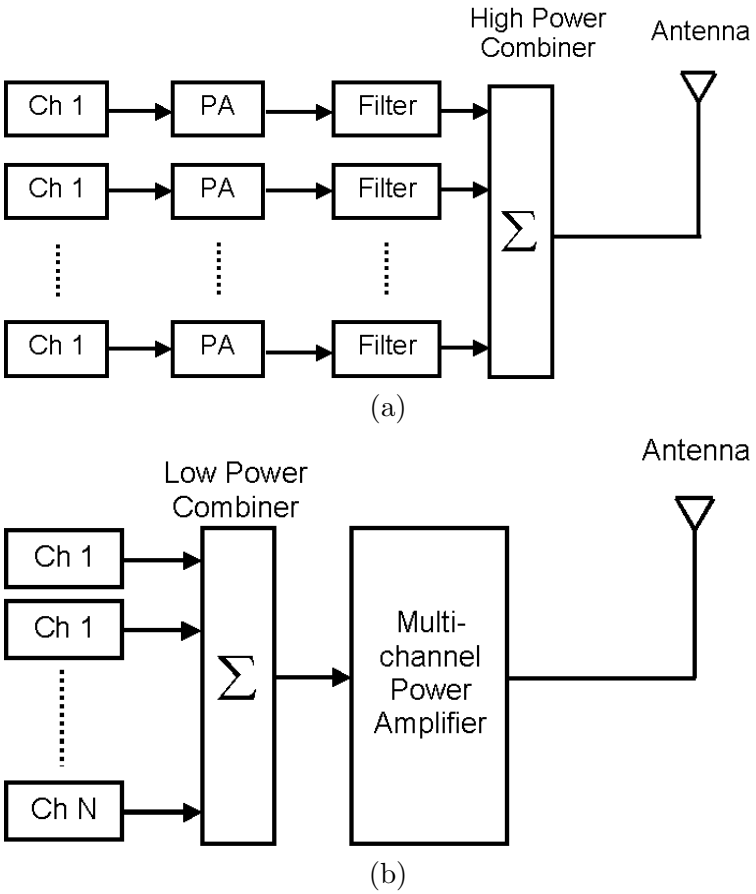

Figure 1.2: Multichannel architectures: Traditional, (a) multiple single channel amplifier system; and (b) single multichannel amplifier system.

their outputs are combined by a tuned high-power power combiner to obtain a multichannel high power signal. While this approach provides less interaction among the input channels, it has many disadvantages. On one hand, the high power combiners employed in this approach suffer from an inherent power loss in addition to the power consumption and the additional cooling of the SCPA. This results in the the amplifier system having low overall efficiency and large size. On the other hand, tuned power combiners complicate channel allocation schemes within a base station. A multichannel power amplifier, see Fig. 1.2(b), that replaces multiple narrowband amplifiers and amplifies multiple channels simultaneously, is expected to eliminate the need for these bulky and expensive power combiners and zonal filters. This in turn, enables the network operator to deploy smaller base stations that are more flexible and have lower cost. On the other hand, the multichannel amplifier concept is

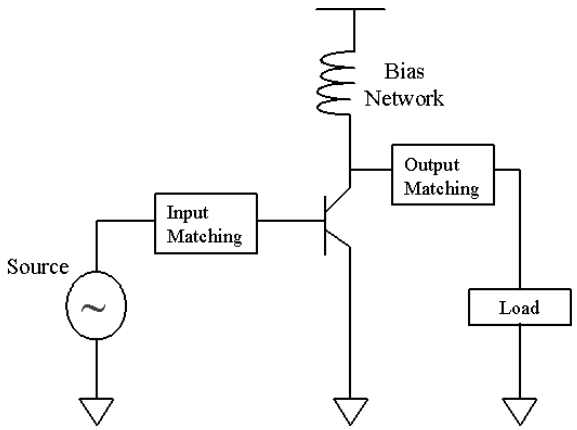

Figure 1.3: Power amplifier circuit

expected to ease dynamic channel allocation schemes by removing the restrictions imposed by the tuned filters and power combiners. In addition, it provides the ability to transmit any modulation format through the amplifier which means that future upgrades of the air interface can be implemented much more easily.

The design of multichannel amplifiers, however, is more challenging as linearity is a great concern. Nonlinearity originates in the active devices incorporated in the design of power amplifiers as shown in Fig. 1.3. Active devices are usually characterized by their nonlinear current-voltage characteristics (I-V) where the response of the device is an instantaneous (memoryless) function of its input. However, this is true only when the junction capacitances of the device are neglected. Junction capacitances in addition to the extra capacitances in the Power Amplifier (PA) circuit give rise to memory effects which makes the response of the circuit depend not only on the instantaneous input but also on the value of the input at past time instances.

Nonlinearity, as will be seen in the following chapters, has a daunting effects on the output waveform, a phenomena called Intermodulation Distortion (IMD) in analog systems and Spectral Regrowth (SR) in digital communication systems. These phenomena inflect severe restrictions on system design, bandwidth and performance and the overall system power budget. In a multichannel amplifier environment, the problem is more severe. This is because many problems arise when a power amplifier is excited by multiple digitally modulated signals. First, multiple signals exhibit a higher Peak to Average Ratio

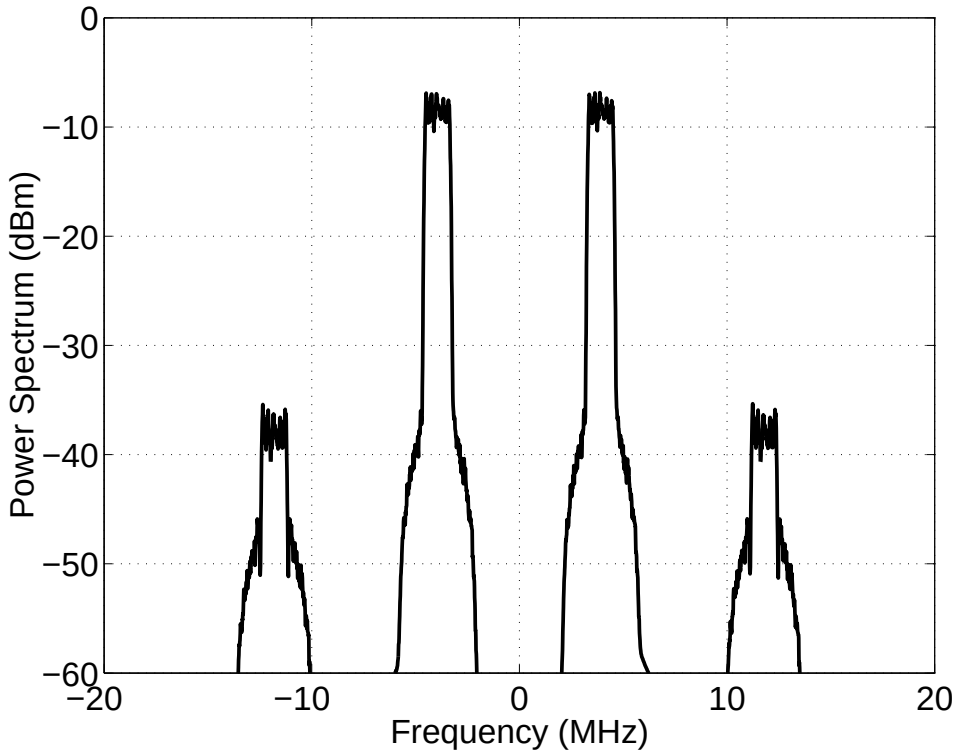

Figure 1.4: Power spectrum of two CDMA signals on a normalized frequency axis; the two CDMA signals are centered at ±4 MHz and intermodulation components at ±12 MHz.

(PAR) than a single signal which intuitively means that the amplifier is required to have higher RF linearity and dynamic range. On the other hand, the interaction of the input signals by nonlinearity introduces new in-band and out- of-band distortion terms because of cross modulation. This is in addition to the spurious intermodulation components at intermodulation frequencies as shown in Fig. 1.4.

One of the scenarios, that is common in a wireless power controlled systems such as a CDMA system, is depicted in Fig. 1.5 [2, 3]. A user within the service area of base station B1 is assigned the channel centered at f_1 but it is blocked by a building. A spurious signal that results from intermodulation of the channels at f_2 and f_3 in base station B2 (which uses a MCPA) is centered at f_1 and may have greater power than the desired signal of B1. This means that the user in the service area of base station B1 is blocked by an interfering signal from base station B2. Another scenario that is most probable is when different frequency channels within the same base station have different power levels when

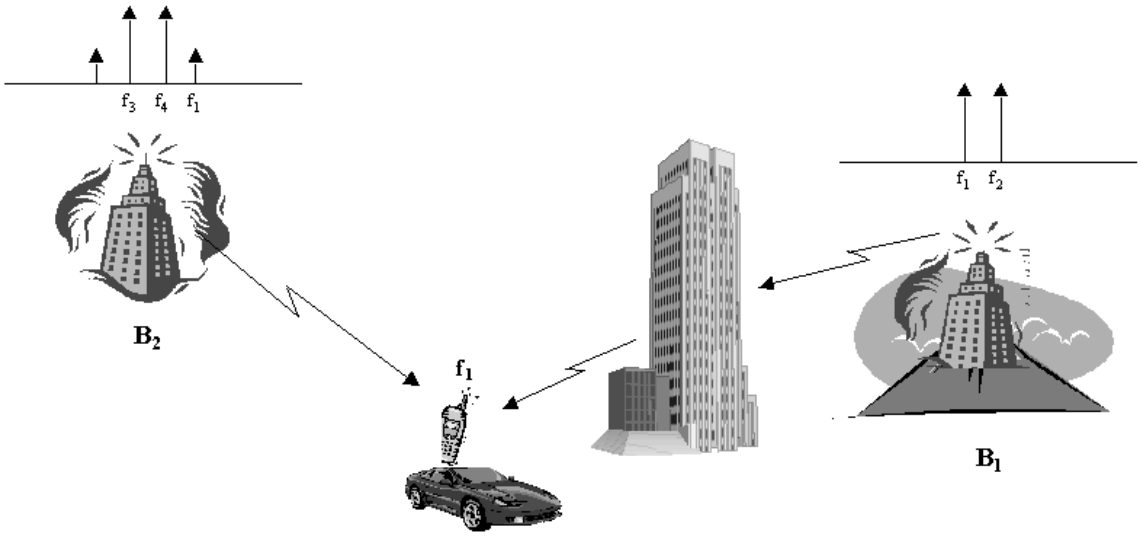

Figure 1.5: Near Far problem in multichannel base station (modified from [2]).

the number of users is not distributed uniformly among various channels. In this case, amplitude modulation is transferred from the high power signal to the low power signal because of cross modulation and this increases the level of distortion in and out of the band of interest.

In a mobile receiver, the interaction of multiple channels because of nonlinearity manifests itself as a desensitization problem. For example, one of the stringent requirements in CDMA receiver design is the proper reception of a CDMA channel in the presence of a single tone jammer [4, 5, 6, 7]. Here, desensitization of the single tone is a measure of the receiver's ability to receive a CDMA signal at its assigned channel frequency and in the presence of a single tone jammer at a given frequency offset from the CDMA signal center frequency. This situation is shown in Fig. 1.6. The single tone jammer models a narrow band Advanced Mobile Phone Service (AMPS) signal transmitted from a nearby AMPS base station. The interference introduced by the jammer results from cross modulation of the jammer and transmitter leakage which, in turn, appears as extra distortion inside the band of the received signal [5, 6].

From the above discussion, there is a need to develop a methodology by which all the above scenarios can be understood and modeled given the versatility of the operating

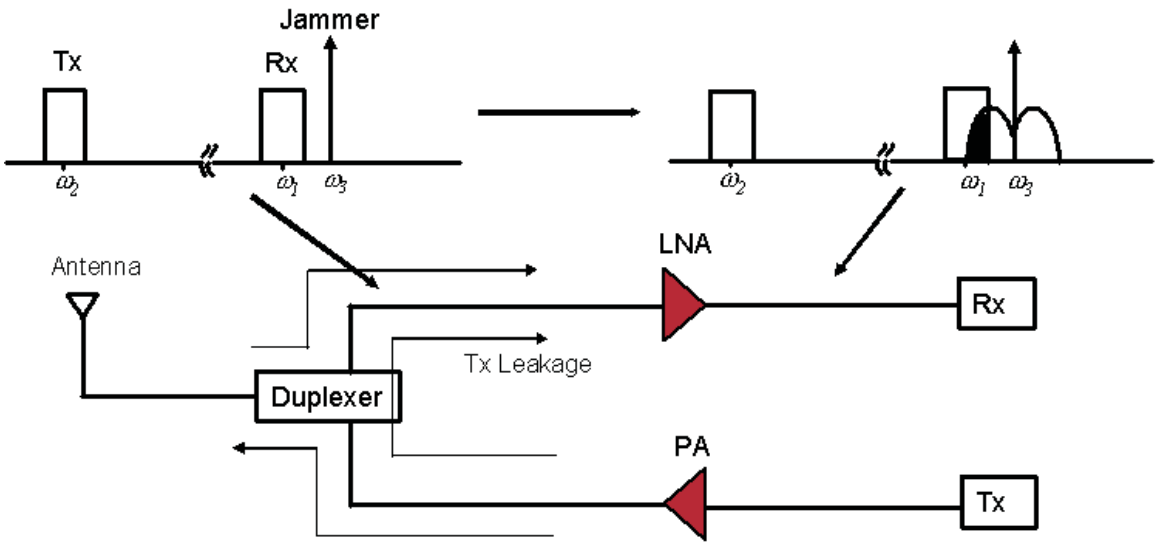

Figure 1.6: Receiver desensitization in reverse link CDMA system

frequency bands and modulation schemes in a mobile communication environment. In this thesis a new behavioral modeling methodology is developed suited to model the interaction of multiple signals in a wideband multichannel system. The modeling technique is based on two basic ideas. The first is the development of a behavioral model to capture the inherent nonlinearity of the devices incorporated in the system design which will take into account their wideband behavior (also known as memory effects). The second is the development of a methodology by which distortion can be characterized in terms of signal statistics.

To the best of the knowledge of the author, this is the first comprehensive study and modeling methodology for the interaction of multiple signals. Here the problem is addressed in a comprehensive manner and the analysis presented here is expected to provide useful guidelines for communication system designers in terms of signal generation, RF circuit design and overall system optimization.

1.2 Thesis Overview

This thesis is divided into three major parts, the first part is a review of major techniques used to model nonlinear amplifiers in addition to the most common approaches of distor-

tion analysis. This part is divided into two chapters: Chapter 2 is a review of the major behavioral modeling techniques and comments on their parameter extraction. Chapter 3 discusses modeling of distortion in analog and digital communication systems and the major measures used as figures of merit for system performance. The second part consists of Chapters 4, 5 and 6 and contains the major contributions of this thesis. Chapter 4 deals with developing the theory for multichannel analysis in nonlinear amplifiers and the development of new techniques modeling multichannel amplifiers. Chapter 5 is a nonlinear statistical analysis of distortion in multichannel amplifiers and chapter 6 is an analysis of communication system performance in the presence of nonlinear distortion where a relationship between the probability of error and nonlinear distortion is developed. The last part consists of Chapters 7 and 8. Chapter 7 uses measurements and simulations to verify the theoretical developments in Chapters 4, 5 and 6. Chapter 8 presents conclusions and suggestions for future work.

1.3 Summary of Original Contributions

1.3.1 Publications

- K. M. Gharaibeh, K. Gard and M. B. Steer, "Statistical modeling of the interaction of multiple signals in nonlinear RF systems," 2002 *IEEE MTT-S International Microwave Symposium Digest*, Vol. 1 ,June 2002, pp. 143–146.

- K. M. Gharaibeh and M. B. Steer, "Technology Choices for Multifunctional Adaptive Radio, Radar and Sensors," *Mediterranean Microwave Conference*, Caceres, Spain, June 2002.

- K. M. Gharaibeh, K. Gard, H. Gutierrez and M. B. Steer, "The importance of nonlinear order in modeling intermodulation distortion and spectral regrowth," *IEEE Radio and Wireless Conference*, (*RAWCON*), Aug. 2002, pp. 161–164.

- K. M. Gharaibeh and M. B. Steer, "Statistical Modeling of Cross Modulation in Multichannel Power Amplifiers Using a New Behavioral Modeling Technique," *IEEE MTT-S International Microwave Symposium Digest*, Vol. 1, June 2003, pp. 343–346.

- K. M. Gharaibeh and M. B. Steer, "Characterization of cross modulation in multichannel amplifiers using a statistically based behavioral modeling technique," *IEEE Trans. Microwave Theory Tech.*, Dec. 2003.

- F. P. Hart, D. G. Stephenson. C. R. Chang, K. M. Gharaibeh, R. G. Johnson and M. B. Steer, "Mathematical foundations of frequency domain modeling of nonlinear circuit and systems using the Arithmetic Operator Method ," *Int. J. RF and Microwave Comp. Aided Engin.*, Oct. 2003.

1.3.2 In Preparation

- K. M. Gharaibeh and M. B. Steer, "Modeling cross modulation in multichannel communication system."

- K. M. Gharaibeh and M. B. Steer, "Performance Analysis of Direct Sequence Spread Spectrum (DS-SS) CDMA System With Amplifier Nonlinearities."

Chapter 2

Review of Behavioral Modeling Techniques

Behavioral modeling of nonlinear systems refers to a class of modeling techniques where a nonlinear system is dealt with as a black box. Unlike circuit level modeling, no information is required about the circuit topology, however, intuitive knowledge helps in developing the model. This is a classical problem in system modeling and is encountered in a variety of fields ranging from physiological systems to circuit theory. The black box model is developed by using an input-output (I-O) set of measurements and then by using system optimization theory, a function or a set of functions along with their parameters are extracted.

System identification techniques are in general divided into two major categories. The first are the nonparametric estimation techniques where no prior or intuitive knowledge is required about the system to be modeled and therefore, no function is suggested apriori to fit the data. This means that the estimation problem requires an excessive search for the function that fits the data well in addition to its parameters using random process theory. Examples of these techniques include kernel smoothing, wavelet theory and neural networks, [8, 9, 10, 11, 12, 13]. The second category includes the parametric estimation techniques which are based on intuitive knowledge about the system. Therefore, a nonlinear function or structure is assumed apriori and the problem reduces to the estimation of its

parameters. Although, parametric estimation is simpler in theory and application than its nonparametric counterparts, it may lead to inaccurate results if there is a lack of intuitive knowledge about the system. However, nonparametric approaches require an excessive search which renders them inefficient when implemented in softwares.

2.1 Behavioral Modeling of Nonlinear Power Amplifiers

In modeling microwave power amplifiers , apriori knowledge is available since nonlinearity originates from active devices which is well understood in circuit theory. Therefore, this nonlinearity takes input-output characteristics that are well-known apriori and then the modeling problem reduces to estimating system parameters using classical parameter estimation theory such as least squares and its variants.

The traditional way of modeling narrowband nonlinear amplifiers is to use the measured AM-AM and AM-PM characteristics which can be developed from simple single-tone measurements. However a multichannel amplifier exhibits a wideband behavior that renders the single-tone measurements insufficient to model its behavior because those characteristics are different at each frequency. This is due to the fact that a wideband amplifier exhibits memory effects where the system response depends not only on the input power level but also on its frequency.

The most common approaches to modeling the wide band behavior (i.e. memory effects) of nonlinear power amplifier are those based on Volterra series analysis. Volterra series analysis represents an analytical approach to modeling nonlinearity since it represents nonlinearity in a similar way in which Taylor series does for analytic functions. However Volterra series retains memory effects of the system and hence it can be described as a Taylor series with memory. The attractiveness of Volterra series representation comes from the fact that its kernels can be related to circuit parameters. For a black box system, Volterra kernels can be developed from input-output measured data using cross correlation techniques [14, 15, 16]. However, the Volterra model is in fact a series representation of a nonlinear analytic function and so it diverges when the nonlinear characteristics are strong. For weakly nonlinear systems only few terms of the series (usually third order) are required to represent the system with acceptable fidelity. On the other hand, the development of higher order (above third order) Volterra kernels is cumbersome and its implementation in

software is inefficient.

A wide variety of models were developed in the literature to overcome the computational complexity of developing Volterra kernels when the system has finite memory. Some models were based on developing parameter estimation techniques that complies with the available measured data. Chen [17], surveyed a wide variety of general nonlinear models based on their structural classification. Kernel relationships of these models with respect to Volterra kernels were derived. The structural classification of nonlinear systems was based on a theory developed by Korenberg [16] which states that any finite memory nonlinear system can be represented by a finite number of parallel Linear-Nonlinear (L-N) or Nonlinear-Linear (N-L) cascades of alternating linear and nonlinear operators. However, these models require that kernel relationships hold for a particular structure to represent the nonlinear system in hand. Boyd and Chua [18] showed that the I-O measurements alone are sufficient to classify these structures because of the unique I-O mappings. Therefore, dependent on the measured data, a certain structure can be accepted or rejected based on satisfying the kernel relationships constituting a sufficient and necessary condition for a system to have a given structure. Parameter estimation of these structures is usually based on measuring the first and second order Volterra or Weiner kernels which are used to define the linear filters incorporated in the given structure. Lee and Shetzen [15] developed an approach for measuring Volterra kernels leading to the complete identification process of a nonlinear system. On the other hand, Frequency domain methods based on the multifrequency excitation were developed in [19, 20, 21, 22] to extract the Vloterra transfer functions. However these methods become inefficient and even computationally prohibitive for high order kernels.

In the following, the major approaches for nonlinear amplifier modeling are reviewed with emphasis on their parameter estimation techniques. First, the Volterra series model and its variants are presented. Special cases of the Volterra model will be presented by defining their kernel relationships. Then, the limiter family of models which is used to model systems that cannot be modeled by the Volterra model or its variants are presented. The objective is to present a unified understanding of the nonlinear behavior and the applicability of various models to a given system.

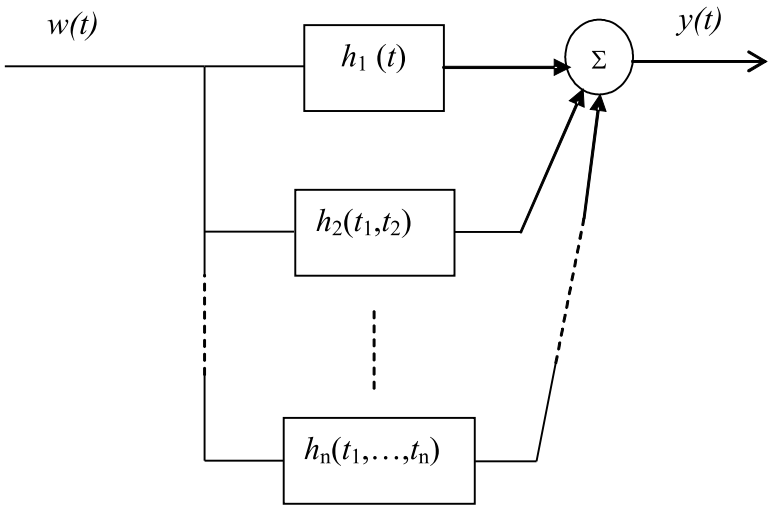

Figure 2.1: A block diagram of the general Volterra model

2.2 General Volterra Series Analysis

A general Volterra series model of a nonlinear system is described by the following functional expansion of continuous functions [22]:

$$y(t) = \sum_{n=1}^{\infty} F_n(w(t)) = \sum_{n=0}^{\infty} y_n(t) \tag{2.1}$$

where $F_n(w(t))$ is the Volterra functional and is defined as

$$F_n(w(t)) = \int_{-\infty}^{\infty} \dots \int_{-\infty}^{\infty} h_n(\lambda_1, \dots, \lambda_n) \prod_{i=1}^{n} w(\lambda_i) d\lambda_i$$

where $h_n(\lambda_1, \dots, \lambda_n)$ is the n- dimensional Volterra kernel which can be symmetric without loss of generality and leads to a unique set of Volterra kernels. Fig. 2.1 shows a graphical representation of the Volterra model. If the nonlinear system is causal and time invariant then it can be expressed as the convolution of the powers of the input signal $w(t)$ with the n-dimensional system kernels as:

$$F_n(w(t)) = \int_{-\infty}^{\infty} \dots \int_{-\infty}^{\infty} h_n(\lambda_1, \dots, \lambda_n) \prod_{i=1}^{n} w(t - \lambda_i) d\lambda_i. \tag{2.2}$$

It is more convenient to write (2.2) in terms of the n-dimensional Volterra transfer functions since these functions are usually easier to extract than their corresponding time kernels.

Therefore $y_n(t)$ can be expressed as

$$y_n(t) = F_n(w(t)) = \int_{-\infty}^{\infty} \dots \int_{-\infty}^{\infty} H_n(f_1, \dots, f_n) \times \prod_{i=1}^{n} W(f_i) e^{j2\pi f_i t} df_i \tag{2.3}$$

Where $H_n(f_1, \dots, f_n)$ is the n-dimensional Volterra Transfer Function (TF) which results from the the n-dimensional Fourier transform of $h_n(\lambda_1, \dots, \lambda_n)$:

$$\begin{aligned} H_n(f_1, \dots, f_n) = \int_{-\infty}^{\infty} \dots \int_{-\infty}^{\infty} h_n(\lambda_1, \dots, \lambda_n) \\ \times e^{-j2\pi(f_1\lambda_1 + \dots + f_n\lambda_n)} d\lambda_1 \dots d\lambda_n \end{aligned} \tag{2.4}$$

and consequently

$$\begin{aligned} h_n(\lambda_1, \dots, \lambda_n) = \int_{-\infty}^{\infty} \dots \int_{-\infty}^{\infty} H_n(f_1, \dots, f_n) \\ \times e^{j2\pi(f_1\lambda_1 + \dots + f_n\lambda_n)} d\lambda_1 \dots d\lambda_n \end{aligned} \tag{2.5}$$

and therefore, the frequency domain description of the n th order response can be expressed as

$$\begin{aligned} Y_n(f) = \int_{-\infty}^{\infty} \dots \int_{-\infty}^{\infty} H_n(f_1, \dots, f_n) \\ \times \delta(f - f_1 \dots - f_n) \prod_{i=1}^{n} W(f_i) e^{j2\pi f_i t} df_i. \end{aligned} \tag{2.6}$$

This is the form in which the Volterra model is most frequently used in modeling electronic systems with sinusoidal or quasi sinusoidal excitation. In the following we discuss the modeling techniques which enables the nonlinear transfer function to be derived directly without the extraction of Volterra kernels. These models make the development of system parameters more tractable by simplifying the kernel relationships. However, for any model kernel relationships must hold. This can be verified in some cases through the intuitive knowledge about the system.

2.3 Single Frequency Volterra Models

Single frequency Volterra models represent a simplified version of a Volterra system by simplifying the branches of the general model, see Fig. 2.1, into cascades of L-N or N-L subsystems. These configurations simplify parameter estimation and reduce computational

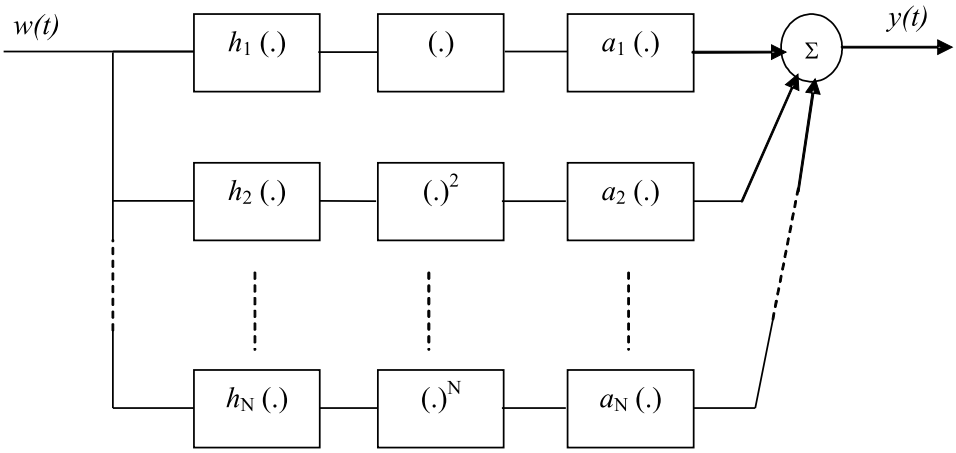

Figure 2.2: Filter-Nonlinearity Volterra model

complexity since all spectral calculations required involve only a single frequency variable instead of several [23]. Single-frequency Volterra models take one of the following topologies: filter-nonlinearity (FN) model and nonlinearity-filter (NF).

A single frequency FN Volterra model is shown in Fig. 2.2 and is characterized by a Volterra kernel that has the following property:

$$\begin{aligned} h_n(\lambda_1, \ldots, \lambda_n) = &\quad a_n h_n(\lambda_1) h_n(\lambda_2) \ldots h_n(\lambda_n) \\ = &\quad a_n \textstyle\prod_{i=1}^{n} h_n(\lambda_i). \end{aligned} \tag{2.7}$$

This can be contrasted to the general form in (2.2) and it follows that the Volterra TF is

$$H_n(f_1, \ldots, f_n) = a_n \prod_{i=1}^{n} H_n(f_i). \tag{2.8}$$

For the NF Volterra model shown in Fig. 2.5, the Volterra kernel has the property:

$$h_n(\lambda_1, \ldots, \lambda_n) = h_n(\lambda_1)\delta(\lambda_1 - \lambda_2) \ldots \delta(\lambda_{n-1} - \lambda_n) \tag{2.9}$$

and it follows that:

$$H_n(f_1, \ldots, f_n) = H(f_1 + \ldots + f_n). \tag{2.10}$$

The primary advantage of the single-frequency Volterra model is the simplicity of its parameter extraction. However it does not represent the broad variety of systems that the

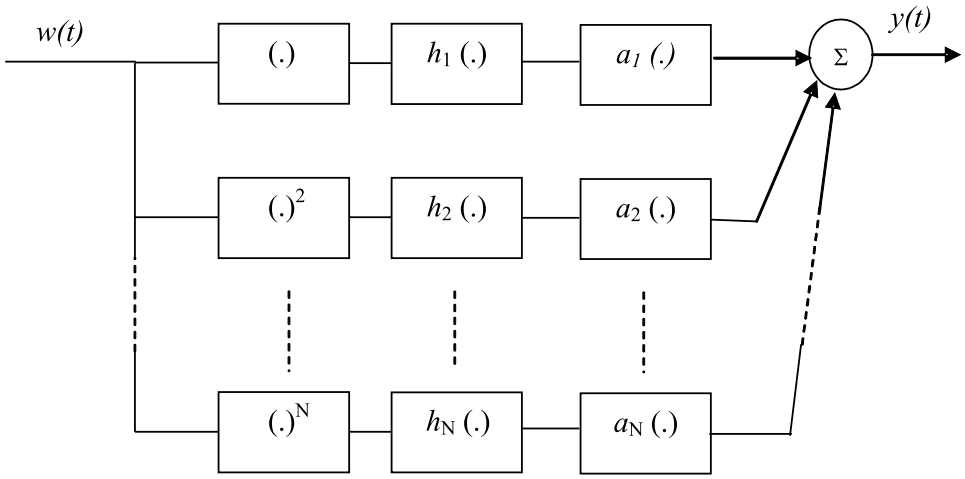

Figure 2.3: Nonlinearity-Filter Model

general Volterra model does, single-frequency model offers a significant simplicity of nonlinear system analysis.

Parameter estimation for the single-frequency Volterra model was discussed in [23] using cross-correlation spectral analysis performed on time domain measured data. These models are regarded as polyspectral models and they showed good performance for TWT high power amplifiers [23]. The identification process used measured AM-AM and AM-PM characteristics and the measured small signal transfer function of the amplifier as apriori information. Then time domain measured I-O data is used to extract the remaining blocks of the model using cross correlation techniques. A detailed analysis of the identification process can be found in [23, 50, 51, 52]. Model parameters were also extracted using multifrequency excitation [24] but only third order nonlinearity was considered.

2.4 Parallel Cascade (Wiener) Model

The parallel Wiener model is a variate of the general Volterra series analysis assuming Gaussian input which results in orthogonal branches of Volterra model. Therefore a Wiener model can be described by replacing the Volterra F functionals by the Wiener G orthogonal

functionals [17]:

$$y(t) = \sum_{n=1}^{\infty} G_n\left(w(t)\right) \tag{2.11}$$

where $G_n(w(t))$ represent the Wiener functional and is defined as

$$G_n(w(t)) = \sum_{p=1}^{n} \int_{-\infty}^{\infty} ... \int_{-\infty}^{\infty} k_{p(n)}(\lambda_1, \ldots, \lambda_p) \prod_{i=1}^{p} w(\lambda_i) d\lambda_i \tag{2.12}$$

where

$$h_{p(n)}(\lambda_1, \ldots, \lambda_p) = \int_{-\infty}^{\infty} ... \int_{-\infty}^{\infty} h_n(\lambda_1, \ldots, \lambda_n) d\lambda_{p+1} \ldots d\lambda_n. \tag{2.13}$$

The above kernel relationship enables the realization of the Volterra model by a parallel cascade of linear and nonlinear elements as shown in Fig. 2.4 [16, 17, 53]. This enables the reformulation of the system equations [17] as

$$\begin{aligned} y(t) &= \sum_{p=1}^{P} y_p(t) \\ y_p(t) &= \sum_{r=0}^{N_p} a_{r,p} u_p^r(t) \end{aligned} \tag{2.14}$$

where

$$u_p(t) = \int_{-\infty}^{\infty} h_p(\lambda) w(t-\lambda) d\lambda = h_p(t) * w(t).$$

Here p is the number of branches and it represents the memory depth and N_p is the maximum order of the polynomial in branch p.

Note that the parallel cascade model represents the system by a finite number of branches with polynomials of finite order. This model was proven adequate for modeling a finite-memory Volterra model having a finite-order. In [16], Korenberg derived an upper bound for the number of cascades required for representing a finite-memory system. Parameter estimation for this model was discussed in [16] using time-domain measurements. In a recent work [53, 26] system parameters were developed using measured two tone test with varying frequency separation.

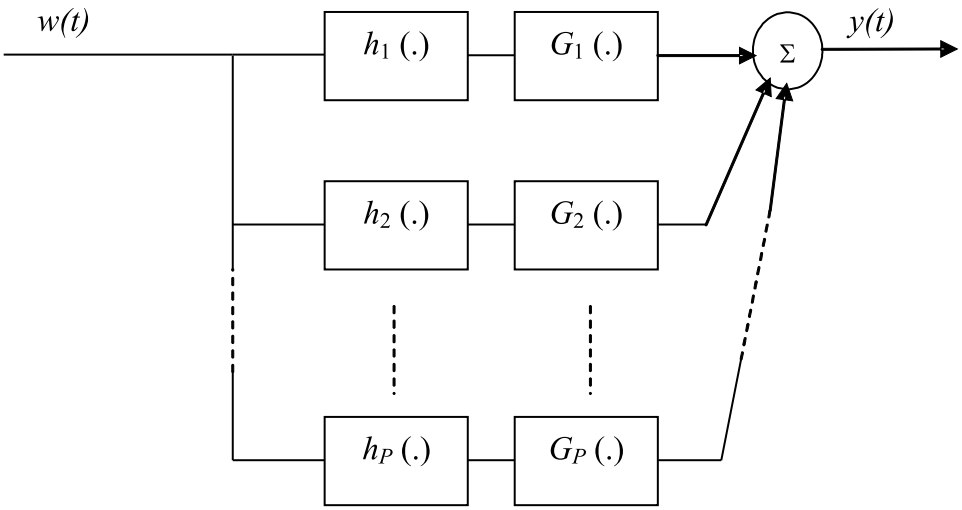

Figure 2.4: Parallel Cascade Model

2.5 Block Models

Block models refer to a class of models where a system is represented by a single cascade of linear and nonlinear elements. These models were suggested in the literature because of the simplicity of their parameter extraction using either direct Vector Network Analyzer (VNA) measurements or cross correlation of time domain measured data [23]. These models, although based on the intuitive knowledge about the system, are theoretically based on special cases of Volterra model and therefore kernel relationships can be developed.

2.5.1 The Two Box and Three Box Approximation

A simplified version of the Volterra model is the two box structure which takes the following form of the Volterra kernel in the frequency domain:

$$H_n(f_1, \ldots, f_n) = a_n H_1(f_1) \ldots H_1(f_n) \ldots \tag{2.15}$$

and for the three box model:

$$H_n(f_1, \ldots, f_n) = a_n H_1(f_1) \ldots H_1(f_n) H_2(f_1 + \ldots + f_n). \tag{2.16}$$

These forms of the Volterra kernels, (2.15) and (2.16), provide a great simplification over the general form since they can be realized by the models shown in Fig 2.5. These

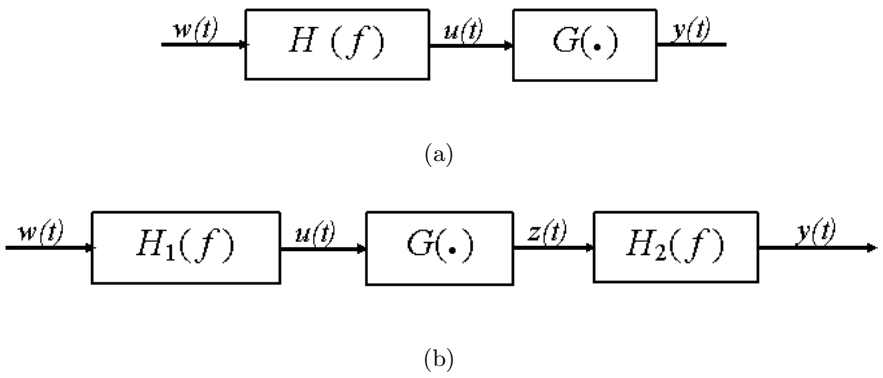

Figure 2.5: Block models: (a) Two box model and (b) three box model.

structures have been successful in representing a wide class of nonlinear systems where the nonlinear operation can be modeled as a cascade of linear operations that represent the finite memory of the system and of a memoryless nonlinearity. These models are called Wiener-Hammerstein models and are used to model a wide variety of nonlinear systems [9, 10, 11, 12, 13, 16]. Parameter extraction of such models are usually based on measuring first and second-order Volterra kernels [17].

2.5.2 Multi-Input Single Output (MISO) Volterra Model

A MISO Volterra model represents a multilateral system or device and is characterized by the following [27]:

$$\begin{aligned} y(t) = \quad & \sum_{n_1=0}^{\infty} \dots \sum_{n_K=0}^{\infty} \int_{-\infty}^{\infty} \dots \int_{-\infty}^{\infty} h_{n_1,n_1,\dots,n_K}(\lambda_{11},\dots,\lambda_{1n_1},\dots,\lambda_{1n_{K1}},\dots,\lambda_{Kn_K}) \\ & w_1(t-\lambda_{11})\dots w_1(t-\lambda_{1n_1})\dots w_K(t-\lambda_{K1})\dots\dots w_K(t-\lambda_{Kn_K}) \\ & d\lambda_{11}\dots d\lambda_{1n_1}\dots d\lambda_{1n_1}\dots d\lambda_{K1}\dots d\lambda_{Kn_K}. \end{aligned} \tag{2.17}$$

A simplified version of the Volterra model is the G-structure [17] which takes the following form of the Volterra kernel in the frequency domain:

$$\begin{aligned} & H_{n_1,n_2,\dots,n_K}(\omega_{11},\dots,\omega_{1n_1},\dots,\omega_{1n_K},\dots,\omega_{Kn_K}) \\ & = a_n \binom{n}{n_1,\dots,n_K} H_{11}(\omega_{11})\dots H_{11}(\omega_{1n_1})\dots H_{1K}(\omega_{K1})\dots H_{1K}(\omega_{Kn_K}) \\ & \times H_2(\omega_{11}+\dots+\omega_{1n_1}+\dots+\omega_{K1}\dots+\omega_{Kn_K}) \end{aligned} \tag{2.18}$$

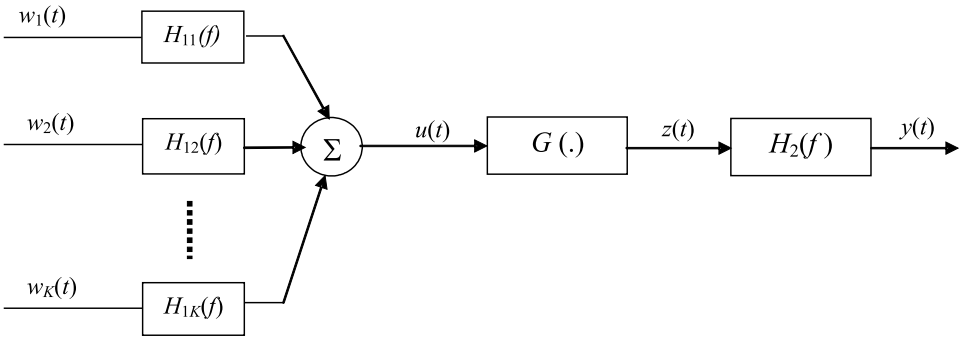

Figure 2.6: MISO model

where

$$\binom{n}{n_1,\ldots,n_K} = \frac{n!}{n_1!\ldots,n_K!}.$$

In a similar way to the single input case, this form of Volterra kernel enables the system model to be realized by the model shown in Fig 2.6. MISO models are usually used to model systems with multiple inputs where each input sees a different input impedance such as a mixer. Parameter estimation for this model is similar to its single input counterpart, however, it requires more extensive computations [27].

2.6 Memoryless and Quasi Memoryless Models

Perhaps the most commonly used model for modeling distortion in power amplifiers is the memoryless model. This model is characterized by a constant Volterra transfer function over frequency, i.e

$$H_n(\underline{f}) = H_n(\underline{0}) = a_n \tag{2.19}$$

where the under bar indicate an n-dimensional vector and it follows that the corresponding Volterra kernel is:

$$h_n(\lambda_1,\ldots,\lambda_n) = a_n\delta(\lambda_1)\delta(\lambda_2)\ldots\delta(\lambda_n). \tag{2.20}$$

Therefore, the model reduces to a power series model with either real or complex coefficients of the form:

$$y(t) = \sum_{n=1}^{N} a_n w^n(t). \tag{2.21}$$

The system is called memoryless if the coefficients a_n are real. These coefficients can be developed from AM-AM power sweep measurements of single tones using a VNA. The system is called quasi memoryless if the coefficients are obtained from AM-AM and AM-PM measurements where polynomial fitting yields a complex power series. The quasi memoryless system takes into account short term memory effects which are manifested as a phase shift in the output waveform that is a function of the input power level. The power series model obtained is popular for its simplicity and the fact that distortion can be directly related to its parameters (coefficients) as will be seen in the following chapter. However, it has its limitations since it does not take into account the long-term memory effects which makes it inadequate for modeling wideband and multichannel systems.

2.7 Other Nonlinear System Models

2.7.1 Generalized Power Series

A Generalized Power Series (GPS) model was pioneered by Steer [19] and is used to determine the steady-state frequency domain description of the output of a nonlinear system. Therefore, for a multifrequency input of the form:

$$w(t) = \sum_{k=0}^{K} w_k(t) = \sum_{k=0}^{K} |W_k| cos(\omega_k t + \phi_k) = \sum_{k=-K}^{K} W_k e^{\omega_k t}$$

then, the nonlinear system can be represented by a GPS as [22]

$$y(t) = A \sum_{n=0}^{\infty} a_n \left[\sum_{k=0}^{K} b_k w_k(t - \tau_{n,k}) \right]^n \tag{2.22}$$

where $b_{k,i}$ are real coefficients, a_n are complex coefficients and $\tau_{n,k}$ is a time delay that depends on the power series order and the index of the input frequency component. The output phasor at a particular frequency is given by

$$Y_\xi = \sum_{n=0}^{\infty} \sum_{\substack{\underbrace{n_1, ..., n_K}_{|n_1|+...+|n_K|=n}}} Re\{\epsilon_n T\}_{\omega_\xi} \tag{2.23}$$

where $\omega_\xi = \sum_{k=1}^{K} n_k \omega_k$ and

$$T = \sum_{\alpha=0}^{\infty} \sum_{\underbrace{s_1,\ldots,s_K}_{s_1+\ldots+s_K=\alpha}} (n+2\alpha)! a_{n+2\alpha} \Phi$$

where

$$\Phi = \prod_{k=1}^{K} \frac{(b_k)^{n_k+2s_k} |W_k|^{|n_k|+s_k} |W_k^*|^{s_k} \Gamma_k^{|n_k|+s_k} \Gamma_k^{s_k}}{s_k!(|n_k|+s_k)!}.$$

and $\Gamma_{k,n} = e^{-j\omega_k \tau_{k,n}}$. The GPS reduces to a memoryless polynomial by setting $\tau = 0$ and $b_k = 1$. The inclusion of complex coefficients and frequency dependent time delays allows a variety of systems to be modeled. The GPS was proved to be equivalent to the single-frequency approximation of the Volterra series in [22]. Parameter extraction can be done by measuring the response to a multifrequency input. In fact, the equivalence of Volterra and GPS series makes the multifrequency excitation suitable to developing the Volterra transfer functions in the frequency domain.

2.7.2 The Limiter Family of Models

The importance of studying distortion introduced by the family of limiter amplifiers arises from the wide variety of applications of those amplifiers either on the conceptual level or on the practical level. In a multicarrier system, a limiter of clipping characteristics is used before a power amplifier to limit the peak envelop power of the input signals in order to prevent the signal from exceeding the power rating of a power amplifier [29]. On the other hand, a soft limiter amplifier model is used to model distortion introduced by linearized power amplifiers in CDMA systems [30]. A predistorted power amplifier can be modeled by a soft limiter model (clipper) which models the perfect cancellation of AM-PM conversion and clipping of AM-AM characteristics by predistortion. A class of memoryless limiter power amplifiers can be modeled by the following parametric form developed in [31]:

$$y(t) = f(w(t)) = \frac{L\text{sgn}(w(t))}{[1 + l/|w(t)|^s]^{1/s}} \tag{2.24}$$

where $\text{sgn}(x)$ is the sign function, L is the asymptotic output level which is used to scale the output, l is the input limit level and s is the knee sharpness parameter. Fig. 2.7 shows the input output characteristics of a limiter amplifier for different values of s. In the following, we discuss special cases of (2.24).

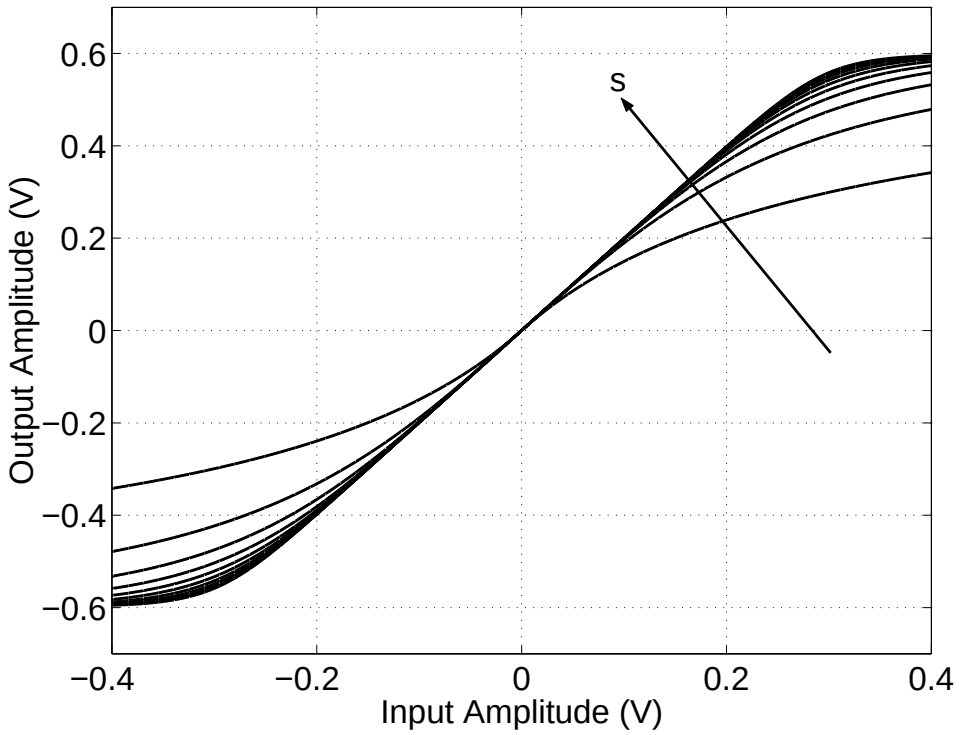

Figure 2.7: Limiter function for different values of smoothing factor s.

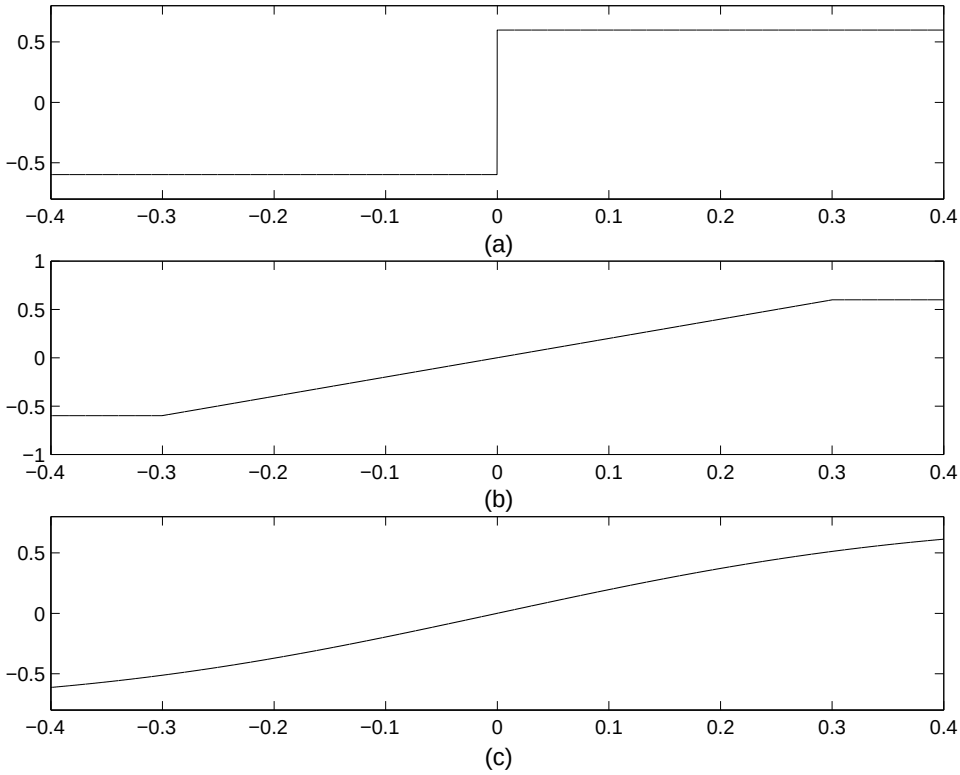

Figure 2.8: Limiter characteristics: (a) hard limiter; (b) soft limiter; and (c) smooth limiter.

Hard limiter Amplifier Model

A hard limiter amplifier is characterized by the model (2.24) with $l = 0$ and choosing s arbitrarily. The resulting transfer characteristics can be written as:

$$y(t) = f(w(t)) = L\text{sgn}(w(t)) \tag{2.25}$$

Fig. 2.8(a) shows the hard limiter characteristics.

Soft Limiter Amplifier Model

A soft limiter or a clipper characteristics shown in Fig. 2.8(b), can be obtained by setting $s = \infty$ and therefore the output of the soft limiter can be written as:

$$y(t) = f(w(t)) = \begin{cases} -l & |w(t)| \leq -l \\ w(t) & -l \leq |w(t)| \leq l \\ l & |w(t)| \geq l \end{cases} \tag{2.26}$$

Smooth Limiter Amplifier Model

A smooth limiter is characterized by the error function as:

$$y(t) = f(w(t)) = \frac{1}{\sqrt{2\pi}} \int_0^{w(t)} e^{\frac{-x^2}{2l^2}} dx \tag{2.27}$$

Where l is used to set the smoothness of the filter. Fig. 2.8 shows the smooth limiter characteristics.

2.8 Conclusion

In this chapter, we have reviewed the most common models of nonlinearity and their relationship to the general Volterra model by defining their kernel relationships. Volterra series analysis provides an analytical approach to arbitrary system level modeling and can be related to circuit parameters. The Volterra model and its variants will be revisited in Chapter 4 when the system input consists of multiple signal. The generalized power series can be related to the Volterra series and it represents an efficient way of modeling severe nonlinearities since it operates in the frequency domain. The limiter amplifier models represent an important group of nonlinear systems where nonlinearity is strong and therefore

cannot be represented by a power series model. These models are characterized using a Gaussian noise process as will be seen in Chapter 4. The variety of models described in this chapter provide an understanding of the nonlinear phenomena in RF and microwave amplifiers. The choice of the model is a tradeoff between the level of needed accuracy and the simplicity of the model parameter extraction and nonlinear system analysis. For the sake of the developments in this dissertation, the three-box block model is chosen because of the simplicity of the statistical analysis that will follow and the simplicity of its parameter extraction. The accuracy of the three-box model will be verified by measurements as will be seen in Chapter 7.

Chapter 3

Modeling of Distortion

One of the most competitive areas of RF and microwave circuit design is the design of highly efficient power amplifiers for cellular radio handsets. The major design constraint is achieving efficiency while achieving maximum specified levels of distortion in the channels adjacent to the channel being used by a particular handset. In some systems, such as analog systems and GSM cellular phone system, frequency planning is required to cope with interference so that the sets of available channels are distributed among the cells in a cluster and the cells within the cluster, and the clusters themselves, are arranged so that the same frequency channels are not used in neighboring cells. Thus, there are always one or two intervening cells between cells that reuse the same channels. In CDMA systems, the concept of clusters in not used and channels are reused in adjacent cells. That is, channels adjacent to a main channel are used for communication in the same cell. Distortion introduced in adjacent channel is therefore more significant than with other systems. In all cellular systems it is necessary for the system design to impose a maximum level on the amount of distortion that can be introduced in adjacent cells. Since it is not possible to design for absolute distortion levels, relative levels of power in an adjacent channel to power radiated in the main channel is specified. The most commonly used measure of this distortion is called adjacent channel power ratio (ACPR) and referring to the ratio of the power in the main channel to the power in the adjacent channel.

The purpose of this chapter is to present a review of the measures of distortion of both analog and digitally modulated signals and to investigate possible relationships

between nonlinearity figures of merit in both systems.

3.1 Analog System Distortion

The nonlinear performance of an amplifier with analog signals is generally quantified using two-tone testing. The troublesome tones at the output of the amplifier are commonly called the third order intermodulation components IM3. This terminology is loose as other intermodulation orders are involved. Third order Intermodulation Ratio (IMR3) is determined by considering the response of two equal amplitude input tones, of frequencies f_1 and f_2. IMR3 is the ratio of the power of the lower (IM3_L) intermodulation tone, here at $2f_1 - f_2$ (or $2f_2 - f_1$) to the power in one of the fundamental tones (f_1 or f_2):

$$\text{IMR3}_L = \frac{P_{IM3_L}}{P_{\text{fund}}} = \frac{P_{2f_1-f_2}}{P_{f_1}} \tag{3.1}$$

and IM3_U is defined in the same way. Generalized power series analysis [19] can be used to model intermodulation distortion of a two-tone signal. The output at a particular frequency ($f_i = n_1 f_1 + n_2 f_2$) is then the vector addition of a number of intermodulation products (IP's). Therefore, using the memoryless version of the GPS in (2.20), then for IM3_L ($n_1 = 2$ and $n_2 = -1$) we have:

$$\text{IMR}_{3L} = K[1 + T] \tag{3.2}$$

where:

$$K = 2a_3 \frac{3!}{2^3} \frac{W_1^2}{2} W_1^*$$

is the intermodulation term, $*$ indicates complex conjugation, W_1 and W_2 are the phasors of the tones at f_1 and f_2 and a_i is the i th order term of the behavioral model which represents a memoryless nonlinear system as a complex power series as in (2.18). The saturation term is defined as [19]:

$$T = \sum_{\alpha=1}^{\infty} \left\{ \left(\frac{(3+2\alpha)!}{3!2^{2\alpha}} \right) \frac{a_{3+2\alpha}}{a_3} \right\} \sum_{s_1+s_2=\alpha} \Phi$$

where

$$\Phi = \frac{|W_1|^{2s_1}}{s_1!(2+s_1)!} \frac{|W_2|^{2s_2}}{S_2!(1+s_2)!}.$$

The intermodulation term K, has a simple relationship to the input tones and varies as the cube of the level of one of the input tones yielding the classic 3:1 slope. However, this is valid only when the saturation term T is zero (for small signals) but as the signal levels become larger, this term grows because of the contribution of the fifth and higher order components. In the following, we discuss traditional measures of nonlinearity and their limitations.

3.1.1 Intercept Points

Traditionally the third order intercept point (IP3) describes nonlinearity of a power amplifier as it is a quantity specified by the manufacturer. By definition, the i th order input intercept point (IIP_i) is the intercept point of extrapolated output power-input power (P_{in}-P_{out}) curve and extrapolated intermodulation power-input power (P_{in}-$P_{\mathrm{IM}i}$) curve where ($P_{\mathrm{IM}i}$) denotes the i th order intermodulation distortion power calculated from a two tone (separated by small frequency difference) test of the nonlinear device. Intercept points represent a good figure of merit for amplifier linearity because they are independent of the input and output powers and are characteristics of the amplifier alone. However, IIPi are extrapolated values and indicate the nonlinear response only in the region where the $P_{\mathrm{IM}i}$ has a slope equal to i. IIP3, for example, is not a reliable indicator of performance outside the region where the P_{IM3} has a slope equal to 3, see Fig. 3.1 and it cannot predict over the entire power range. Therefore, IIP_i may not be the proper parameter to characterize nonlinearity with non-constant envelope modulated signal. In addition, an intercept point of order i is constant only when that particular i th intermodulation order is present alone. Since single order nonlinearity in real nonlinear systems is rarely present, the intercept point concept does not accurately represent nonlinearity.

3.1.2 1 dB Compression Point

A very common parameter of nonlinearity is the 1 dB compression point. The 1 dB compression point is the input power at which the extrapolated linear response is greater than that power by 1 dB. Using the model in [19], the output of the nonlinear device for a single-

tone input is expressed as

$$Y = a_1 W + \sum_{\alpha=1}^{\alpha_m} \left\{ \left(\frac{(1+2\alpha)!}{2^{2\alpha}\alpha!(1+\alpha)!} \right) \right\} a_{1+2\alpha} |W|^{2\alpha} W, \tag{3.3}$$

that is as

$$Y = a_1 W + \frac{3}{4}|W|^2 W + \frac{5}{8}|W|^4 W + \ldots.$$

A 1 dB compression point correspond to a factor of $10^{-1/20} = 0.89$ change in voltage gain. Therefore, the corresponding value of W where the power drops to 1 dB below the linear gain is found by solving

$$Y = a_1 W + \frac{3}{4}|W|^2 W + \frac{5}{8}|W|^4 W + \ldots = 0.89W. \tag{3.4}$$

Note that the value of the 1 dB compression point is also dependent on other intermodulation products above third oeder. The relation between the 1 dB compression point and the third order intercept point can be understood by considering a pure third order nonlinearity where the value of W in (3.4) (neglecting terms of order > 3) can be expressed as

$$W_{1\text{dB}} = \sqrt{.11 \frac{4}{3} \left| \frac{a_1}{a_3} \right|} \tag{3.5}$$

and the value of W at the intercept point is

$$W_{\text{IP3}} = \sqrt{\frac{4}{3} |\frac{a_1}{a_3}|} \tag{3.6}$$

therefore, IIP3-$P_{1\text{dB}}$ (= 9.6 dB) is a fundamental lower limit for the difference. This difference becomes higher when higher order terms are considered because of the decrease in $P_{1\text{dB}}$ as the influence of fifth and higher order intermodulation products is becoming more significant. This imposes a restriction on the applicability of IIP3 as measure of nonlinearity, where it becomes more applicable when $P_{1\text{dB}}$ is higher. In chapter 7, we will discuss by a practical example the applicability of $P_{1\text{dB}}$ and IIP3 and their relationship to digital system distortion.

3.2 Digital Signal Distortion

With digitally modulated signals the nonlinear behavior of PAs results in two main impairments to the output spectrum. The first is gain compression which results in in-band distortion and the second is increasing the relative distortion levels in the adjacent channels—a

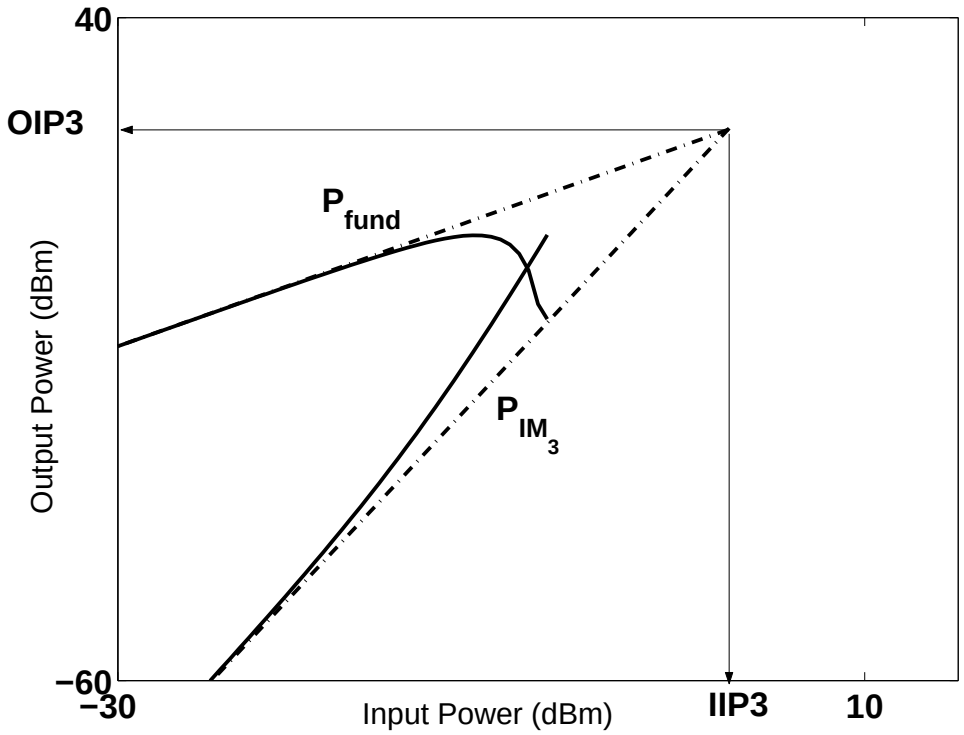

Figure 3.1: Third order Intercept Point.

process called Spectral Regrowth (SR) which limits system performance. Generally, systems with linear modulation schemes (QPSK, QAM, etc.) are more susceptible to PA nonlinearity because of their nonconstant envelope. Therefore operating a PA near the compression point results in clipping of the signal amplitude which appears as spectral regrowth and gain compression. From a constellation diagram point of view, the nonlinear behavior is manifested as compression and rotation of the signal constellation which means that nonlinear distortion results in increasing system probability of error.

In order to model distortion in a digital communication system, the output Power Spectral Density (PSD) must be estimated. Gard *et. al* [32, 33, 34, 35] developed a statistical technique by which distortion can be accurately estimated in a single channel nonlinear amplifier. The analysis was based on using a memoryless model to develop the autocorrelation function at the output of the nonlinear model and then the ACPR is estimated from the output spectrum which is obtained from the Fourier transform of the autocorrelation function. Therefore, following [32], the autocorrelation function is defined as

$$R_{yy}(\tau) = E[\tilde{y}(t)\tilde{y}(t+\tau)] \tag{3.7}$$

where E is the expected value. The autocorrelation function is a measure of the correlation of the signal with time-shifted replicas of itself and therefore, its Fourier transform represents the frequency contents of the random process. A quadrature digitally modulated CDMA signal can be represented as a filtered In-phase (I) and quadrature (Q) channels modulated at a carrier frequency. Therefore, the transmitted signal can be written as

$$\begin{aligned} w(t) &= i(t)\cos(\omega_c t) + q(t)\sin(\omega_c t) \\ &= A(t)\cos(\omega_c t + \Phi(t)) \\ &= \frac{1}{2}[\tilde{w}(t)e^{j\omega_c t} + \tilde{w}^*(t)e^{-j\omega_c t}]. \end{aligned} \tag{3.8}$$

where

$$\tilde{w}(t) = i(t) + jq(t) = A(t)e^{j\Phi(t)}$$

is the complex envelope of the modulated signal $w(t)$. The complex envelope $\tilde{w}(t)$ has a bandwidth B and its components $i(t)$ and $q(t)$ can be treated as real uncorrelated stationary random processes [32]. Applying (3.8) to the instantaneous nonlinear characteristics $G(w(t))$ as in (2.18) and taking the component centered at the carrier results in the following

envelop characteristics:

$$\tilde{y}(t) = \sum_{n=1}^{N} b_n \tilde{w}_k^n(t) \tag{3.9}$$

where $b_n = \frac{a_n}{2^{n-1}}\binom{n}{\frac{n+1}{2}}$ and represent the envelope coefficients. Now, let $\tilde{w}(t) = \tilde{w}_1$ and $\tilde{w}(t+\tau) = \tilde{w}_2$ then by using (3.7), the output autocorrelation can be formulated as [32]:

$$R_{yy}(\tau) = \sum_{n=1}^{N}\sum_{m=1}^{N} b_n b_m^* R_{\tilde{w}_n \tilde{w}_m}(\tau) \tag{3.10}$$

where

$$R_{w_n w_m}(\tau) = E\left[\tilde{w}_1^{\frac{(n+1)}{2}} \tilde{w}_1^{*\frac{(n-1)}{2}} \tilde{w}_2^{\frac{(n-1)}{2}} \tilde{w}_2^{*\frac{(n+1)}{2}}\right]. \tag{3.11}$$

and the output power spectrum is obtained from the Fourier transform of the output autocorrelation function (Weiner-Khintchine theorem [36]):

$$S_{yy}(f) = \sum_{n=1}^{N}\sum_{m=1}^{N} b_n b_m^* S_{nm}(\tau) \tag{3.12}$$

where

$$S_{nm}(f) = \int_{-\infty}^{\infty} R_{\tilde{w}_n \tilde{w}_m}(\tau) e^{-j\omega\tau d\tau}.$$

Therefore, the output spectrum is a sum of the Fourier transform of each component of the autocorrelation function weighted by the appropriate power series coefficient. Fig. 3.2 shows the output spectrum of the nonlinear model divided into linear and intermodulation components.

The effect of SR is mitigated in many systems by not using adjacent channels in the same geographical cell. However it is still necessary to establish a lower limit on the ratio of the power in the main channel to the amount of power induced in the adjacent channel. This ratio is known as Adjacent Channel Power Ratio ACPR. ACPR is defined as

$$ACPR = \frac{\int_{f_3}^{f_4} S_{yy}(f)df}{\int_{f_1}^{f_2} S_{yy}(f)df}. \tag{3.13}$$

Frequencies f_3 and f_4 are the frequency limits of the main channel while f_1 and f_2 are the limits of the lower adjacent channel. Fig. 3.3 clarifies the definition of ACPR. In the IS-95 CDMA mobile system standard [45] ACPR is defined as the ratio of the adjacent channel power in a 30 kHz resolution bandwidth ($f_4 - f_3$=30 kHz), swept over the adjacent channel, to the total power in the main channel ($f_2 - f_1$=1.23 MHz).

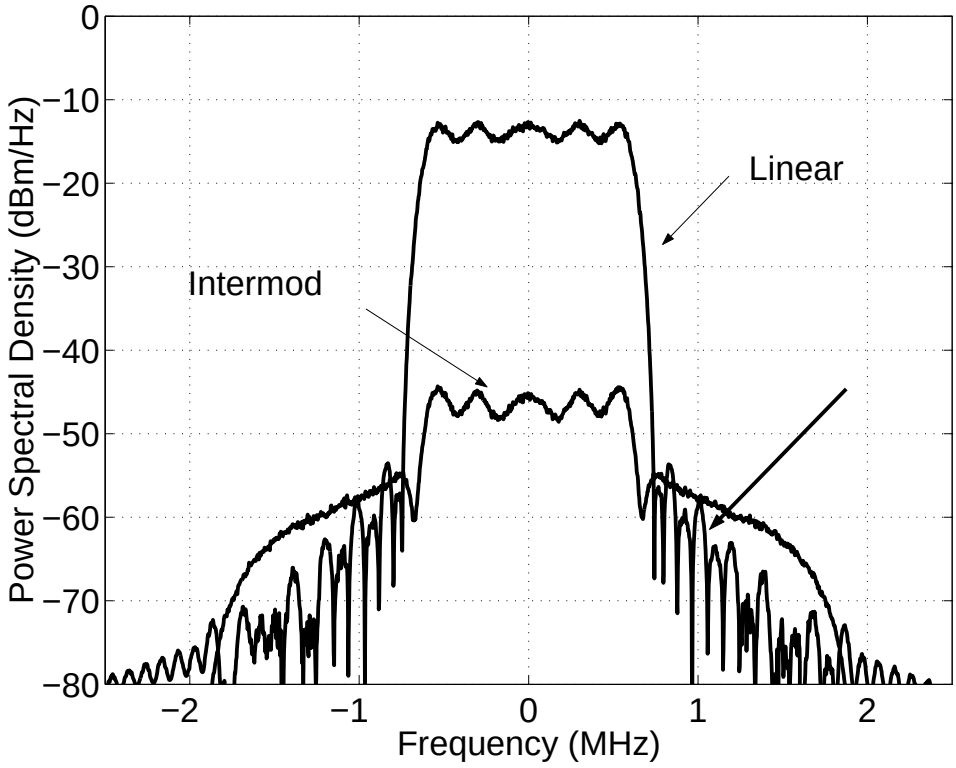

Figure 3.2: Output power spectral density of a nonlinear PA driven by an reverse link IS-95 CDMA signal.

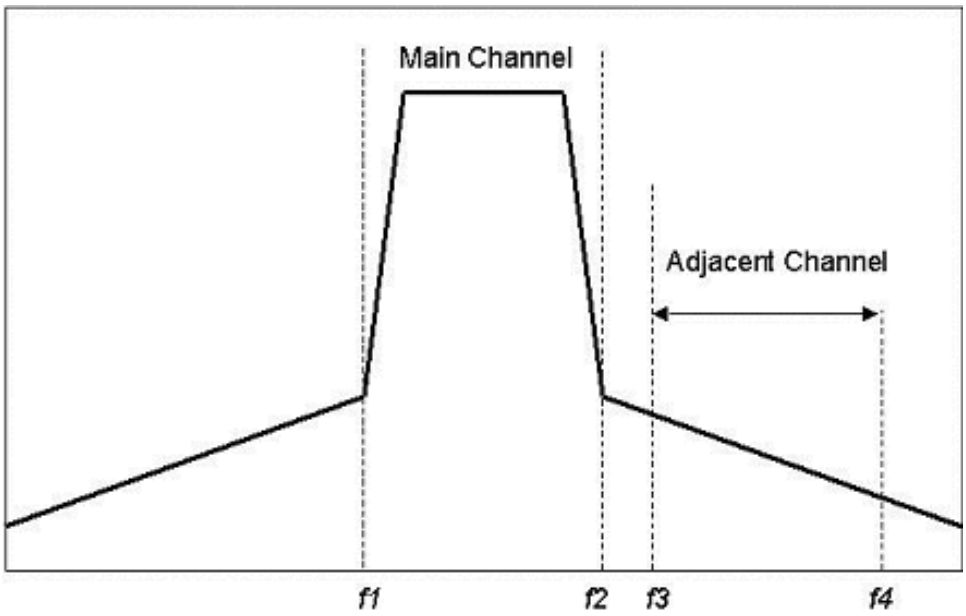

Figure 3.3: Definition of ACPR

3.3 The limiter Family

Distortion that results from passing communication signals through a limiter amplifier was studied in [37, 38, 39, 40, 41, 42, 43]. Here we use the Price theorem [44] which enables the calculation of the autocorrelation function for an input that has a gaussian distribution. The validity and the limitations of such an assumption will be thoroughly discussed in Chapter 6. Here we develop closed forms for the output autocorrelation function of the limiter amplifier models. The output autocorrelation of the amplifier can be written as:

$$\begin{aligned} R_{yy}(\tau) &= E[y(t)y(t+\tau)] \\ &= E[f(w(t))f(w(t+\tau))]. \end{aligned} \tag{3.14}$$

Now, let $w(t) = w_1$ and $w(t+\tau) = w_2$ then, using the Price theorem [44], the output autocorrelation function for a zero mean Gaussian input signal can be computed using the following relation:

$$\frac{\partial^k R_{yy}(\tau)}{\partial R^k_{ww}(\tau)} = E[f^{(k)}(w_1)f^{(k)}(w_2)]$$

$$= \int_{-\infty}^{\infty}\int_{-\infty}^{\infty} \frac{f^{(k)}(w_1)f^{(k)}(w_2)}{2\pi\sqrt{1-R^2_{\tilde{w}\tilde{w}}(\tau)}} \times \exp\left\{\frac{-1}{2(1-R^2_{\tilde{w}\tilde{w}}(\tau))}\left[\frac{w_1^2}{\sigma^2_{w_1}}+\frac{w_2^2}{\sigma^2_{w_2}}-\frac{2R_{\tilde{w}\tilde{w}}(\tau)}{\sigma^2_{w_1}\sigma^2_{w_2}}\right]\right\} dw_1 dw_2 \quad (3.15)$$

where $f^{(k)}(w)$ denotes the k th derivative of $f(w)$ with respect to w and $\sigma^2_{w_1}$,$\sigma^2_{w_2}$ are the variances of the random variables w_1, w_2 respectively. In the following, we discuss the derivation of the autocorrelation function for the limiter amplifier models presented in Section 2.7.2 using the Gaussian input assumption.

Hard limiter Model

For the hard-limiter amplifier models, we take the case where $k = 1$, then $f^{(k)}(w)$ is a first order delta function of area $2L$ and centered at $w = 0$. Substituting into (3.15) and integrating, we get [44]:

$$\frac{\partial R_{yy}(\tau)}{\partial R_{\tilde{w}\tilde{w}}(\tau)} = \frac{2L^2}{\pi\sqrt{1-R^2_{\tilde{w}w}(\tau)}} \quad (3.16)$$

and the output autocorrelation function can be obtained by integrating (3.16) and taking the condition that $R_{yy}(\tau) = 0$ when $R_{ww}(\tau) = 0$ and hence, we get:

$$\begin{aligned} R_{yy}(\tau) &= \frac{2L^2}{\pi\sqrt{1-R^2_{ww}(\tau)}} dR_{ww} \\ &= \frac{2L^2}{\pi}\sin^{-1}\left[\frac{R_{ww}(\tau)}{R_{ww}(0)}\right]. \end{aligned} \quad (3.17)$$

This form is called Van Vleck's result [44] which relates the input autocorrelation to the output autocorrelation by the inverse sine function.

Smooth Limiter

The output autocorrelation function of a smooth filter can be found using Price theorem in a simple compact form as [44]:

$$\frac{\partial R_{yy}(\tau)}{\partial R_{ww}(\tau)} = \frac{L^2}{2\pi\sqrt{(1+l^{-2})^2 - l^{-4}R^2_{ww}(\tau)}} \quad (3.18)$$

and by integrating 3.18, we get the output autocorrelation function as:

$$R_{yy}(\tau) = \frac{(lL)^2}{2\pi}\sin^{-1}\left[\frac{R_{ww}(\tau)}{(1+l^2)R_{ww}(0)}\right]. \quad (3.19)$$

Soft Limiter

For a soft limiter, the output autocorrelation can be obtained using 2.21 and setting $k = 2$ in 3.15, therefore:

$$\frac{\partial^2 R_{yy}(\tau)}{\partial R_{ww}^2(\tau)} = \frac{\exp\left[\frac{l^2}{1+\rho_{ww}(\tau)}\right] - \exp\left[\frac{l^2}{1-\rho_{ww}(\tau)}\right]}{\pi\sqrt{1-\rho_{ww}^2(\tau)}} \tag{3.20}$$

where $\rho_{ww(\tau)} = R_{ww(\tau)}/R_{ww}(0)$ and the output autocorrelation function can be found by integrating 3.20 where we get [46]:

$$R_{yy}(\tau) = R_{ww}(0)\left[\text{erf}^2\left(\frac{l}{\sqrt{2}\sigma_w}\right)\frac{R_{ww}(\tau)}{R_{ww}(0)} + \sum_{n=2}^{\infty} C_n\left[\frac{R_{ww}(\tau)}{R_{ww}(0)}\right]^{n+1}\right] \tag{3.21}$$

where erf is the error function and C_n is defined as

$$C_n = \frac{4H_{n-1}^2\left(\frac{l}{\sqrt{2}\sigma_w}\right)}{\pi 2^n (n+1)!} e^{\frac{-l^2}{\sigma_w^2}}$$

where H_n is a Hermite polynomial of order n. The output spectrum for the limiter amplifiers discussed above was simulated assuming the the input signal can be approximated by a NBGN process which have a box shaped PSD. This assumption will be discussed in chapter 5 and we will show that it is a good approximation in some cases. Fig 3.4 shows the output PSD of three kinds of limiter amplifier using the calculated autocorrelation functions for an input with box shaped spectral density (NBGN).

3.4 Relationship between IMR and ACPR

The intermodulation Distortion Ratio (IMR) is an adequate performance measures for the nonlinear behavior of RF amplifiers with analog modulated signals such as FM. This is because these signals can be represented as a number of discrete tones and so two-tone testing accurately captures nonlinear behavior. However, relating two-tone properties to spectral distortion with digitally modulated signals has proved elusive. With digitally modulated signals, the level of spectral regrowth of the spectrum in neighboring channels is a fundamental performance parameter with distortion quantified by ACPR. A relationship between the IMR of discrete-tone signals and spectral regrowth of digitally-modulated signals has long been supposed as they are both due to the same nonlinear processes.

The relationship between the IMR and the ACPR can be established by using the 3 rd order power series representation of the nonlinear characteristics and using (3.6) where we have:

$$a_1 = G$$

$$a_3 = \frac{-2G}{3\text{IIP3}}$$

and G is the linear gain. Therefore, using these simple relationships in (3.12), the output spectrum can be directly related to IIP3. Note that this is only valid for the third order assumption. A relationship between IIP3 and ACPR can be established by assuming that the PSD of the input signal has a defined shape such the PSD of NBGN process which is proved to be an acceptable assumption in some situations. However, this assumption was proven inadequate [48] for the reverse link of a CDMA system. In Chapter 7 we will explore possible relationships using simulations and measurements to show that lower-order nonlinear modeling can be used to capture discrete tone distortion but high-order modeling is important for capturing the response with digitally modulated signals. This is because the nonlinear amplifier is then presenting its most extreme nonlinearity at the peaks of the signals. Therefore the relationship between the two mentioned measures of nonlinearity cannot be established specifically for high drive levels. In Chapter 7 we will demonstrate by measurements and simulations that higher order nonlinear modeling must be used in the behavioral modeling of RF systems with digitally modulated signals than in the behavioral modeling of two-tone response.

3.5 Conclusion

In this chapter we discussed distortion introduced by nonlinear amplifiers both in analog and digital communication systems. The analysis here establishes the basis for modeling of distortion in PAs and the measures of nonlinearity presented in this chapter will be used in the context of multichannel amplifiers modeling. In addition, the relationship between analog and digital system distortion was discussed and further analysis and results will be shown in Chapter 7 which are part of the original contributions of this dissertation.

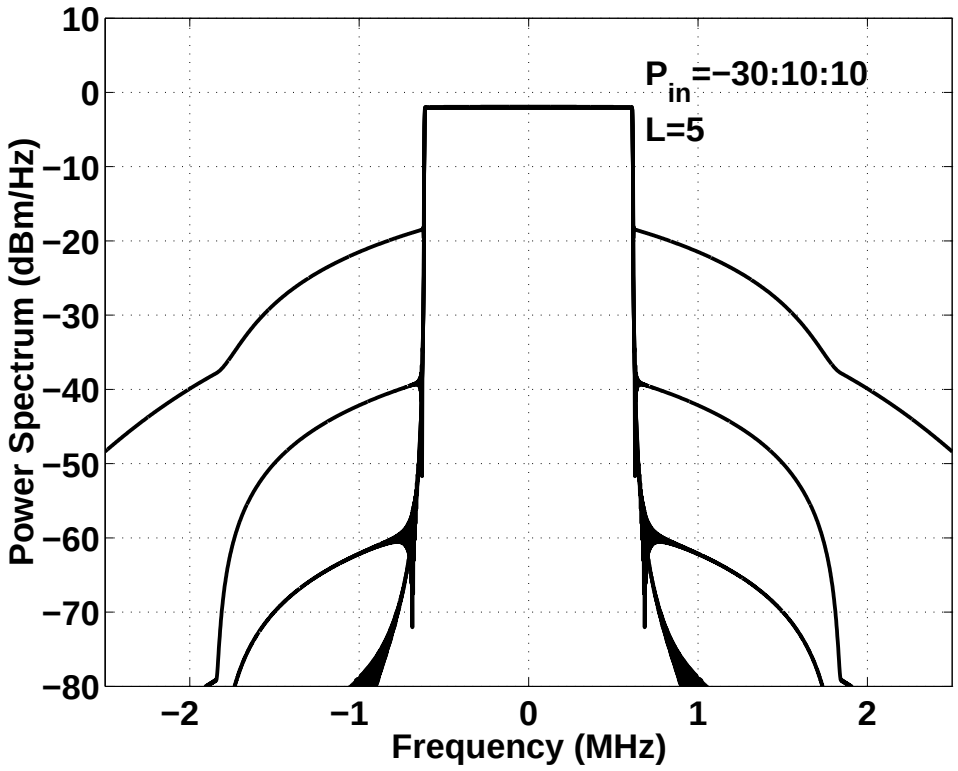
P in =−30:10:10
L=5
Power Spectrum (dBm/Hz)
Frequency (MHz)
10
0
−10
−20
−30
−40
−50
−60
−70
−80
−2
−1
0
1
2

(a)

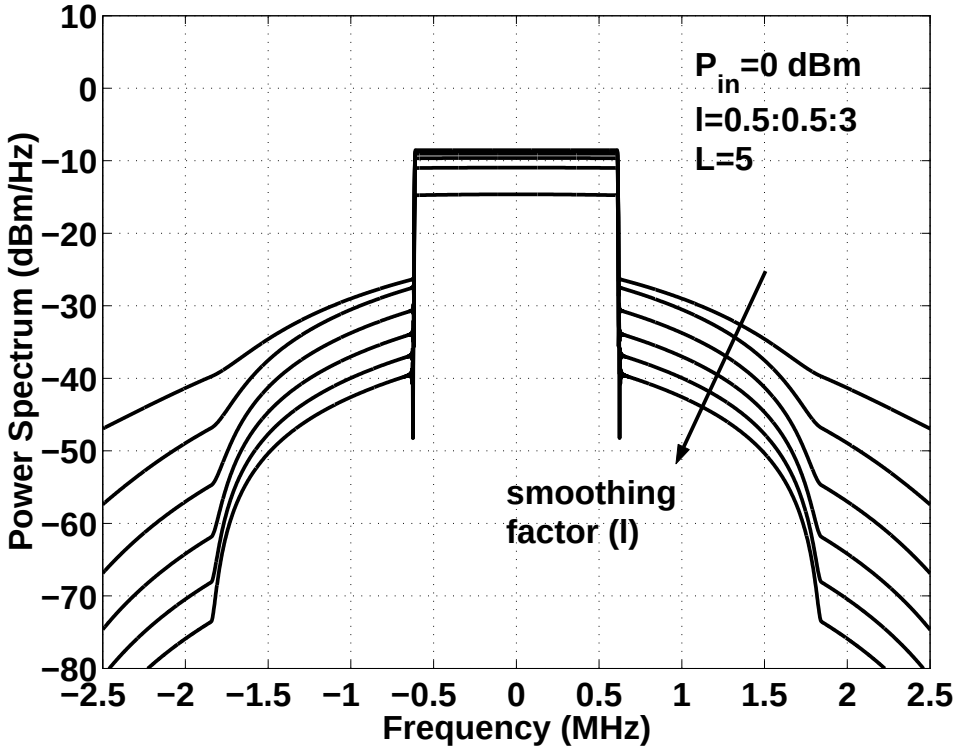
P in =0 dBm
l=0.5:0.5:3
L=5
smoothing
factor (l)
Power Spectrum (dBm/Hz)
Frequency (MHz)
10
0
−10
−20
−30
−40
−50
−60
−70
−80
−2.5
−2
−1.5
−1
−0.5
0
0.5
1
1.5
2
2.5

(b)

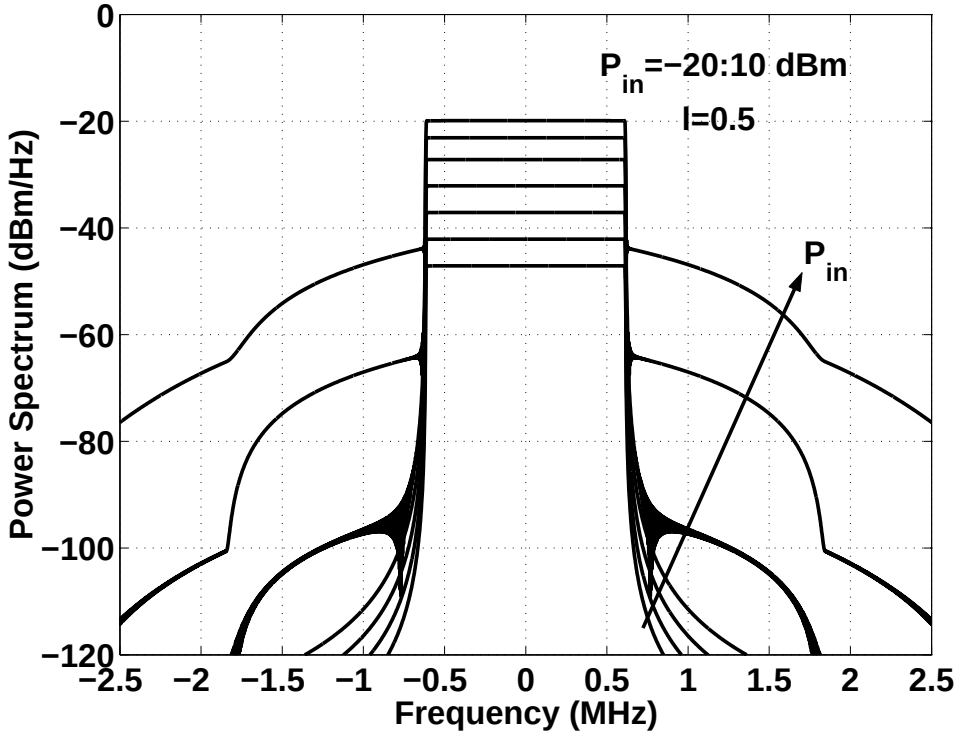

(c)

Figure 3.4: Output power spectral densities: (a) hard limiter; (b) smooth limiter; and (c) soft limiter.

Chapter 4

Behavioral Modeling of Multichannel Systems

With a multichannel input the nonlinear behavior results in components at all the intermodulation frequencies of the input frequencies. Therefore the output of the nonlinear system at a certain intermodulation frequency consists of contributions from all the input signals. In this chapter the complex envelope of the output at a particular frequency (which results from the intermodulation of input channels) is derived, as shown in Fig. 4.1. The complex envelope form is needed since all the simulations will be performed at the envelope level. Envelope simulations offer an advantage over time domain simulations as the sampling frequency is commensurate with the bandwidth of individual channels and not with the frequency separation of input channels. This makes the simulation of multiple channels more practical and more numerically efficient. This analysis will be used in the distortion analysis of MCPA in the following chapters where the envelope model will be used to derive the output spectrum by which distortion can be estimated. This chapter is divided into three main parts. The first part is an analysis of multiple signals using Volterra series analysis and its variants as described in Chapter 2. The second part deals with the the three-box approximation of the Volterra model which will be adopted to model multichannel amplifiers and its parameter extraction. The last part discusses parameter extraction

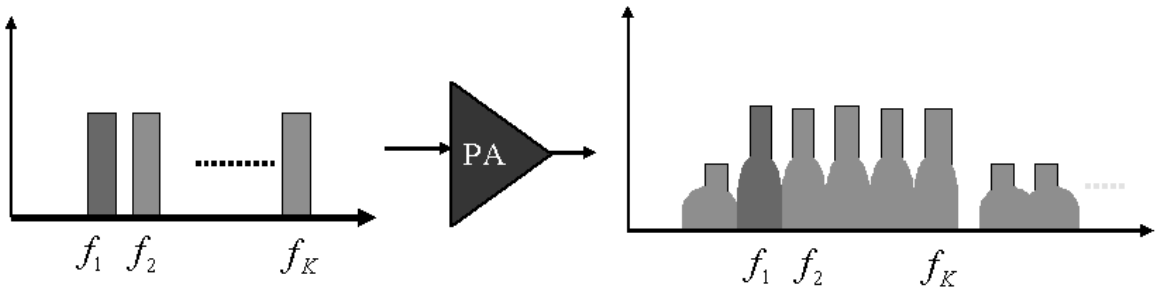

Figure 4.1: Envelope Simulations

of the memoryless and the three-box model.

4.1 Multichannel Analysis of Volterra Series and Its Variants

Volterra series represents the output of the system as a convolution of powers of the input with the Volterra kernels. In order to develop a theoretical analysis for the interaction of multiple signals by the nonlinear behavior, we use the analyses of general Volterra series addressed in [21, 22, 49] to develop the output waveform for the models described in Chapter 2. We start the analysis by considering an input that consists of the sum of K modulated carriers applied to a nonlinear amplifier so that:

$$w(t) = \sum_{k=1}^{K} w_k(t). \tag{4.1}$$

We will assume that the signals $w_k(t)$ are modulated RF carriers with center frequencies ξ_k and have equal bandwidths B_k. Now let $\tilde{w}_k(t)$ be the complex envelope of $w_k(t)$, then the $w_k(t)$ can be written in complex envelope form as

$$\begin{aligned} w_k(t) &= Re\{\tilde{w}_k(t)e^{j2\pi\xi_k t}\} \\ &= \frac{1}{2}\tilde{w}_k(t)e^{j2\pi\xi_k t} + \frac{1}{2}\tilde{w}_k^*(t)e^{-j2\pi\xi_k t}. \end{aligned} \tag{4.2}$$

Taking the Fourier transform of (4.2) yields

$$W_k(f) = \frac{1}{2}\tilde{W}_k(f-\xi_k) + \frac{1}{2}\tilde{W}_k^*(-f-\xi_k).$$

Then $w(t)$ and its Fourier transform can be written as

$$w(t) = \frac{1}{2} \sum_{k=-K}^{K} \tilde{w}_k(t) e^{j2\pi\xi_k t}$$

and

$$W(f) = \frac{1}{2} \sum_{k=-K}^{K} \tilde{W}_k(f - \xi_k) \tag{4.3}$$

respectively, where $\tilde{w}_{-k} = \tilde{w}_k^*$ and $\xi_{-k} = -\xi_k^*$. The output of the Volterra system for a multiple input can be expressed by substituting (4.3) into (2.3), therefore

$$y_n(t) = \int_{-\infty}^{\infty} \dots \int_{-\infty}^{\infty} H_n(f_1, \dots, f_n) \times \prod_{i=1}^{n} \frac{1}{2} \sum_{k=-K}^{K} \tilde{W}_k(f_i - \xi_k) e^{j2\pi f_i t} df_i.$$

Now since [22]

$$\prod_{i=1}^{n} \frac{1}{2} \sum_{k=-K}^{K} \tilde{W}_k(f_i - \xi_k) = \frac{1}{2^n} \sum_{k_1=-K}^{K} \dots \sum_{k_n=-K}^{K} \prod_{i=1}^{n} \tilde{W}_{k_i}(f_i - \xi_{k_i})$$

then the output $y_n(t)$ can be written as

$$y_n(t) = \frac{1}{2^n} \sum_{k_1=-K}^{K} \dots \sum_{k_n=-K}^{K} \Lambda(t; \underline{\xi}) \tag{4.4}$$

where $\underline{\xi} = (\xi_{k_1}, \dots, \xi_{k_n})$ is an n-dimensional vector and represents the intermodulation frequency vector where each k_i ranges from $-K$ to K. The function Λ represents the following integral [49]:

$$\Lambda(t; \underline{\xi}) = \int_{-\infty}^{\infty} \dots \int_{-\infty}^{\infty} H_n(f_1, \dots, f_n) \prod_{i=1}^{n} \tilde{W}_{k_i}(f_i - \xi_{k_i}) e^{j2\pi f_i t} df_i.$$

The integral Λ represents the component of the output waveform centered at the sum frequency $\xi = (\xi_{k_1} + \dots + \xi_{k_n})$ [49]. In the frequency vector $\underline{\xi}$, each distinct frequency ξ_{k_i} occurs n_k times where $\sum_{k=-K}^{K} n_k = n$, therefore, there are $\binom{n}{n_{-K}, \dots, n_K}$ such integrals. The component of $y_n(t)$ centered at ξ due to the intermodulation of input components centered at the frequency vector $(\xi_{k_1}, \dots, \xi_{k_n})$ can be expressed in complex envelope form as [49]

$$\tilde{y}_{n,\xi}(t) = \frac{1}{2^{n-1}} \sum_{n_{-K}+\dots+n_K=n} \binom{n}{n_{-K}, \dots, n_K} \int_{-\infty}^{\infty} \dots \int_{-\infty}^{\infty} \tilde{H}_{n,\underline{\xi}}(\underline{f}) \prod_{i=1}^{n} \tilde{W}_{k_i}(f_i) e^{j2\pi f_i t} df_i \tag{4.5}$$

where $\tilde{H}_{n,\underline{\xi}}(\underline{f})$ is the baseband equivalent of $H_n(\underline{f})$ with respect to the frequency vector $\underline{\xi}$ and the total output of the system is

$$\begin{aligned}\tilde{y}_{\xi}(t) &= \sum_{n=0}^{\infty} \frac{1}{2^{n-1}} \sum_{n_{-K}+\ldots+n_K=n} \binom{n}{n_{-K},\ldots,n_K} \\ &\quad \times \int_{-\infty}^{\infty} \ldots \int_{-\infty}^{\infty} \tilde{H}_{n,\underline{\xi}}(\underline{f}) \prod_{i=1}^{n} \tilde{W}_{k_i}(f_i) e^{j2\pi f_i t} df_i. \end{aligned} \tag{4.6}$$

This formulation establishes the basis for the analysis which follows for the models discussed in Chapter 2. In the following the output of each of these models will be derived for multiple input excitation.

4.1.1 Memoryless System

As discussed in Chapter 2, a memoryless system is characterized by a constant Volterra transfer function over frequency. Therefore, using the kernel relationship in (2.19) and substituting in (4.6) yields

$$\begin{aligned}\tilde{y}_{n,\xi}(t) &= \frac{1}{2^{n-1}} \sum_{n_{-K}+\ldots+n_K=n} \binom{n}{n_{-K},\ldots,n_K} \int_{-\infty}^{\infty} \ldots \int_{-\infty}^{\infty} \tilde{a}_n \prod_{i=1}^{n} \tilde{W}_{k_i}(f_i) e^{j2\pi f_i t} df_i \\ &= \frac{a_n}{2^{n-1}} \binom{n}{n_{-K},\ldots,n_K} \prod_{i=1}^{n} \tilde{w}_{k_i}(t). \end{aligned} \tag{4.7}$$

Now since

$$\prod_{i=1}^{n} \tilde{w}_{k_i}(t) = \prod_{k=-K}^{K} \tilde{w}_k^{n_k}(t) \tag{4.8}$$

then the complex envelope of the output $y(t)$ reduces to

$$\tilde{y}_{\xi}(t) = \sum_{n=1}^{N} \frac{a_n}{2^{n-1}} \sum_{n_{-K}+\ldots+n_K=n} \binom{n}{n_{-K},\ldots,n_K} \prod_{k=-K}^{K} \tilde{w}_k^{n_k}(t) \tag{4.9}$$

where $\sum_{k=-K}^{K} n_k = n$.

4.1.2 Filter-Nonlinearity Model

For the FN model, we use the kernel relationship (2.7) and then it follows that the output $y_n(t)$ can be written as

$$y_n(t) = \int_{-\infty}^{\infty} \ldots \int_{-\infty}^{\infty} a_n \prod_{i=1}^{n} h_n(\lambda_i) w(t-\lambda_i) d\lambda_i$$

$$
\begin{aligned}
&= \int_{-\infty}^{\infty} \cdots \int_{-\infty}^{\infty} a_n \prod_{i=1}^{n} H_n(f_i) W(f_i) e^{j2\pi f_i t} df_i \\
&= \int_{-\infty}^{\infty} \cdots \int_{-\infty}^{\infty} a_n \prod_{i=1}^{n} U_n(f_i) e^{j2\pi f_i t} df_i \\
&= a_n u_n^n(t) \qquad (4.10)
\end{aligned}
$$

where

$$u_n(t) = \int_{-\infty}^{\infty} H_n(f) W(f) e^{j2\pi ft} e^{j2\pi ft} df = \int_{-\infty}^{\infty} U_n(f) e^{j2\pi ft} df$$

represents the filtered input. Therefore, the n th order output consists of powers of the filtered input waveforms by the the linear filter of the n th branch. Applying the same analysis of the memoryless nonlinearity, the complex envelope of the output signal in the vicinity of a frequency ξ due to the intermodulation of input components centered at a frequency vector $\underline{\xi}$ can be written as

$$\tilde{y}_{n,\xi}(t) = \frac{a_n}{2^{n-1}} \sum_{n_{-K}+\ldots+n_K=n} \binom{n}{n_{-K}, \ldots, n_K} \prod_{i=1}^{n} \tilde{u}_{n,k_i}(t) \qquad (4.11)$$

where

$$\tilde{u}_{n,k}(t) = \int_{-\infty}^{\infty} \tilde{h}_{n;\xi_k}(\lambda) \tilde{w}_k(t-\lambda) d\lambda$$

and $\tilde{h}_{n;\xi_k}(t)$ is the baseband equivalent of the filter of the n th branch with respect to frequency ξ_k. Using (4.8) the complex envelope of (4.11) reduces to a power series model with filtered inputs $u(t)$:

$$\tilde{y}_{\xi}(t) = \sum_{n=1}^{N} \frac{a_n}{2^{n-1}} \sum_{n_{-K}+\ldots+n_K=n} \binom{n}{n_{-K}, \ldots, n_K} \prod_{k=-K}^{K} \tilde{u}_{n,k}^{n_k}(t) \qquad (4.12)$$

4.1.3 Nonlinearity-Filter Model

For the NF model, the kernel relationship (2.9) enables the output of the system to be written as

$$y_n(t) = \int_{-\infty}^{\infty} h_n(\lambda) w^n(t-\lambda) d\lambda. \qquad (4.13)$$

Now, let $w^n(t) = v_n(t)$, then using (4.9) for the memoryless nonlinearity, the complex envelope of the output $v_n(t)$ with respect to frequency ξ is

$$\tilde{v}_{n,\xi}(t) = \frac{1}{2^{n-1}} \sum_{n_{-K}+\ldots+n_K=n} \binom{n}{n_{-K}, \ldots, n_K} \prod_{k=-K}^{K} \tilde{w}_k^{n_k}(t)$$

and hence, the complex envelope of the output waveform $y(t)$ is

$$\tilde{y}_\xi(t) = \sum_{n=1}^{N} \frac{1}{2^{n-1}} \sum_{n_{-K}+\ldots+n_K=n} \binom{n}{n_{-K},\ldots,n_K} \int_{-\infty}^{\infty} \tilde{h}_{n,\xi}(\lambda) \prod_{k=-K}^{K} \tilde{w}_k^{n_k}(t-\lambda)d\lambda \quad (4.14)$$

where $\tilde{h}_{n,\xi}$ is the baseband equivalent of the filter $h_n(t)$ with respect to the frequency ξ.

4.1.4 Parallel Cascade (Wiener) Model

The parallel cascade model can be treated in a similar way. Given the input- output relationship (2.11), and using the multiple envelope signal $w(t)$, we can write

$$y(t) = \sum_{p=1}^{P} y_p(t)$$

$$y_p(t) = \sum_{r=0}^{N_p} a_{r,p} u_p^r(t)$$

where

$$\begin{aligned} u_p(t) &= \int_{-\infty}^{\infty} h_p(\lambda) w(t-\lambda) d\lambda \\ &= \sum_{k=1}^{K} \int_{-\infty}^{\infty} h_p(\lambda) w_k(t-\lambda) d\lambda \\ &= \sum_{k=1}^{K} u_{p,k}(t). \end{aligned}$$

The output of the p th branch $y_p(t)$ can then be written as

$$y_p(t) = \sum_{r=0}^{N_p} a_{r,p} \left(\sum_{k=1}^{K} u_{p,k}(t) \right)^r.$$

The complex envelope of the output of the p th branch with respect to frequency ξ can be expressed using (4.9) as

$$\tilde{y}_{p,\xi}(t) = \sum_{r=1}^{N_p} \frac{a_{r,p}}{2^{r-1}} \binom{r}{n_{-K},\ldots,n_K} \prod_{k=-K}^{K} \tilde{u}_{p,k}^{n_k}(t)$$

where

$$\tilde{u}_{p,k}(t) = \int_{-\infty}^{\infty} \tilde{h}_{p;\xi_k}(\lambda) \tilde{w}_k(t-\lambda) d\lambda.$$

Therefore, the complex envelope of the total output is

$$\tilde{y}_\xi(t) = \sum_{p=1}^{P} \sum_{r=1}^{N_p} \frac{a_{r,p}}{2^{r-1}} \binom{r}{n_{-K}, \ldots, n_K} \prod_{k=-K}^{K} \tilde{u}_{p,k}^{n_k}(t) \tag{4.15}$$

where $\tilde{u}(t)$ is the complex envelope of $u(t)$ and $\sum_{k=-K}^{K} n_k = r$.

4.1.5 Multi-Input Single Output Nonlinear Model

Using (2.17) and the frequency-domain kernel relationship (2.18), the output $z(t)$ of the memoryless block can be written as

$$\begin{aligned} z(t) = \quad & \sum_{n_1=0}^{\infty} \cdots \sum_{n_K=0}^{\infty} a_n \binom{n}{n_1, \ldots, n_K} \int_{-\infty}^{\infty} \cdots \int_{-\infty}^{\infty} \\ & h_{11}(\lambda_{11}) w_1(t-\lambda_{11}) \ldots h_{11}(\lambda_{1n_1}) w_1(t-\lambda_{1n_1}) \ldots \\ & h_{1K}(\lambda_{K1}) w_K(t-\lambda_{K1}) \ldots h_{1K}(\lambda_{Kn_K}) w_K(t-\lambda_{Kn_K}) \\ & d\lambda_{11} \ldots d\lambda_{1n_1} \ldots d\lambda_{1n_1} \ldots d\lambda_{K1} \ldots d\lambda_{Kn_K} \\ = \quad & \sum_{n=0}^{\infty} \sum_{n_1+\ldots+n_K=n} a_n \binom{n}{n_1, \ldots, n_K} \int_{-\infty}^{\infty} \cdots \int_{-\infty}^{\infty} h_{11}(\lambda_{11}) w_1(t-\lambda_{11}) \ldots \\ & h_{11}(\lambda_{1n_1}) w_1(t-\lambda_{1n_1}) \ldots h_{1K}(\lambda_{K1}) w_K(t-\lambda_{K1}) \ldots h_{1K}(\lambda_{Kn_K}) w_K(t-\lambda_{Kn_K}) \\ & d\lambda_{11} \ldots d\lambda_{1n_1} \ldots d\lambda_{1n_1} \ldots d\lambda_{K1} \ldots d\lambda_{Kn_K}. \end{aligned} \tag{4.16}$$

Note that because of the kernel relationship (2.18), the integrand now is separable which means that the multiple integral in (4.16) can be written as the product of individual integrals and hence the output of the memoryless block can be written as

$$\begin{aligned} z(t) &= \sum_{n=0}^{\infty} a_n \left(\sum_{k=1}^{K} \int_{-\infty}^{\infty} h_{1k}(\lambda) w_k(t-\lambda) d\lambda \right)^n \\ &= \sum_{n=0}^{\infty} z_n(t) \end{aligned}$$

where

$$z_n(t) = a_n \left(\sum_{k=1}^{K} u_k(t) \right)^n$$

and

$$u_k(t) = \int_{-\infty}^{\infty} h_{1k}(\lambda) w_k(t-\lambda) d\lambda.$$

The complex envelope of the output $z(t)$ with respect to the frequency ξ can be developed in a similar way to the memoryless nonlinearity. Therefore:

$$\tilde{z}_{n;\xi}(t) = \frac{a_n}{2^{n-1}} \sum_{n_{-K}+\ldots+n_K} \binom{n}{n_{-K},\ldots,n_K} \prod_{k=-K}^{K} \tilde{u}_k^{n_k}(t) \tag{4.17}$$

where

$$\tilde{u}_k(t) = \int_{-\infty}^{\infty} \tilde{h}_{1k;\xi}(\lambda)\tilde{w}_k(t-\lambda)d\lambda$$

and hence, the complex envelope of the total output waveform $y(t)$ is

$$\tilde{y}_\xi(t) = \sum_{n=1}^{N} \frac{1}{2^{n-1}} \sum_{n_{-K}+\ldots+n_K=n} \binom{n}{n_{-K},\ldots,n_K} \int_{-\infty}^{\infty} \tilde{h}_{2,\xi}(\lambda) \prod_{k=-K}^{K} \tilde{u}_k^{n_k}(t-\lambda)d\lambda \tag{4.18}$$

where $\tilde{h}_{2,\xi}(t)$ is the baseband equivalent of the output filter $h_2(t)$ with respect to frequency ξ.

4.2 Multichannel Analysis of the Three Box Model

The three-box approximation of the Volterra model, despite its simplicity, captures the behavior of a class of power amplifiers including memory effects and serves the objective of studying the interaction of the multiple channels. Memory effects are manifested as multiple AM-AM curves at different frequencies which have the same shape as shown in Fig 4.2. If the amplifier circuit exhibits different shapes for the nonlinear characteristics, then the system cannot be approximated by the three-box model and it requires a more sophisticated model. The phenomena of dissimilar nonlinear characteristics is due to the memory effects caused by nonlinear parasitic capacitances of the nonlinear device. However the model can be improved by considering more complicated structures that give better accuracy.
The three-box structure was investigated in [50] and [51] and used to adequately model memory effects of single input nonlinear amplifiers where its parameters were extracted using time-domain measurements. The three-box model shown in Fig. 4.3 consists of three major blocks: an input Linear Time Invariant (LTI) filter with frequency response $H_1(f)$, a static nonlinearity G and an output LTI filter with a frequency response $H_2(f)$. In our present work the static nonlinearity, is described by the power series

$$z(t) = \sum_{n=0}^{N} a_n u^n(t).$$

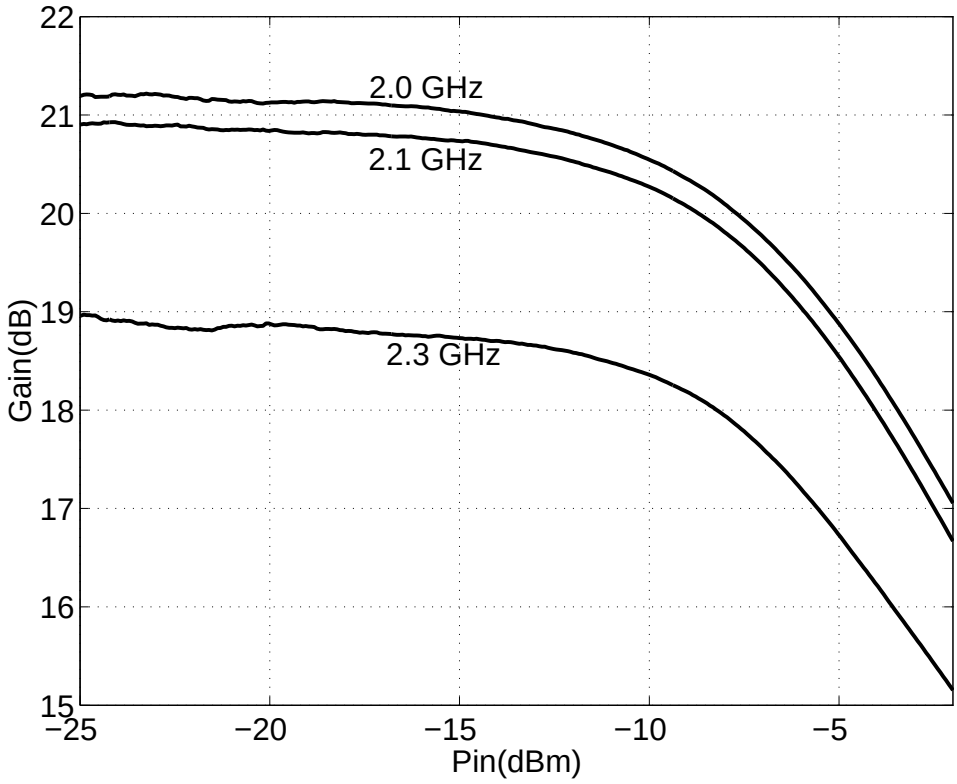

Figure 4.2: AM-AM characteristics taken at different frequencies

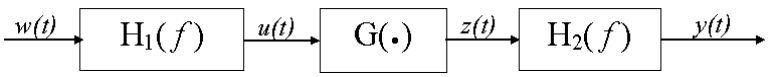

Figure 4.3: Three box model.

Now consider a multichannel input signal $w(t)$ defined in (4.1) applied to the nonlinear amplifier then the signal $u(t)$ at the output of the input filter can be written as a convolution of the input signal with the input filter impulse response as

$$\begin{aligned} u(t) &= \int_{-\infty}^{\infty} h_1(\lambda) w(t-\lambda) d\lambda \\ &= \sum_{k=1}^{K} u_k(t) \end{aligned}$$

where $h_1(t)$ is the impulse response of the input filter and

$$u_k(t) = \int_{-\infty}^{\infty} h_1(\lambda) w_k(t-\lambda) d\lambda.$$

The output of the nonlinear block is then

$$z(t) = \sum_{n=0}^{N} z_n(t)$$

where

$$z_n(t) = a_n \left(\sum_{k=1}^{K} u_k(t) \right)^n \tag{4.19}$$

is the n th order nonlinear response. Finally, the total output of the model is

$$\begin{aligned} y(t) &= \int_{-\infty}^{\infty} h_2(\lambda) z(t-\lambda) d\lambda \\ &= \sum_{n=1}^{N} \int_{-\infty}^{\infty} h_2(\lambda) z_n(t-\lambda) d\lambda \end{aligned} \tag{4.20}$$

where $h_2(t)$ is the impulse response of the output filter. In order to estimate distortion (particularly cross modulation) introduced by the interaction of multiple signals, a closed form expression for the output waveform at a particular frequency in complex envelope form is derived. The input to the nonlinear block, $u_k(t)$, can be written in complex form as [31]

$$\tilde{u}_k(t) = \int_{-\infty}^{\infty} \tilde{h}_{1;\xi_k}(\lambda) \tilde{w}_k(t-\lambda) d\lambda$$

where $\tilde{h}_{1;\xi_k}(t)$ is the base band equivalent impulse response of the input filter with respect to frequency ξ_k and $\tilde{w}_k(t)$ is the complex envelope of the input signal $w_k(t)$. Hence, the total input to the nonlinear block can be written as a complex conjugate pair as

$$u(t) = \sum_{k=-K}^{K} \frac{1}{2} \tilde{u}_k(t) e^{j2\pi\xi_k t}$$

where the minus sign notation here indicates complex conjugation so that $\tilde{u}_{-k} = \tilde{u}_k^*$ and $\xi_{-k} = -\xi_k$. Following the analyses presented in Section 4.1 for Volterra series, the n th order output of the nonlinear block becomes

$$\begin{aligned} z_n(t) &= \frac{a_n}{2^n}\left(\sum_{k=-K}^{K}\tilde{u}_k(t)e^{j2\pi\xi_k t}\right)^n \\ &= \frac{a_n}{2^n}\sum_{k_1=-K}^{K}\cdots\sum_{k_n=-K}^{K}\prod_{i=1}^{n}\tilde{u}_{k_i}(t)e^{j2\pi\xi_{k_i}t} \\ &= \frac{a_n}{2^n}\sum_{k_1=-K}^{K}\cdots\sum_{k_n=-K}^{K}A(t)e^{j2\pi(\xi_{k_1}+\ldots+\xi_{k_n})t} \end{aligned} \tag{4.21}$$

where $A(t) = \prod_{i=1}^{n}\tilde{u}_{k_i}(t)$. The output $y(t)$ consists of components centered at all the intermodulation frequencies that result from the permutations of the input carrier frequencies represented by the frequency vector $(\xi_{k_1}, \ldots, \xi_{k_n})$. Therefore, the component of $z_n(t)$ centered at frequency $\xi = \xi_{k_1} + \ldots + \xi_{k_n}$ due to the intermodulation of input components (centered at the frequency vector $(\xi_{k_1}, \ldots, \xi_{k_n})$) can be expressed as [49]

$$z_{n,\xi}(t) = \sum_{n_{-K}\xi_k+\ldots n_K\xi_k=\xi}\frac{a_n}{2^n}\binom{n}{n_{-K},\ldots,n_K}\left(A(t)e^{j2\pi\xi t} + A^*(t)e^{-j2\pi\xi t}\right)$$

where

$$\binom{n}{n_{-K},\ldots,n_K} = \frac{n!}{n_K!\ldots n_{-K}!}$$

is the multinomial coefficient. Thus the complex envelope of the output signal at the output of the nonlinear block and in the vicinity of a frequency ξ is

$$\begin{aligned} \tilde{z}_{n,\xi}(t) &= \sum_{\xi_{k_1}+\ldots+\xi_{k_n}=\xi}\frac{a_n}{2^{n-1}}\binom{n}{n_{-K},\ldots,n_K}A(t) \\ &= \sum_{n_{-K}+\ldots+n_K=n}\frac{a_n}{2^{n-1}}\binom{n}{n_{-K},\ldots,n_K}\prod_{k=-K}^{K}\tilde{u}_k^{n_k}(t) \end{aligned} \tag{4.22}$$

where $\xi = \sum_{k=-K}^{K} n_k\xi_k = \sum_{i=1}^{n}\xi_{k_i}$ and $\sum_{k=-K}^{K} n_k = n$. The complex envelope of the output $y(t)$ can now be written in complex envelope form as

$$\tilde{y}_\xi(t) = \sum_{n=1}^{N}\int_{-\infty}^{\infty}\tilde{h}_{2;\xi}(\lambda)\tilde{z}_{n,\xi}(t)(t-\lambda)d\lambda \tag{4.23}$$

where $\tilde{h}_{2;\xi}(t)$ is the base band equivalent impulse response of the output filter with respect to frequency ξ. This expression enables the complex envelope of the output waveform to

be related to the complex envelope of the input waveforms. In addition this expression enables cross modulation to be distinguished from intermodulation as will be seen in the next section.

The development up to this point applies for an arbitrary number of channels, i.e. values of K. In the rest of this section we will consider two particular cases. Closed forms for the output waveform are developed when a single channel is input ($K = 1$) and with two channel input ($K = 2$).

4.2.1 Single Channel

Consider the case where the input consists of a single narrow band signal, $K = 1$, with carrier frequency ξ_1. Then the output complex envelope at the fundamental frequency, ξ_1, is, from (4.22),

$$\tilde{z}_{n,\xi_1}(t) = \sum_{n_{-1}+n_1=n} \frac{a_n}{2^{n-1}} \binom{n}{n_{-1}, n_1} \tilde{w}_{-1}^{n_{-1}} \tilde{w}_1^{n_1}(t) \tag{4.24}$$

The contributing frequency vectors at frequency ξ_1, are all permutations of the vector $(\xi_1, \xi_1, -\xi_1)$ for $n = 3$; and $(\xi_1, \xi_1, \xi_1, -\xi_1, -\xi_1)$ for $n = 5$; and so on. Therefore, $n_{-1} = (n-1)/2$ and $n_1 = (n+1)/2$, and so (4.24) becomes

$$\tilde{z}_{\xi_1}(t) = \sum_{n=1}^{N} b_n \tilde{u}_{-1}^{\frac{n-1}{2}} \tilde{u}_1^{\frac{n+1}{2}} \tag{4.25}$$

where

$$b_n = \frac{a_n}{2^{n-1}} \binom{n}{\frac{n-1}{2}, \frac{n+1}{2}}. \tag{4.26}$$

The interpretation of this result is as follows. In a single channel system, the complex envelope of the n th order output signal $\tilde{y}_{\xi_1}(t)$ centered at the carrier frequency ξ_1, is obtained from the complex envelope of the input signal given the nonlinear behavioral model (described by the power series coefficients and filter impulse responses after applying (4.23)). In the case of discrete tones this expression represents the gain-compression characteristics. The output complex envelope at any of the harmonics can also be derived in compact form as in (4.25) using the appropriate frequency vectors.

4.2.2 Two Channels

Now, a two channel input ($K = 2$) will be considered. The two channels are described by their complex envelopes $\tilde{u}_1(t)$ and $\tilde{u}_2(t)$ (at the output of the input filter) with respect to the frequencies ξ_1 and ξ_2 respectively. First, an expression for gain compression and gain saturation will be derived by deriving the output envelope response centered at one of the carriers. Following a similar approach to that used above, the complex envelope of the output waveform at the first carrier (ξ_1) is

$$\tilde{z}_{n,\xi_1}(t) = \sum_{n_{-2}+n_{-1}+n_1+n_2=n} \frac{a_n}{2^{n-1}} \binom{n}{n_{-2}, n_{-1}, n_1, n_2} \tilde{u}_{-2}^{n_{-2}} \tilde{u}_{-1}^{n_{-1}} \tilde{u}_1^{n_1} \tilde{u}_2^{n_2} \tag{4.27}$$

The contributing vectors at frequency ξ_1 are all permutations of the following vectors $(\xi_1, \xi_1, -\xi_1)$ and $(\xi_1, \xi_2, -\xi_2)$ for $n = 3$; and the vectors $(\xi_1, \xi_1, \xi_1, -\xi_1, -\xi_1)$, $(\xi_1, \xi_1, -\xi_1, \xi_2, -\xi_2)$ and $(\xi_1, \xi_2, \xi_2, -\xi_2, -\xi_2)$ for $n = 5$ and so on. By induction, $n_{-2} = l, n_{-1} = ((n-1)/2) - l, n_1 = ((n+1)/2) - l, n_2 = l$, and hence (4.27) can be written as the sum of the contributions defined by each of the above frequency vectors as

$$\tilde{z}_{\xi_1}(t) = \sum_{n=1}^{N} \sum_{l=0}^{\frac{n-1}{2}} b_{n,l} \tilde{u}_{-2}^{l} \tilde{u}_{-1}^{\frac{n-1}{2}-l} \tilde{u}_1^{\frac{n+1}{2}-l} \tilde{u}_2^{l} \tag{4.28}$$

where

$$b_{n,l} = \frac{a_n}{2^{n-1}} \binom{n}{l, \frac{n-1}{2} - l, \frac{n+1}{2} - l, l}. \tag{4.29}$$

This expression captures gain compression — the effect on the output $\tilde{z}_{\xi_1}$ due to the level of the input $\tilde{u}_1$ centered at the same frequency ξ_1; and gain saturation — the effect on the output $\tilde{z}_{\xi_1}$ due to the level of the input $\tilde{u}_2$ in the other channel centered at ξ_2. Since the second channel is modulated, gain saturation manifests itself as cross modulation.

The intermodulation products can be derived in the same way by describing the nonlinear components by their frequency vectors. The lower intermodulation component $\mathrm{IM3}_L$ is centered at frequency $(2\xi_1 - \xi_2)$ and the contributing vectors at frequency $2\xi_1 - \xi_2$ are all the permutations of the vector $(\xi_1, \xi_1, -\xi_2)$ for $n = 3$ and the vectors $(\xi_1, \xi_1, \xi_1, -\xi_1, -\xi_2)$ and $(\xi_1, \xi_1, -\xi_2, -\xi_2, \xi_2)$ for $n = 5$ and so on. By induction, $n_{-2} = l+1, n_{-1} = ((n-3)/2) - l, n_1 = ((n+1)/2) - l, n_2 = l$. Thus, the output complex envelope centered at frequency $(2\xi_1 - \xi_2)$ is

$$\tilde{z}(t)_{2\xi_1-\xi_2} = \sum_{n=3}^{N} \sum_{l=0}^{\frac{n-3}{2}} b_{n,l} \tilde{u}_{-2}^{l+1} \tilde{u}_{-1}^{\frac{n-3}{2}-l} \tilde{u}_1^{\frac{n+1}{2}-l} \tilde{u}_2^{l} \tag{4.30}$$

and for the upper intermodulation component, $\mathrm{IM3}_U$, the output complex envelope centered at frequency $(2\xi_2 - \xi_1)$ is

$$\tilde{z}(t)_{2\xi_2-\xi_1} = \sum_{n=3}^{N} \sum_{l=0}^{\frac{n-3}{2}} b_{n,l} \tilde{u}_{-2}^{\frac{n-3}{2}-l} \tilde{u}_{-1}^{l+1} \tilde{u}_{1}^{l} \tilde{u}_{2}^{\frac{n+1}{2}-l} \tag{4.31}$$

where

$$b_{n,l} = \frac{a_n}{2^{n-1}} \binom{n}{\frac{n-3}{2} - l, l+1, l, \frac{n+1}{2} - l}. \tag{4.32}$$

The output $y(t)$ is then obtained for all the above output components after application of (4.23).

4.2.3 Summary

In Subsections A and B, the input-output behaviors of the nonlinear block were developed for one and two input channels. The full system response is obtained by incorporating the output filter response described by the convolution operations in (4.23). A memoryless system can be dealt with as a special case where the linear filters have an impulse response $h_1(\lambda) = h_2(\lambda) = \delta(\lambda)$ and therefore, $\tilde{u}_k(t) = \tilde{w}_k(t)$ and the model reduces to a power series model. The case where $K > 2$ can be developed in the same way, however, a compact form similar to (4.28) cannot be reached. Alternatively, the Arithmetic Operator Method (AOM) presented in [28] and used for discrete tones can be used here to develop the output spectral components. For the purpose of understanding the interaction of multiple digitally modulated signals in a nonlinearity, the case where $K = 2$ is sufficient.

What we have developed so far is a complex envelope formulation for the output of the nonlinear amplifier. The complex envelope formulation is needed since all the simulations reported in this paper are performed at the envelope level. Envelope simulations are time efficient since the sampling frequency is commensurate with the bandwidth of the individual channels and do not depend on the frequency separation of channels.

4.3 Model Parameter Extraction

Behavioral model parameter extraction involves using measured I-O data to develop the parameters of the model blocks. In a memoryless system parameter extraction is done by

fitting a nonlinear function to the measured I-O data. The function is usually chosen apriori and least squares is used as a fitting criterion. Examples of functional fits are polynomial fit, Bessel function, etc. For the block models, parameter extraction requires the extraction of the linear filter responses in addition to the memoryless nonlinearity. In this section, we develop model parameter extraction for the memoryless and the three-box model. The extraction procedures presented here involve using the capabilities of the Agilent 8510 VNA where no time domain measurements are needed. This facilitates the implementation of the model in software using simple measurements.

4.3.1 Memoryless Model

A memoryless model accurately characterizes a nonlinear system (or device) when it has no significant memory within the signal bandwidth. A memoryless system can be dealt with as a special case of the three-box model where the linear filters have an impulse response $h_1(t) = h_2(t) = \delta(t)$ and it follows that $\tilde{y} = \tilde{z}$ and $\tilde{u} = \tilde{w}$. Therefore model parameter extraction reduces to extracting the power series coefficients of the form:

$$y(t) = \sum_{n=1}^{N} a_n w^n(t) \tag{4.33}$$

The coefficients a_n are called instantaneous coefficients and represent the instantaneous input-output characteristics. The traditional way of extracting these coefficients is by performing a power sweep of a single tone to obtain the AM-AM and AM-PM characteristics using a VNA. However, the AM-AM and AM-PM characteristics represent the envelope characteristics since the output of the amplifier is measured at the first zone only. The envelope characteristics can be developed using (4.25) and setting $\tilde{y} = \tilde{z}$ and $\tilde{u} = \tilde{w}$ as

$$\tilde{y}(t) = \tilde{w}(t)G(\tilde{w}(t)) \tag{4.34}$$

where G is the complex gain function and can be written as

$$\begin{aligned} G(\tilde{w}(t)) &= \frac{a_n}{2^{n-1}} \binom{n}{\frac{n+1}{2}} \tilde{w}^{\frac{n-1}{2}}(t) \\ &= \sum_{n=1}^{N} b_n \tilde{w}^{\frac{n-1}{2}}(t) \end{aligned} \tag{4.35}$$

The new coefficients b_n represent the relationship between the input and the output complex envelopes at the fundamental frequency and

$$b_n = \frac{a_n}{2^{n-1}} \binom{n}{\frac{n+1}{2}}. \tag{4.36}$$

This result can also be obtained from GPS analysis as in [32] or from the Tchebychev integral which relates the an arbitrary nonlinear instantaneous model to its envelope counterpart [31]. The set of coefficients b_n is what is obtained by fitting a polynomial to the measured AM-AM and AM-PM characteristics. Since the envelope characteristics have odd symmetry, then only odd-order envelope coefficients can be obtained from measurements. The odd order coefficients (a_n) can then be developed from their envelope counterparts (b_n) using (4.36). Fortunately, only the odd order components contribute to intermodulation and cross-modulation components that lie inside the bandwidth of the input signals.

In the case of two-channel analysis, single tone characteristics are not sufficient. Although the model is still considered as being memoryless, the AM-PM characteristics change at different frequencies and therefore, the envelope coefficients extracted at a certain frequency do not necessarily represent the instantaneous coefficients. In order to develop the model coefficients, we write the envelope characteristics using (4.29) and setting $\tilde{y} = \tilde{z}$ and $\tilde{u} = \tilde{w}$ as

$$\tilde{y}_{\xi_1}(t) = \tilde{w_1} G(|\tilde{w}_1|, |\tilde{w}_2|) \tag{4.37}$$

where G represents the complex gain compression function and is a function of the levels of both signal envelopes: it can then be written as

$$G(|\tilde{w}_1|, |\tilde{w}_2|) = \sum_{n=1}^{N} \sum_{l=0}^{\frac{n-1}{2}} b_{n,l} |\tilde{w}_1|^{n-2l-1} |\tilde{w}_2|^{2l}. \tag{4.38}$$

where

$$b_{n,l} = \frac{a_n}{2^{n-1}} \binom{n}{l, \frac{n-1}{2} - l, \frac{n+1}{2} - l, l}. \tag{4.39}$$

The new set of coefficients $b_{n,l}$ represents the relationship between the input and the output complex envelopes of the first carrier. This formulation is needed because this is, in fact, the model that can be extracted from measurements. In order to extract the model coefficients we introduce a new technique. The idea is that the input power of the first tone is swept while the power of the second tone is fixed at a certain power level. The process is repeated

for each power step of the second tone. In this way multiple curves for the nonlinear characteristics (AM-AM and AM-PM conversions) are obtained. A two-dimensional (2D) curve fitting yields the set of coefficients $b_{n,k}$, thus the multichannel behavioral model is obtained. The number of coefficients is equal to $((N+1)(N+3)/8)$.

4.3.2 Three-Box Model

Parameter extraction of the three-box model has been extensively investigated [31, 50, 51, 52]. Here the simplified intuitive approach presented in [31] is used to develop the model parameters. The system model, Fig. 4.3, consists of an LTI input filter, a static nonlinearity, and an LTI output filter. Following [31], the transfer functions of the linear filters are be obtained by measuring the gain characteristics at saturation $H_{\text{sat}}(f)$ (for example at the 1 dB compression point), and measuring the small signal linear frequency response $H_{\text{ss}}(f)$. Therefore, the transfer function of the pre filter is

$$H_1(f) = \frac{H_{\text{ss}}(f)}{|H_{\text{sat}}(f)||H_{\text{ss}}(f_{\text{ref}})|} \tag{4.40}$$

and that of the output filter is

$$H_2(f) = \frac{H_{\text{sat}}(f)}{|H_{\text{sat}}(f_{\text{ref}})|} \tag{4.41}$$

where f_{ref} is the reference frequency at which the nonlinear block will be extracted. Note that as indicated in [31], this characterization is intuitive and assumes that the amplifier exhibits limiting behavior. Note also that this assumption requires linearity of the phase-frequency response of the amplifier so that $\angle H_{\text{sat}}(f) = \angle H_1(f) + \Phi(P_{\text{sat}}, f_{\text{ref}})$. This assumption is not always valid but for the case in hand, it is.

Finally, the static nonlinearity, the middle block in Fig. 4.3, is extracted as the measured single-tone AM-AM and AM-PM characteristics taken at the reference carrier frequency f_{ref}. To obtain the reference coefficients, the AM-AM and AM-PM characteristics are chosen to be measured at the middle frequency of the band of interest. Then the envelope coefficients are extracted as from the AM-AM and AM-PM measured characteristics by polynomial fit.

4.4 Conclusion

In this chapter, we have presented an analysis of nonlinearity with multiple inputs. The analysis was done using Volterra model as well as for the models presented in Chapter 2 at the complex envelope level. The analysis of multiple channels was extended for the three-box model to include the derivation of a closed form for the output waveform in complex envelop form which will be used in the analysis of distortion which will follow. In addition, we have developed parameter extraction procedures for both the memoryless and the three-box model. The memoryless model with its novel parameter extraction technique can be used for small separations between the input signals, i.e. when the AM-AM characteristics are constant with frequency while the AM-PM characteristics vary. The three-box model is more general and can be used for any frequency separation provided that the nonlinear characteristics have the same shape. This model will be very useful for the analysis which will follow where a statistical model for modeling distortion in multichannel amplifiers will be developed.

Chapter 5

Distortion In Multichannel Digital Communication Systems

This chapter deals with developing a nonlinear statistical model by which distortion in CDMA systems can be predicted. The model is based on random process theory and enables distortion to be related to the statistical properties of digitally modulated signals. The analysis uses the behavioral models discussed in Chapter 4, in particular the memoryless model and the three-box model to develop the autocorrelation function at the output of the nonlinear system. In addition, we derive the output autocorrelation function assuming that the input signals can be approximated by a gaussian process which is an acceptable assumption in some cases. The autocorrelation function is used to compute the output spectrum by which distortion can me modeled. The objective is to develop a model that can be implemented in a commercial software using measured behavioral model parameters. The analysis presented in this chapter is intended to model distortion in a multichannel system and therefore single and two channel inputs will be discussed.

5.1 Background

The traditional approach to characterizing distortion in multichannel power amplifiers is to test the amplifier with n tones and examine the intermodulation capability of the power amplifier [90]. However this cannot accurately characterize distortion when the amplifier is driven by digitally modulated signals. Bennet *et al* [30], studied the power rating of multichannel amplifiers by examining the peak envelope power of various modulation schemes. It was shown that for a large number of channels, savings in the power rating may be made by limiting the input envelope. However no estimates of distortion were presented. Wang *et. al* [54], used the fifth order Volterra series analysis to model intermodulation and cross-modulation distortions under two-channel CDMA excitation with 5 MHz isolation bandwidth. The model was based on the assumption that a CDMA signal can be approximated by a narrow band gaussian process—a rough assumption. The approach used was limited to small frequency separation. Aparin *et al.* [5], studied the cross-modulation distortion in CDMA receivers that results from the interaction of transmitter leakage and the existence of a strong jammer in the receiver band by Low Noise Amplifier (LNA) nonlinearity. The analysis of cross-modulation distortion was based on Volterra series analysis to capture the frequency dependent characteristics of the amplifier. The analysis was limited to a third order nonlinear model and discrepancies between measured and simulated values of cross-modulation were reported due to the higher order nonlinearities. There was considerable complexity in deriving the Volterra kernels from circuit model parameters. The same problem was studied by Ko *et al.* [55] who derived an empirical formula for estimating the cross-modulation power distortion caused by the presence of single-tone jammer and transmitter leakage in CDMA mobile phones. The analysis was made using discrete tones and a third order memoryless nonlinearity which makes the work a rough estimate of cross-modulation.

The major problem with all of these analyses is the relatively low order of the nonlinearity that was considered. Also most of the work assumes that CDMA signals can be approximated either by a single tone or by narrowband Gaussian noise process at best. In the analysis that will follow, these assumptions are removed as we use a behavioral model that considers any order of nonlinearity in addition to using exact signal realizations. The focus here is on both sides of the mechanism by which distortion is introduced in a communication system. The first is the inherent nonlinearity of the system where a model

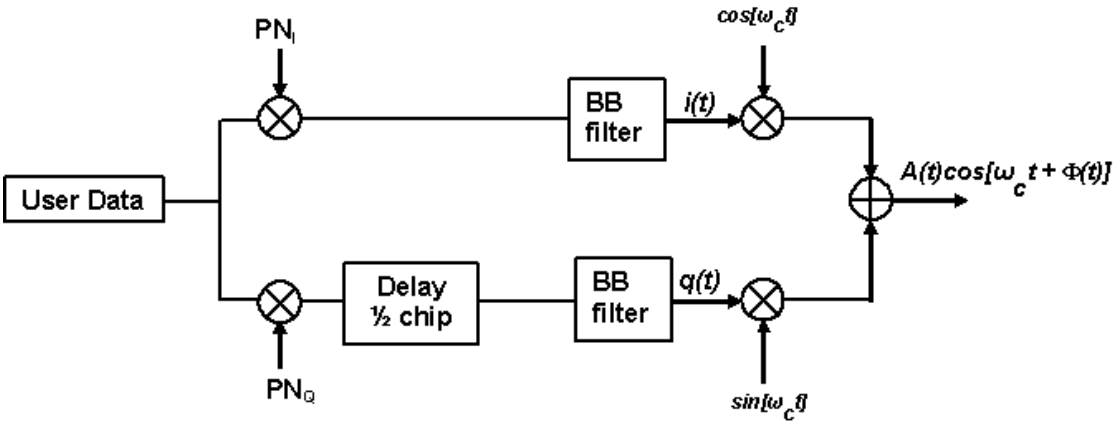

Figure 5.1: Block diagram of reverse link IS-95 CDMA system

that takes into account memory effects is used and the second is the statistics of the signal where we show their impact on the level of distortion.

5.2 CDMA Signal Model and Statistics

We consider the signal model of an IS-95 CDMA cellular system where nonlinearity is a great concern. An IS-95 CDMA system uses linear modulation schemes (QPSK for the forward link and OQPSK for the reverse link) and therefore is more susceptible to amplifier nonlinearities than other cellular systems. However the statistical model of distortion is general and can be with any signal format. In the following we present the modulation schemes and the statistical properties of both the forward and reverse link where their second order statistics (the autocorrelation function) is derived.

5.2.1 CDMA Reverse Link Signal Model and Statistics

The modulation scheme for the reverse link in an IS-95 CDMA system is shown in Fig. 5.1 [56]. Coded user data is split into in-phase (I) and a quadrature (Q) channels and spread by orthogonal Pseudo Noise (PN) codes at a rate of 1.2288 mega-chips per second (Mcps). The Q sequence is delayed by a half PN chip time resulting in offset quadrature phase shift keying

(OQPSK). The resulting spread data is then passed through a baseband filter. The IS-95 50-tap Finite Impulse Response (FIR) baseband pulse-shaping filter can be approximated by the following Infinite Impulse Response (IIR) with an acceptable accuracy

$$h(t) = B\text{sinc}(Bt) = B\frac{\sin(\pi Bx)}{\pi Bx} \tag{5.1}$$

where B is the reciprocal of the PN code rate (1.2288 MHz) [48]. The filtered I and Q channels are quadrature modulated at the carrier frequency and the transmitted signal can be written as:

$$\begin{aligned} w(t) &= i(t)cos(\omega_c t) + q(t)sin(\omega_c t) \\ &= A(t)cos(\omega_c t + \Phi(t)) \\ &= \frac{1}{2}[\tilde{w}(t)e^{j\omega_c t} + \tilde{w}^*(t)e^{-j\omega_c t}]. \end{aligned} \tag{5.2}$$

where

$$\tilde{w}(t) = i(t) + jq(t) = A(t)e^{j\Phi(t)}$$

is the complex envelope of the modulated signal $w(t)$. The complex envelope $\tilde{w}(t)$ has a bandwidth of B. The quadrature components, $i(t)$ and $q(t)$ can be written as:

$$\begin{aligned} i(t) &= \frac{1}{\sqrt{2}}\sum_{n=-\infty}^{\infty}\rho d(nT)I(nT)h(t - nT + \frac{\varphi}{\pi}) \\ q(t) &= \frac{1}{\sqrt{2}}\sum_{n=-\infty}^{\infty}\rho d(nT)Q(nT)h(t - (n+\frac{1}{2})T + \frac{\varphi}{\pi}). \end{aligned} \tag{5.3}$$

where ρ is a constant used to set the input power level, T is the chip period and φ is a random phase uniformly distributed in $[0, 2\pi]$ independent of the sampled process $d(nT)$. The data sequence $d(nT)$ are random numbers taking the values ± 1 with equal probability and represent user data. Fig. 5.2 shows a realization of a reverse link CDMA signal. The statistics of the CDMA signal are defined by its autocorrelation function. The autocorrelation of the quadrature process $\tilde{w}(t)$ is defined as:

$$\begin{aligned} R_{\tilde{w}\tilde{w}}(\tau) &= E[\tilde{w}(t)\tilde{w}^*(t+\tau)] \\ &= E[(i(t) + jq(t))(i(t+\tau) - jq(t+\tau))] \\ &= R_{ii}(\tau) - jR_{iq}(\tau) + jR_{qi}(\tau) + R_{qq}(\tau) \end{aligned} \tag{5.4}$$

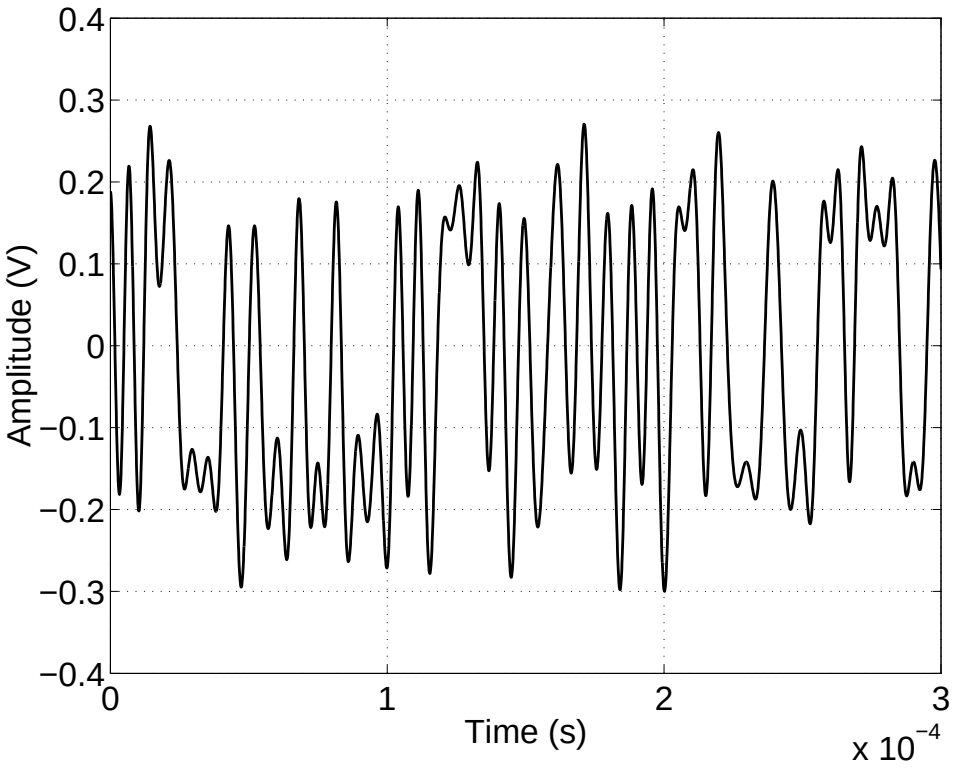

Figure 5.2: time domain realization of reverse link IS-95 CDMA signal

where E is the expected value. Using (5.3), the autocorrelation functions of the real processes $i(t)$ and $q(t)$ is

$$\begin{aligned}
R_{ii}(\tau) &= \frac{1}{2}E\sum_n\sum_m \rho d(nT)d(mT)I(nT)I(mT) \\
&\quad \times h(t-nT+\frac{\varphi}{\pi})h(t-mT+\tau+\frac{\varphi}{\pi}) \\
R_{iq}(\tau) &= \frac{1}{2}E\sum_n\sum_m \rho d(nT)d(mT)I(nT)Q(mT) \\
&\quad \times h(t-nT+\frac{\varphi}{\pi})h(t-(m+\frac{1}{2})T+\tau+\frac{\varphi}{\pi}) \\
R_{qq}(\tau) &= \frac{1}{2}E\sum_n\sum_m \rho d(nT)d(mT)Q(nT)Q(mT) \\
&\quad \times h(t-(n+\frac{1}{2})T+\frac{\varphi}{\pi})h(t-(m+\frac{1}{2})T+\tau+\frac{\varphi}{\pi}) \\
R_{qi}(\tau) &= \frac{1}{2}E\sum_n\sum_m \rho d(nT)d(mT)Q(nT)I(mT) \\
&\quad \times h(t-(n+\frac{1}{2})T+\frac{\varphi}{\pi})h(t-mT+\tau+\frac{\varphi}{\pi}). \qquad (5.5)
\end{aligned}$$

The above autocorrelation functions are simplified by using the statistical properties of the PN and data sequences. First, the statistical properties of the PN sequences are given by [57]:

$$E[I(n)I(m)] = E[Q(n)Q(m)] = \begin{cases} 1 & \text{if } n=m \\ 0 & \text{otherwise} \end{cases} \qquad (5.6)$$

and

$$E[I(n)Q(m)] = 0. \qquad (5.7)$$

The data sequences d_i are assumed to be independent identically distributed random variables (iid) [57], therefore:

$$E\left[d_i(nT)d_j(nT)\right] = \begin{cases} 1 & \text{if } i=j \\ 0 & \text{otherwise} \end{cases} \qquad (5.8)$$

and therefore, the correlation functions in (5.5) reduce to

$$\begin{aligned}
R_{ii}(\tau) &= \frac{1}{2}\sum_n \rho^2 E\left[d(nT)^2\right] E_\varphi[h(t-nT+\frac{\varphi}{\pi})h(t-nT+\tau+\frac{\varphi}{\pi})] \\
R_{qq}(\tau) &= \frac{1}{2}\sum_n \rho^2 E\left[d(nT)^2\right] E_\varphi[h(t-(n+\frac{1}{2})T+\frac{\varphi}{\pi})h(t-(n+\frac{1}{2})T+\tau+\frac{\varphi}{\pi})] \\
R_{iq}(\tau) &= 0 \\
R_{qi}(\tau) &= 0. \qquad (5.9)
\end{aligned}$$

The phase φ is assumed to be random and uniformly distributed in $[0, 2\pi]$. Using the properties of the joint moments of pulse trains [48] we have:

$$E_\varphi \left[\sum_n [h(t - nT + \frac{\varphi}{\pi}) h(t - nT + \tau + \frac{\varphi}{\pi}) \right] = h(\tau). \tag{5.10}$$

and

$$E_\varphi \left[\sum_n [h(t - (n + \frac{1}{2})T + \frac{\varphi}{\pi}) h(t - (n + \frac{1}{2})T + \tau + \frac{\varphi}{\pi}) \right] = h(\tau). \tag{5.11}$$

Consequently (5.9) reduces to

$$\begin{aligned} R_{ii}(\tau) &= \frac{1}{2}\sigma_{\tilde{w}}^2 h(\tau) \\ R_{qq}(\tau) &= \frac{1}{2}\sigma_{\tilde{w}}^2 h(\tau) \\ R_{iq}(\tau) &= R_{qi}(\tau) = 0. \end{aligned}$$

where $\sigma_{\tilde{w}}^2 = \rho^2$ and it follows that the autocorrelation function in (5.4) is

$$R_{\tilde{w}\tilde{w}}(\tau) \quad = \sigma_{\tilde{w}}^2 h(\tau). \tag{5.12}$$

Therefore, the process $\tilde{w}(t)$ is a Wide Sense Stationary (WSS) random process since the autocorrelation function $R_{\tilde{w}\tilde{w}}(\tau)$ is a function of the time shift (τ). Note that the autocorrelation function of the reverse link and the Narrow Band Gaussian Noise (NBGN) process are the same provided that the baseband filter can be approximated by the sinc function. This assumption will be discussed in more details in the following sections.

5.2.2 CDMA Forward Link Signal Model and Statistics

The modulation scheme of the IS-95 forward link CDMA system is shown in Fig. 5.3. Baseband coded user data is generated at a rate of 19.2 kbps (kilo bits per second) [56]. Each users' data is first spread by a Walsh code providing orthogonality with other users and then these are summed to yield the composite signal at a rate of 1.2288 Mcps. The resulting data stream is split into I and Q channels, spread by the orthogonal Pseudo Noise (PN) codes generated at a rate of 1.2288 Mcps and then passed through a baseband filter with impulse response defined in (5.1). The PN codes are base station specific and are used

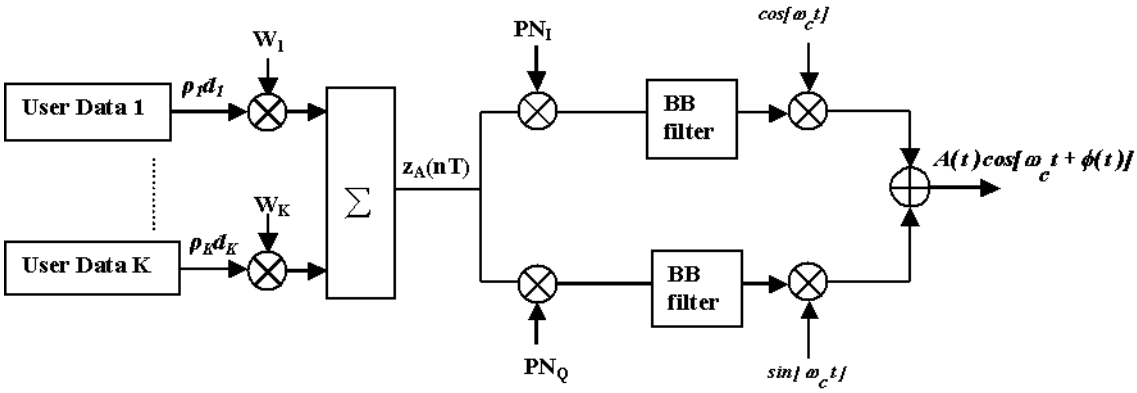

Figure 5.3: Block diagram of forward link IS-95 CDMA system

with each carrier. According to the modulation scheme of the forward link, the complex envelope of the transmitted signal can be written as

$$\tilde{w}(t) = \frac{1}{\sqrt{2}} \sum_{-\infty}^{\infty} \tilde{w}_A(nT) \left[I(nT) + jQ(nT) \right] h(t - nT + \frac{\varphi}{\pi}) \tag{5.13}$$

where φ is a random phase uniformly distributed in $[0, 2\pi]$ independent of the sampled process $\tilde{w}_A(nT)$. This signal represents the sampled coded CDMA signal and can be expressed as

$$\tilde{w}_A(nT) = \sum_{i=0}^{K-1} \rho_i d_i(nT) W_i(nT) \tag{5.14}$$

where ρ_i is a power scaling factor and $W_i(nT)$ are the Walsh code chips of the i th user and $d_i(nT)$ represent the i th user data. Each $d_i(nT)$ is constant within the bit period, i.e. $d_i(nT) = \pm 1$ for $0 \leq n \leq K$ where K represents the number of users and equals to the number of chips in each Walsh code. The quadrature components, $i(t)$ and $q(t)$ can now be written as

$$\begin{aligned} i(t) &= \frac{1}{\sqrt{2}} \sum_{n=-\infty}^{\infty} \tilde{w}_A(nT) I(nT) h(t - nT + \frac{\varphi}{\pi}) \\ q(t) &= \frac{1}{\sqrt{2}} \sum_{n=-\infty}^{\infty} \tilde{w}_A(nT) Q(nT) h(t - nT + \frac{\varphi}{\pi}). \end{aligned} \tag{5.15}$$

The statistics of the CDMA signal are defined by its autocorrelation function. The autocorrelation of the quadrature process $\tilde{w}(t)$ is defined as:

$$\begin{aligned} R_{\tilde{w}\tilde{w}}(\tau) &= E[\tilde{w}(t)\tilde{w}^*(t+\tau)] \\ &= E[(i(t)+jq(t))(i(t+\tau)-jq(t+\tau))] \\ &= R_{ii}(\tau) - jR_{iq}(\tau) + jR_{qi}(\tau) + R_{qq}(\tau) \end{aligned} \tag{5.16}$$

Using (5.15), the autocorrelation functions of the real processes $i(t)$ and $q(t)$ can be written as:

$$\begin{aligned} R_{ii}(\tau) &= \frac{1}{2}E\sum_n\sum_m \tilde{w}_A(nT)\tilde{w}_A(mT)I(nT)I(mT)h(t-nT+\frac{\varphi}{\pi})h(t-mT+\tau+\frac{\varphi}{\pi}) \\ R_{iq}(\tau) &= \frac{1}{2}E\sum_n\sum_m \tilde{w}_A(nT)\tilde{w}_A(mT)I(nT)Q(mT)h(t-nT+\frac{\varphi}{\pi})h(t-mT+\tau+\frac{\varphi}{\pi}) \\ R_{qq}(\tau) &= \frac{1}{2}E\sum_n\sum_m \tilde{w}_A(nT)\tilde{w}_A(mT)Q(nT)Q(mT)h(t-nT+\frac{\varphi}{\pi})h(t-mT+\tau+\frac{\varphi}{\pi}) \\ R_{qi}(\tau) &= \frac{1}{2}E\sum_n\sum_m \tilde{w}_A(nT)\tilde{w}_A(mT)Q(nT)I(mT)h(t-nT+\frac{\varphi}{\pi})h(t-mT+\tau+\frac{\varphi}{\pi}). \end{aligned} \tag{5.17}$$

Using (5.6) and (5.7) the autocorrelation functions in (5.17) reduce to:

$$\begin{aligned} R_{ii}(\tau) &= \frac{1}{2}\sum_n E\left[\tilde{w}_A(nT)^2\right] E_\varphi[h(t-nT+\frac{\varphi}{\pi})h(t-nT+\tau+\frac{\varphi}{\pi})] \\ R_{qq}(\tau) &= \frac{1}{2}\sum_n E\left[\tilde{w}_A(nT)^2\right] E_\varphi[h(t-nT+\frac{\varphi}{\pi})h(t-nT+\tau+\frac{\varphi}{\pi})] \\ R_{iq}(\tau) &= 0 \\ R_{qi}(\tau) &= 0. \end{aligned} \tag{5.18}$$

The statistics of the sampled process $\tilde{w}_A(nT)$ are known since it represents the input coded data. To find the expected values in (5.18), we use the statistics of the data samples, PN codes and Walsh codes. Therefore, using (5.15), we have:

$$\begin{aligned} E[\tilde{w}_A^2(nT)] &= \sum_{i,j}^{K-1} E\left[\rho_i\rho_j d_i(nT)d_j(nT)W_i(nT)W_j(nT)\right] \\ &= \sum_{i,j}^{K-1} \rho_i\rho_j E\left[d_i(nT)d_j(nT)\right] E\left[W_i(nT)W_j(nT)\right]. \end{aligned} \tag{5.19}$$

The data sequences d_i are assumed to be independent identically distributed random variables (iid), independent from the Walsh codes. The statistical properties of Walsh codes are discussed in [57]. Each Walsh code is generated from a set of Hadamard basis functions resulting in orthogonal codes. It follows from (5.9) that (5.19) reduces to

$$E\left[\tilde{w}_A^2(nT)\right] = \sum_{i=0}^{K-1} \rho_i^2 = \sigma_{\tilde{w}}^2 \tag{5.20}$$

In a similar manner to the reverse link, the phase φ is assumed to be random and uniformly distributed in $[0, 2\pi]$ and therefore the identities (5.10) and (5.11) hold. Consequently (5.18) reduces to

$$\begin{aligned} R_{ii}(\tau) &= \frac{1}{2}\sigma_{\tilde{w}}^2 h(\tau) \\ R_{qq}(\tau) &= \frac{1}{2}\sigma_{\tilde{w}}^2 h(\tau) \\ R_{iq}(\tau) &= R_{qi}(\tau) = 0. \end{aligned}$$

and it follows that the autocorrelation function is

$$R_{\tilde{w}\tilde{w}}(\tau) \quad = \sigma_{\tilde{w}}^2 h(\tau). \tag{5.21}$$

Therefore, $\tilde{w}(t)$ is a Wide Sense Stationary (WSS) random process since the autocorrelation function $R_{ww}(\tau)$ is a function of the time shift (τ) only. In fact, it is the random phase φ that makes the process a WSS process. If this phase does not exist, then the process is considered as a cyclostationary process with the bit period T_b. However, this affects only the higher order moments and not the second order statistics $(R_{zz}(\tau))$ which is still stationary (independent of time) and therefore, the analysis above is still valid.

To establish the cross correlation function of two forward link CDMA signals, let the complex envelopes of the two signals be $\tilde{w_1}(t)$ and $\tilde{w_1}(t)$ then, the cross correlation function is defined as

$$\begin{aligned} R_{\tilde{w_1}\tilde{w_2}}(\tau) &= E[\tilde{w_1}(t)\tilde{w_2}^*(t+\tau)] \\ &= \sum_n \sum_m E[\tilde{w_1}(nT)\tilde{w_2}^*(mT)]h(t - nT + \frac{\varphi}{\pi})h(t - mT + \tau + \frac{\varphi}{\pi}) \end{aligned} \tag{5.22}$$

where, using (5.14);

$$\begin{aligned} E\left[\tilde{w_1}(nT)\tilde{w_2}^*(mT)\right] &= E[\tilde{w_1}_A(nT)\left\{I(nT) + jQ(nT)\right\}\tilde{w_2}_A(mT)\left\{I(mT) - jQ(mT)\right\}] \\ &= E\left[\tilde{w_1}_A(nT)\tilde{w_2}_A(nT)\right]. \end{aligned} \tag{5.23}$$

The cross-correlation function of the sampled processes $\tilde{w}_{1A}(nT)$ and $\tilde{w}_{2A}(nT)$ can now be evaluated using the definition of the sampled processes $\tilde{w}_1(nT)$ and $\tilde{w}_2(nT)$ in (5.14) and knowing the-cross correlation properties of the data sequences and Walsh codes of the two channels, therefore

$$\begin{aligned} E\left[\tilde{w}_{1A}(nT)\tilde{w}_{2A}(nT)\right] &= \sum_{i,j}^{K-1} E\left[\rho_i \xi_j d_i^{\tilde{w}_1}(nT) d_j^{\tilde{w}_2}(nT) W_i(nT) W_j(nT)\right] \\ &= \sum_{i,j}^{K-1} \rho_i \xi_j E\left[d_i^{\tilde{w}_1}(nT) d_j^{\tilde{w}_2}(nT)\right] E\left[W_i(nT) W_j(nT)\right] \end{aligned}$$

where $d_i^{\tilde{w}_1}$ and $d_i^{\tilde{w}_2}$ represent the data bits of the i th user in the first and second channel respectively. Now, assuming that the data bits of the two channels are statistically independent yields:

$$E\left[d_i^{\tilde{w}_1}(nT) d_j^{\tilde{w}_2}(nT)\right] = E\left[d_i^{\tilde{w}_1}(nT)\right] E\left[d_i^{\tilde{w}_2}(nT)\right] = 0$$

and it follows that (5.13) reduces to

$$R_{\tilde{w}_1 \tilde{w}_2}(\tau) = 0 \tag{5.24}$$

which means that two processes $\tilde{w}_1$ and $\tilde{w}_2$ are orthogonal when the data samples are independent due to the statistical properties of Walsh codes and the PN spreading codes. However, the two processes cannot be considered as uncorrelated or statistically independent unless they are assumed to be Gaussian. This assumption will be discussed in the following sections.

5.3 Nonlinear Statistical Analysis with Multiple Channels

As discussed in Chapter 3, with a digitally modulated signal, distortion introduced by nonlinearities is typically characterized by the level of spectral regrowth and in-band distortion. In order to estimate distortion, the output spectrum must be estimated from the input waveform and the behavioral model. In this section, we develop the output autocorrelation function for single and multiple input channels. The output spectrum is computed from the Fourier transform of the autocorrelation function. The contribution here is in the development of a generalized autocorrelation using the multichannel analysis presented in

Chapter 4. We use the multichannel behavioral model analysis along with the signal model to develop a closed form for the output autocorrelation function. Unlike single channel statistical modeling [32, 33, 34, 35, 48, 60, 61, 93], the analysis presented here is general and enables the estimation of extra distortion terms such as cross-modulation and the spurious intermodulation signals. The autocorrelation formulation will be based on both the memoryless model and the three-box model.

5.3.1 Memoryless Model

As discussed in Chapter 3, a memoryless model is characterized by a power series with real or complex coefficients. In the analysis that will follow we use the power series representation and the analysis presented in Chapter 4 to develop the a formulation for the output autocorrelation function for one and two channel input. The memoryless model is dealt with as a special case of the three-box model analysis where the linear filter responses are excluded.

Single Channel

The autocorrelation function of the output signal is defined as

$$R_{yy}(\tau) = E[\tilde{y}(t)\tilde{y}^*(t+\tau)]. \tag{5.25}$$

Now considering only the output component centered at the fundamental frequency ξ_1 (first zonal output) then by using (4.24) and setting $\tilde{u} = \tilde{w}$ and $\tilde{y} = \tilde{z}$ (for the memoryless case), the output autocorrelation can be written as

$$\begin{aligned} R_{yy;\xi_1}(\tau) &= E[\tilde{y}_{\xi_1}(t)\tilde{y}^*_{\xi_1}(t+\tau)] \\ &= \sum_{n=1}^{N}\sum_{m=1}^{N} b_n b_m^* R_{w_n w_m}(\tau) \end{aligned} \tag{5.26}$$

where

$$R_{w_n w_m}(\tau) = E[\tilde{w}_1^{\frac{(n+1)}{2}}(t)\tilde{w}_{-1}^{\frac{(n-1)}{2}}(t)\tilde{w}_1^{\frac{(m-1)}{2}}(t+\tau)\tilde{w}_{-1}^{\frac{(m+1)}{2}}(t+\tau)]. \tag{5.27}$$

The above expression is similar to the single channel formulation in [32]. In [48] it was shown that the output autocorrelation function is a function of the time shift (τ) provided

that the process $\tilde{w}(t)$ is Wide Sense Stationary (WSS) random processe. Note that the statistics of the modulated signal $w(t)$ are the same as the statistics of its complex envelope since the carrier contains no information. The PSD of the output signal can be found from the Fourier transform of the autocorrelation function (Weiner-Khintchine theorem [36]) as:

$$S_{yy;\xi_1}(f) = \sum_{n=1}^{N}\sum_{m=1}^{N} b_n b_m^* S_{nm}(\tau) \tag{5.28}$$

where

$$S_{nm}(f) = \int_{-\infty}^{\infty} R_{w_n w_m}(\tau) e^{-j\omega\tau d\tau}.$$

The expression (5.28) is a general output PSD and consists of $[(N+1)/2]^2$ terms. These terms can be divided into two groups: The first group represents the linear output with gain compression ($n = 1$ or $m = 1$) and the second group represent the intermodulation distortions ($n > 1$ and $m > 1$). The nonlinear terms in the autocorrelation function are responsible for the nonlinear distortion. This means that distortion can be controlled by changing the statistics of the signal for a given nonlinearity. In a forward link CDMA system, this can be done by the proper choice of the number of users in the two channels, using a different set of orthogonal codes, or introducing a data coding scheme that will result in a better distortion performance [57, 58, 59, 63].

Two Channels

For the case of two channels the output autocorrelation function can be derived using (5.25). Therefore using (4.28) and setting $\tilde{u} = \tilde{w}$ and $\tilde{y} = \tilde{z}$ (for the memoryless case), then the output autocorrelation of the signal centered at the first carrier frequency ξ_1 is

$$R_{yy;\xi_1}(\tau) = \sum_{n=1}^{N}\sum_{m=1}^{N}\sum_{l=0}^{\frac{n-1}{2}}\sum_{k=0}^{\frac{m-1}{2}} b_{n,l} b_{m,k}^* R_{w_n w_m w_l w_k}(\tau) \tag{5.29}$$

where

$$\begin{aligned} R_{w_n w_m w_l w_k}(\tau) = \; & E[\tilde{w}_1^{\frac{(n+1)}{2}-l}(t)\tilde{w}_{-1}^{\frac{(n-1)}{2}-l}(t)\tilde{w}_1^{\frac{(m-1)}{2}-k}(t+\tau)\tilde{w}_{-1}^{\frac{(m+1)}{2}-k}(t+\tau) \\ & \times \tilde{w}_2^{l}(t)\tilde{w}_{-2}^{l}(t)\tilde{w}_2^{k}(t+\tau)\tilde{w}_{-2}^{k}(t+\tau)] \end{aligned} \tag{5.30}$$

The above expression reduces to the single channel formulation when $w_2(t) = 0$ and setting k and l to 0. The PSD of the output signal can be computed from the Fourier transform of

the autocorrelation function as

$$S_{yy;\xi_1}(f) = \sum_{n=1}^{N}\sum_{m=1}^{N}\sum_{l=0}^{\frac{n-1}{2}}\sum_{k=0}^{\frac{m-1}{2}} b_{n,l}b^*_{m,k}S_{nmlk}(\tau) \tag{5.31}$$

where

$$S_{nmlk}(f) = \int_{-\infty}^{\infty} R_{w_n w_m w_l w_k}(\tau)e^{-j\omega\tau d\tau}.$$

The expression (5.31) consists of $[(N+1)/2]^2 \times [(N+3)/4]^2$ terms. These terms can be divided into three major groups: The first group represents the linear output with gain compression ($l = 0, k = 0, n = 1$ or $m = 1$), the second group represent the intermodulation distortions ($l = 0, k = 0,\ n > 1$ and $m > 1$), and the third group represents the cross-modulation distortion caused by the presence of the second signal ($l > 0, k > 0$). In this way, the development of the statistical model provides the accurate characterization of cross-modulation distortion. Note that the formulation of the autocorrelation function in (5.32) provides an insight into the effect of the self and joint statistics of the two signals on the level of distortion. This means that this distortion can be controlled by changing the statistics of the two signals. In a forward link CDMA system, this can be done by the proper choice of the number of users in the two channels.

The receiver desensitization problem can be treated as a special case of the above analysis. Let the input signal $w(t)$ consist of a single tone jammer $w_1(t) = A_1 cos(\omega_1 t + \theta)$ and a transmitter leakage CDMA signal be $w_2(t) = A_2(t)cos(\omega_2 t + \Phi(t))$. Therefore, $\tilde{w}_1(t) = A_1 e^{j\theta}$ and $\tilde{w}_2(t) = A_2(t)e^{j(\Phi(t))}$ and then the output autocorrelation at the jammer center frequency can be expressed as in (5.29) with

$$R_{w_n w_m w_l w_k}(\tau) = A_1^{n+m-2l-2k} E[\tilde{w}_2(t)^l \tilde{w}_2(t)^{*l} \tilde{w}_2(t+\tau)^k \tilde{w}_2(t+\tau)^{*k}]. \tag{5.32}$$

Summary

In the above subsections we derived the autocorrelation function for the single and two-channel cases using the memoryless model. Note that this formulation does not include the variation of the model parameters with frequency. However, the analysis is needed since it gives an insight on the impact of the statistical properties of the signals on distortion. The analysis in the following section will be done using the three-box model which includes the effect of memory on the level of distortion.

5.3.2 Three-Box Model

The analysis presented here is an extension to the autocorrelation analysis presented in the previous section of a memoryless multichannel amplifier. Here we use the three-box model analysis and couple it with autocorrelation analysis to develop the output spectrum for a nonlinear system with memory at any intermodulation frequency. The objective is to combine the frequency variations of the behavioral model (which are captured by the linear filter responses) in the autocorrelation analysis so that memory effects ar included in the estimation of distortion.

Single Channel

Consider a signal $w_1(t)$ modulated at frequency ξ_1 and applied at the input of the nonlinear amplifier. Referring to the three-box behavioral model in Fig. 4.3 and considering only the output component centered at the fundamental frequency ξ_1 (first zonal output) then by using (4.24) the autocorrelation function of the output of the second block is

$$\begin{aligned} R_{\tilde{z}\tilde{z};\xi_1}(\tau) &= E[\tilde{z}_{\xi_1}(t)\tilde{z}^*_{\xi_1}(t+\tau)] \\ &= \sum_{n=1}^{N}\sum_{m=1}^{N} b_n b_m^* R_{\tilde{u}_n\tilde{u}_m}(\tau) \end{aligned} \tag{5.33}$$

where

$$\begin{aligned} R_{\tilde{u}_n\tilde{u}_m}(\tau) &= E[\tilde{u}_1^{\frac{(n+1)}{2}}(t)\tilde{u}_{-1}^{\frac{(n-1)}{2}}(t)\tilde{u}_1^{\frac{(m-1)}{2}}(t+\tau)\tilde{u}_{-1}^{\frac{(m+1)}{2}}(t+\tau)] \\ &= R_{\tilde{w}_n\tilde{w}_m}(\tau)\left|\tilde{h}_{1;\xi_1}(0)\right|^{n+m} \end{aligned} \tag{5.34}$$

$$R_{\tilde{w}_n\tilde{w}_m}(\tau) = \quad E[\tilde{w}_1^{\frac{(n+1)}{2}}(t)\tilde{w}_{-1}^{\frac{(n-1)}{2}}(t)\tilde{w}_1^{\frac{(m-1)}{2}}(t+\tau)\tilde{w}_{-1}^{\frac{(m+1)}{2}}(t+\tau)]$$

and $\tilde{h}_{1;\xi_1}(t)$ is the baseband equivalent of the impulse response of the input filter with respect to the frequency ξ_1. Note that (5.34) is derived assuming that the input filter response is constant within each signal bandwidth. The PSD of the output signal $\tilde{z}_{\xi_1}(t)$ is obtained from the Fourier transform of the autocorrelation function as

$$S_{\tilde{z}\tilde{z};\xi_1}(f) = \sum_{n=1}^{N}\sum_{m=1}^{N} b_n b_m^* S_{\tilde{u};nm}(f) \tag{5.35}$$

where

$$S_{\tilde{u};nm}(f) = |\tilde{H}_{1;\xi_1}(0)|^{n+m} S_{\tilde{w};nm}(f)$$

$$S_{\tilde{w};nm}(f) = \int_{-\infty}^{\infty} R_{\tilde{w}_n \tilde{w}_m}(\tau) e^{-j\omega\tau d\tau}.$$

The PSD at the output of the system is

$$\begin{aligned} S_{\tilde{y}\tilde{y};\xi_1}(f) &= |\tilde{H}_{2;\xi_1}(f)|^2 S_{\tilde{z}\tilde{z};\xi_1}(f) \\ &= |\tilde{H}_{2;\xi_1}(f)|^2 |\tilde{H}_{1;\xi_1}(0)|^{n+m} S_{\tilde{w}\tilde{w};\xi_1}(f) \end{aligned} \tag{5.36}$$

where $\tilde{H}_{1;\xi_1}(f)$ and $\tilde{H}_{2;\xi_1}(f)$ are the baseband equivalent of the transfer functions of the input and output filters with respect to frequency ξ_1. Note that the output spectrum is weighted by powers of the impulse responses of the input and output filter. The derivations here assume that the input filter response in constant within the signal bandwidth. This is an acceptable assumption since the amplifier is expected to have more significant variations of the impulse response at high drive levels and this is included by the response of output filter.

Two Channels

For the two channel case consider two modulated carriers $w_1(t)$ and $w_2(t)$ modulated at frequencies ξ_1 and ξ_2 where $\xi_2 > \xi_1$ and applied at the input of the nonlinear amplifier. Then using (4.28), the autocorrelation function of the output component of the second block centered at frequency ξ_1 is

$$\begin{aligned} R_{\tilde{z}\tilde{z};\xi_1}(\tau) &= E[\tilde{z}_{\xi_1}(t)\tilde{z}_{\xi_1}(t+\tau)] \\ &= \sum_{n=1}^{N}\sum_{m=1}^{N}\sum_{l=0}^{\frac{n-1}{2}}\sum_{k=0}^{\frac{m-1}{2}} b_{n,l} b^*_{m,k} R_{\tilde{u}_n \tilde{u}_m \tilde{u}_l \tilde{u}_k}(\tau). \end{aligned} \tag{5.37}$$

where

$$\begin{aligned} R_{\tilde{u}_n \tilde{u}_m \tilde{u}_l \tilde{u}_k}(\tau) &= E[\tilde{u}_1^{\frac{(n+1)}{2}-l}(t)\tilde{u}_{-1}^{\frac{(n-1)}{2}-l}(t)\tilde{u}_1^{\frac{(m-1)}{2}-k}(t+\tau)\tilde{u}_{-1}^{\frac{(m+1)}{2}-k}(t+\tau) \\ &\quad \times \tilde{u}_2^l(t)\tilde{u}_{-2}^l(t)\tilde{u}_2^k(t+\tau)\tilde{u}_{-2}^k(t+\tau)] \\ &= R_{\tilde{w}_n \tilde{w}_m \tilde{w}_l \tilde{w}_k}(\tau) \left|\tilde{h}_{1;\xi_1}(0)\right|^{n+m-2l-2k} \left|\tilde{h}_{1;\xi_2}(0)\right|^{2l+2k} \end{aligned} \tag{5.38}$$

and

$$R_{\tilde{w}_n\tilde{w}_m\tilde{w}_l\tilde{w}_k}(\tau) = E[\tilde{w}_1^{\frac{(n+1)}{2}-l}(t)\tilde{w}_{-1}^{\frac{(n-1)}{2}-l}(t)\tilde{w}_1^{\frac{(m-1)}{2}-k}(t+\tau)\tilde{w}_{-1}^{\frac{(m+1)}{2}-k}(t+\tau) \times\tilde{w}_2^l(t)\tilde{w}_{-2}^l(t)\tilde{w}_2^k(t+\tau)\tilde{w}_{-2}^k(t+\tau)]. \tag{5.39}$$

where $\tilde{h}_{1;\xi_1}(t)$ and $\tilde{h}_{1;\xi_2}(t)$ are the baseband equivalent of the impulse responses of the input filter with respect to the frequencies ξ_1 and ξ_1 respectively. Again (5.38) is derived assuming that the input filter response is constant within each signal bandwidth. The PSD of the output signal $\tilde{z}_{\xi_1}(t)$ is obtained from the Fourier transform of the autocorrelation function as:

$$S_{\tilde{z}\tilde{z};\xi_1}(f) = \sum_{n=1}^{N}\sum_{m=1}^{N}\sum_{l=0}^{\frac{n-1}{2}}\sum_{k=0}^{\frac{m-1}{2}} b_{n,l}b_{m,k}^* S_{\tilde{u};nmlk}(f) \tag{5.40}$$

where

$$S_{\tilde{u};nmlk}(f) = |\tilde{H}_{1;\xi_1}(0)|^{n+m-2l-2k}|\tilde{H}_{1;\xi_2}(0)|^{2l+2k}S_{\tilde{w};nmlk}(f)$$

$$S_{\tilde{w};nmlk}(f) = \int_{-\infty}^{\infty} R_{\tilde{w}_n\tilde{w}_m\tilde{w}_l\tilde{w}_k}(\tau)e^{-j\omega\tau d\tau}.$$

The PSD at the output of the system is

$$S_{\tilde{y}\tilde{y};\xi_1}(f) = |\tilde{H}_{2;\xi_1}(f)|^2 S_{\tilde{z}\tilde{z}}(f) \tag{5.41}$$

where $\tilde{H}_{1;\xi_i}(f)$ and $\tilde{H}_{2;\xi_i}(f)$ are the baseband equivalent transfer functions of the input and output filters with respect to frequency ξ_i.

The output autocorrelation function of the intermodulation components can be developed in the same way. Therefore, for the upper and lower intermodulation components, using (4.30) and (4.31), the output autocorrelation function is

$$R_{\tilde{z}\tilde{z};\xi_{\mathrm{IM3}}}(\tau) = \sum_{n=3}^{N}\sum_{m=3}^{N}\sum_{l=0}^{\frac{n-3}{2}}\sum_{k=0}^{\frac{m-3}{2}} b_{n,l}b_{m,k}^* R_{\tilde{u}_n\tilde{u}_m\tilde{u}_l\tilde{u}_k}(\tau). \tag{5.42}$$

where ξ_{IM3} is the intermodulation frequency. Thus, for the upper intermodulation component (at $\xi_{\mathrm{IM3}} = 2\xi_2 - \xi_1$) we have

$$R_{\tilde{u}_n\tilde{u}_m\tilde{u}_l\tilde{u}_k}(\tau) = R_{\tilde{w}_n\tilde{w}_m\tilde{w}_l\tilde{w}_k}(\tau)|\tilde{h}_{1;\xi_1}(0)|^{2l+2k+2}|\tilde{h}_{1;\xi_2}(0)|^{n+m-2l-2k-2} \tag{5.43}$$

where

$$\begin{aligned} R_{\tilde{w}_n\tilde{w}_m\tilde{w}_l\tilde{w}_k}(\tau) &= E[\tilde{w}_1^l(t)\tilde{w}_{-1}^{l+1}(t)\tilde{w}_1^{k+1}(t+\tau)\tilde{w}_{-1}^k(t+\tau)\tilde{w}_2^{\frac{(n+1)}{2}-l}(t) \\ &\quad \times\tilde{w}_{-2}^{\frac{(n-3)}{2}-l}(t)\tilde{w}_2^{\frac{(m-3)}{2}-k}(t+\tau)\tilde{w}_{-2}^{\frac{(m+1)}{2}-k}(t+\tau)] \end{aligned}$$

and for the lower intermodulation component (at $\xi_{\mathrm{IM3}} = 2\xi_1 - \xi_2$):

$$R_{\tilde{u}_n\tilde{u}_m\tilde{u}_l\tilde{u}_k}(\tau) = R_{\tilde{w}_n\tilde{w}_m\tilde{w}_l\tilde{w}_k}|\tilde{h}_{1;\xi_1}(0)|^{n+m-2l-2k-2}|\tilde{h}_{1;\xi_2}(0)|^{2l+2k+2} \tag{5.44}$$

where

$$\begin{aligned} R_{\tilde{w}_n\tilde{w}_m\tilde{w}_l\tilde{w}_k}(\tau) &= E[\tilde{w}_1^{\frac{(n+1)}{2}-l}(t)\tilde{w}_{-1}^{\frac{(n-3)}{2}-l}(t)\tilde{w}_1^{\frac{(m-3)}{2}-k}(t+\tau)\tilde{w}_{-1}^{\frac{(m+1)}{2}-k}(t+\tau) \\ &\quad \times\tilde{w}_2^l(t)\tilde{w}_{-2}^{l+1}(t)\tilde{w}_2^{k+1}(t+\tau)\tilde{w}_{-2}^k(t+\tau)] \end{aligned}$$

The output PSD of the intermodulation components is obtained in a similar way to the component at ξ_1, therefore

$$S_{\tilde{z}\tilde{z};\xi_{\mathrm{IM3_U}}}(f) = \sum_{n=1}^{N}\sum_{m=1}^{N}\sum_{l=0}^{\frac{n-3}{2}}\sum_{k=0}^{\frac{m-3}{2}} b_{n,l}b_{m,k}^* S_{\tilde{u};nmlk}(f) \tag{5.45}$$

where

$$S_{\tilde{u};nmlk}(f) = |\tilde{H}_{1;\xi_1}(0)|^{2l+2k+2}|\tilde{H}_{1;\xi_2}(0)|^{n+m-2l-2k-2}S_{\tilde{w};nmlk}(f)$$

$$S_{\tilde{w};nmlk}(f) = \int_{-\infty}^{\infty} R_{\tilde{w}_n\tilde{w}_m\tilde{w}_l\tilde{w}_k}(\tau)e^{-j\omega\tau d\tau}.$$

and for $\mathrm{IM3}_L$:

$$S_{\tilde{z}\tilde{z};\xi_{\mathrm{IM3_L}}}(f) = \sum_{n=1}^{N}\sum_{m=1}^{N}\sum_{l=0}^{\frac{n-3}{2}}\sum_{k=0}^{\frac{m-3}{2}} b_{n,l}b_{m,k}^* S_{\tilde{u};nmlk}(f) \tag{5.46}$$

where

$$S_{\tilde{u};nmlk}(f) = |\tilde{H}_{1;\xi_1}(0)|^{n+m-2l-2k-2}|\tilde{H}_{1;\xi_2}(0)|^{2l+2k+2}S_{\tilde{w};nmlk}(f)$$

$$S_{\tilde{w};nmlk}(f) = \int_{-\infty}^{\infty} R_{\tilde{w}_n\tilde{w}_m\tilde{w}_l\tilde{w}_k}(\tau)e^{-j\omega\tau d\tau}.$$

The PSD at the output of the system for all the above cases is

$$S_{\tilde{y}\tilde{y};\xi_i}(f) = |\tilde{H}_{2;\xi_i}(f)|^2 S_{\tilde{z}\tilde{z}}(f) \tag{5.47}$$

where ξ_i is the intermodulation frequency and $\tilde{H}_{1;\xi_i}(f)$ and $\tilde{H}_{2;\xi_i}(f)$ are the baseband equivalent transfer functions of the input and output filters with respect to the frequency ξ_i.

The above results enable the autocorrelation function of the outputs centered at the fundamental and intermodulation frequencies to be computed by combining the effects of the input and output filters as well as the nonlinear block. In a similar way to the single channel case, the output PSD is simply the PSD of the memoryless nonlinearity multiplied by powers of the magnitude frequency response of the linear filters. The assumption that the transfer function of the input filter is constant within the signal bandwidth is again a reasonable assumption for modeling a wideband multichannel amplifier. Wideband multichannel amplifiers are expected to have a flat response within each channel bandwidth which is usually much smaller than the overall bandwidth of the amplifier.

Summary

In the above subsections we have derived formulae to compute the output PSD using the three-box model and signal realizations. This enables the easy implementation of the model in software where measured filter responses are multiplied by the output PSD. The output PSD is generated from the Fourier transform of the autocorrelation functions which are computed for the particular digitally modulated signals and at a particular output frequency.

5.4 Gaussian Assumption

The formulation of the autocorrelation function of the output of nonlinearity is greatly simplified if the input signals are assumed to be Gaussian processes. In [48] it was shown that the Gaussian assumption is not always an acceptable assumption specially for the reverse link where a difference of 6 dB in estimating ACPR was reported. However the Gaussian assumption is acceptable for the forward link signal since the forward link signal consists of the sum of multiple user data which means that its probability distribution, by central limit theorem, approaches a Gaussian distribution. In Section 5.2 we showed that the second order statistic is the same for both a CDMA signal and Gaussian noise. However, the higher order moments are different for each. In this section we use the properties of the moments of complex Gaussian random variables to obtain a simplified formulation for the autocorrelation function for a single and two-channel cases. For illustration purposes we

will restrict ourselves to a maximum nonlinear order of 3 of the behavioral model, however this can be generalized to any order of nonlinearity.

5.4.1 Single Channel

Using the output autocorrelation function formulated in (5.26), and letting $\tilde{w}(t) = \tilde{w}_1$, $\tilde{w}(t+\tau) = \tilde{w}_2$, $\tilde{w}_{-1}(t) = w^*(t)$ and $\tilde{w}_{-1}(t+\tau) = w^*(t+\tau)$, the output autocorrelation function for third order nonlinearity is

$$\begin{aligned} R_{\tilde{y}\tilde{y}}(\tau) = \quad & |b_1|^2 E[\tilde{w}_1 \tilde{w}_2^*] + b_1 b_3^* E[\tilde{w}_1 \tilde{w}_2^{*^2} \tilde{w}_2] + b_1^* b_3 E[\tilde{w}_1^2 \tilde{w}_1^* \tilde{w}_2^*] \\ & + |b_3|^2 E[\tilde{w}_1^2 \tilde{w}_1^* \tilde{w}_2^{*^2} \tilde{w}_2] \end{aligned} \tag{5.48}$$

If the random process $\tilde{w}(t)$ is a zero mean Gaussian then the following property of zero mean Gaussian random variables applies [32]:

$$\begin{aligned} & E[x_1 x_2 \dots x_s x_1^* x_2^* \dots x_t^*] \\ & = \begin{cases} \sum_\pi E[x_{\pi(1)} x_1^*] E[x_{\pi(2)} x_2^*] \dots E[x_{\pi(s)} x_s^*] & s = t \\ 0 & \text{otherwise.} \end{cases} \end{aligned} \tag{5.49}$$

The summation is over all the permutations π of the set of integers {1,2,...,s}. Therefore, the output autocorrelation function for third order nonlinearity ($n = 3$), can be written as (see B)

$$\begin{aligned} R_{\tilde{y}\tilde{y}}(\tau) = \quad & R_{\tilde{w}\tilde{w}}(\tau) \left[|b_1|^2 + 4Re[(b_1 b_3^*)] R_{\tilde{w}\tilde{w}}(0) + 4|b_3|^2 R_{\tilde{w}\tilde{w}}^2(0) \right] \\ & + 2|b_3|^2 R_{\tilde{w}\tilde{w}}^3(\tau) \end{aligned} \tag{5.50}$$

This result means that the output autocorrelation function can be written in terms of the second order statistic (the input autocorrelation function $R_{\tilde{w}\tilde{w}}$) which provides a great simplification over the generalized autocorrelation analysis. It is worth noting here that the second order statistic (the input autocorrelation function) is the same for CDMA and NBGN, however, higher order moments are different. Therefore, the Gaussian assumption leads to inaccurate results when modeling distortion in the reverse link. The Gaussian assumption was shown to be fairly acceptable for the forward link since the transmitted signal consist of a big number of Walsh-coded data sequences which, by central limit theorem, approaches the Gaussian distribution [48]. However the accuracy of such an assumption decreases if the composite signal is lightly loaded.

5.4.2 Two Channels

Using the orthogonality of the two signals as proved in (5.22) and letting $\tilde{w}_1(t) = r_1$, $\tilde{w}_1(t+\tau) = r_2$, $\tilde{w}_2(t) = s_1$ and $\tilde{w}_2(t+\tau) = s_2$, and the replacing the minus sign subscript by the $(*)$ to indicate the conjugation then (5.30) can be written as

$$R_{w_n w_m w_l w_k}(\tau) = E\left[r_1^{\frac{(n+1)}{2}-l} r_1^{*\frac{(n-1)}{2}-l} r_2^{\frac{(n-1)}{2}-k} r_2^{*\frac{(n+1)}{2}-k}\right] E\left[s_1^l s_1^{*l} s_2^k s_2^{*k}\right]. \tag{5.51}$$

For illustration purposes, we will restrict ourselves to writing down the third order response. Thus using (5.29) the output autocorrelation function for third order nonlinearity is

$$\begin{aligned} R_{\tilde{y}\tilde{y};\xi_1}(\tau) &= |b_{1,0}|^2 E[r_1 r_2^*] + b_{1,0} b_{3,0}^* E[r_1 r_2^{*^2} r_2] + b_{1,0}^* b_{3,0} E[r_1^2 r_1^* r_2^*] + |b_{3,0}|^2 E[r_1^2 r_1^* r_2^{*^2} r_2] \\ &+ b_{1,0} b_{3,1}^* E[r_1 r_2^*] E[s_2 s_2^*] + b_{3,0} b_{3,1}^* E[r_1^2 r_1^* r_2^*] E[s_2 s_2^*] + b_{1,0}^* b_{3,1} E[r_1 r_2^*] E[s_1 s_1^*] \\ &+ b_{3,0}^* b_{3,1} E[r_1 r_2 r_2^{*^2}] E[s_1 s_1^*] + |b_{3,1}|^2 E[r_1 r_2^*] E[s_1 s_1^* s_2 s_2^*]. \end{aligned} \tag{5.52}$$

Using the properties of Gaussian random processes in (5.49) and collecting the power-like terms, the output autocorrelation function for a third order nonlinearity ($n = 3$) can be written as (see appendix B)

$$\begin{aligned} R_{\tilde{y}\tilde{y};\xi_1}(\tau) &= R_{rr}(\tau)[|b_{1,0}|^2 + 4Re[(b_{1,0} b_{3,0}^*)] R_{rr}(0) + 2Re[(b_{1,0} b_{3,1}^*)] R_{ss}(0) \\ &+ 4Re[(b_{3,0} b_{3,1}^*)] R_{ss}(0) R_{rr}(0) + 4|b_{3,0}|^2 R_{rr}^2(0) + |b_{3,1}|^2 R_{ss}^2(0)] \\ &+ |b_{3,1}|^2 R_{ss}^2(\tau) R_{rr}(\tau) + 2|b_{3,0}|^2 R_{rr}^3(\tau) \end{aligned} \tag{5.53}$$

Again, the output autocorrelation is now a function of the input autocorrelation functions of the input signals. Note that the cross terms are represented by the product of the autocorrelation functions of the two signals. In Chapter 7 we will demonstrate the accuracy of the Gaussian assumption for both the forward and the reverse link by comparing it with the spectrum generated from signal realizations.

5.5 Conclusion

In this chapter we have developed a nonlinear statistical analysis for single and multiple channel inputs. The analysis is based on both the memoryless and the three-box approximation of the Volterra model which captures memory effects of a nonlinear power amplifier. The three-box model was shown to capture the behavior of a nonlinear amplifier with similar

shapes of the AM-AM characteristics. This enables the accurate estimation of intermodulation and cross-modulation distortions which are of great concern in multichannel PA design. In Chapter 7 it will be shown that using the three-box model provides better accuracy in the estimation of distortion than the memoryless model which uses single tone characteristics. This is because the nonlinear response with multiple channels depends on the frequency separation of the channels as well as their power levels. The statistical analysis presented in this chapter can be generalized to model an arbitrary number of input signals.

Chapter 6

Probability of Error

As discussed in Chapter 3, the nonlinear characteristics of RF and Microwave amplifiers result in two main impairments to the output spectrum which limit system performance. The first is in-band distortion which is manifested as a degradation of the system Bit Error Rate (BER), and the second is Spectral Regrowth (SR) which is responsible of increasing the relative distortion levels in the adjacent channels. Generally, systems with linear modulation schemes (QPSK, QAM, etc.) are more susceptible to PA nonlinearity because of their nonconstant envelope.

Analysis of BER degradation due to PA nonlinearity has been extensively investigated in the literature. Because of the lack of a statistical model for modeling the nonlinear distortion, most of these analyses were based on simulations [64, 65, 66]. On the other hand, the assumption that the signal and its distortion can be represented by a Gaussian random process provided a means for developing an analytical analysis that relates system performance (BER) to nonlinear distortion. The Gaussian assumption enables the treatment of the signal and its distortion as uncorrelated processes and, therefore, simple analytical form for the BER of the system can be derived. Analytical characterization of BER due to amplifier nonlinearities has been extensively studied for Orthogonal Frequency-Division Multiplexing (OFDM) systems since OFDM signals exhibit a high PAR which makes the system BER more sensitive to amplifiers nonlinearities than other systems. In [67, 68, 69, 70] an analytical analysis of BER in an OFDM system due to amplifier nonlinearities was developed. These analyses were based on using either the limiter amplifier model (hard limiter

and clipper) or the functional form of the AM-AM and AM-PM conversions known as the Saleh model [71]. The analysis enabled the BER to be related to nonlinear model coefficients under the assumption that the signal and its distortion can be assumed to have a Gaussian distribution which is an acceptable assumption for an OFDM signals [68, 72]. An analytical analysis of BER was developed in [73, 74] for OFDM system with amplifier nonlinearities by relating BER to nonlinear distortion using the PSD of the nonlinear distortion. In [75, 76, 77], an analytical framework for predicting the performance of a Direct Sequence-Spread Spectrum (DS-SS) system due to amplifier nonlinearities was studied. The analysis was based on using the Saleh model to model the AM-AM and AM-PM characteristics of the amplifier and the Gaussian assumption.

The main problem with all these analyses is that system performance analysis was not based on considering the PSD of nonlinear distortion which is a more realistic measure of distortion than simple nonlinear model parameters. In this chapter, we use our understanding of distortion to develop a relationship between in-band distortion and BER in an IS-95 CDMA system. The main contribution of this chapter is the development of a model by which the in-band distortion can be related analytically to the system BER. The in-band distortion is computed from the simulated output spectrum which is developed using signal realizations and measured AM-AM and AM-PM characteristics as discussed in Chapter 5. The analytical model is verified using simulations where the forward link transmit/receive system with a nonlinear amplifier is simulated in MATLAB.

6.1 Signal Model and Statistics

The modulation scheme for the forward link in an IS-95 CDMA system was discussed in Chapter 5. The transmitted signal can be written as

$$\begin{aligned} w(t) &= i(t)\cos(\omega_c t) + q(t)\sin(\omega_c t) \\ &= A(t)\cos(\omega_c t + \Phi(t)) \\ &= \frac{1}{2}[\tilde{w}(t)e^{j\omega_c t} + \tilde{w}^*(t)e^{-j\omega_c t}]. \end{aligned} \tag{6.1}$$

where

$$\tilde{w}(t) = i(t) + jq(t) = A(t)e^{j\Phi(t)}$$

is the complex envelope of the modulated signal $w(t)$. The complex envelope of the transmitted signal defined in (5.13) can be written as

$$\begin{aligned}\tilde{w}(t) &= \frac{1}{\sqrt{2}} \sum_{l=-\infty}^{\infty} \sum_{i=0}^{K-1} \sum_{n=0}^{K-1} \rho d_i(lT_b) W_i(nT) \\ &\quad \times [I(nT) + jQ(nT)]\, h(t - nT - lT_b). \end{aligned} \tag{6.2}$$

Without loss of generality, (6.2) can be written as

$$\tilde{w}(t) = \frac{1}{\sqrt{2}} \sum_{l=-\infty}^{\infty} \sum_{i=0}^{K-1} \sum_{n=0}^{K-1} \rho c_i(lT_b) p_i(t - nT - lT_b) \tag{6.3}$$

where $p_i(t - nT) = W_i(nT)\,[I(nT) + jQ(nT)]\,h(t - nT)$. The output of the nonlinear amplifier can be written in a complex envelope form as:

$$\tilde{y}(t) = \sum_{n=1}^{N} b_n \tilde{w}^n(t). \tag{6.4}$$

Using the Gaussian assumption the output autocorrelation function for third order nonlinearity ($N = 3$) and can be written, as in (5.50), as

$$\begin{aligned} R_{\tilde{y}\tilde{y}}(\tau) &= |\alpha_1|^2 R_{\tilde{w}\tilde{w}}(\tau) + |\alpha_2|^2 R^3_{\tilde{w}\tilde{w}}(\tau) \\ &= |\alpha_1|^2 R_{\tilde{w}\tilde{w}}(\tau) + R_{\tilde{d}\tilde{d}} \end{aligned} \tag{6.5}$$

where

$$\begin{aligned} |\alpha_1|^2 &= |b_1|^2 + 4Re[b_1 b_3^*] R_{\tilde{w}\tilde{w}}(0) + 4|b_3|^2 R^2_{\tilde{w}\tilde{w}}(0) \\ |\alpha_2|^2 &= 2|b_3|^2. \end{aligned} \tag{6.6}$$

The formulation of the autocorrelation function in this way means that the two processes $\tilde{w}(t)$ and $\tilde{d}(t)$ are uncorrelated random processes. This formulation coincides with the generalized form of Bussgang's theorem [75]. Note that this formulation enables the output signal to be written as a useful component $\tilde{w}(t)$ combined with a distortion component $\tilde{d}(t)$ uncorrelated from the useful component. Therefore, the output of the nonlinear system can now be written as

$$\tilde{y}(t) = |\alpha_1| \tilde{w}(t) + \tilde{d}(t). \tag{6.7}$$

Note that (6.7) enables the nonlinear distortion to be treated as an additive noise similar to the AWGN and so makes analytical formulation of the BER more tractable as will be seen in the following section.

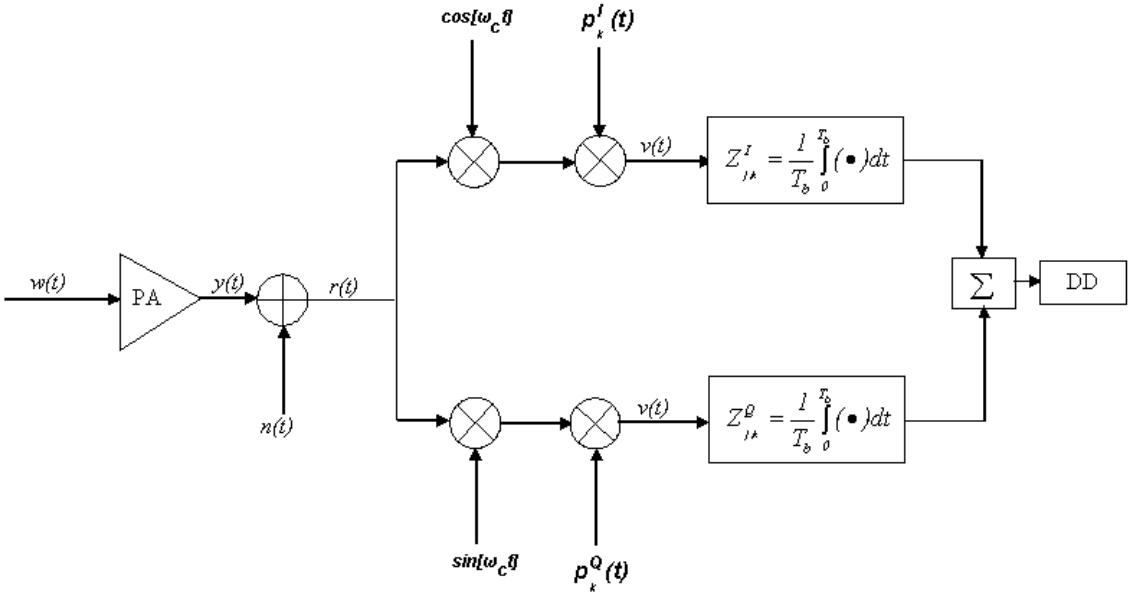

Figure 6.1: Block diagram of DS-SS receiver

6.2 Performance Analysis

A forward link wireless CDMA system can be assumed to be synchronous since the composite signal is generated at the transmitter where synchronization of different users is possible [78]. The system also uses orthogonal Walsh codes which makes the Multiple Access Interference (MAI) absent. However, this is not always true because the orthogonality can be corrupted by the multi-path behavior of a cellular system. For the purpose of studying the effect of nonlinear distortion on the system bit error rate, we will neglect the effects of fading. These assumptions are useful for the case in hand which is to study the performance of the system in the presence of nonlinear amplifier distortion. In order to determine the bit error probability, the statistics of the transmitted signal and the receiver architecture must be defined. The receiver of an IS-95 forward link is shown in Fig. 6.1 [79]. The received signal $r(t)$ is expressed as

$$r(t) = |\alpha_1| w(t) + d(t) + n(t)$$

where $n(t)$ is an additive white Gaussian noise having zero mean and a two-sided power spectral density of $N_o/2$. The received waveform is first demodulated and then multiplied by the spreading code of the k th user of the I and Q branches. The resulting waveform $v^{(k)}(t)$ for the I channels can be written as

$$v_I^{(k)}(t) = |\alpha_1| w(t) p_k^I(t) \cos(\omega_c t)$$
$$+ d(t) p_k^I(t) \cos(\omega_c t) + n(t) p_k^I(t) \cos(\omega_c t).$$

The decision variable $Z_{j,k}^I$ at the output of the integrate and dump circuit for the j th bit and the k th user can be written as

$$Z_{j,k}^I = D_0^I + D_d^I + D_n^I$$

where D_0^I is the useful component which represents the linear output of the signal, D_d^I represents the nonlinear distortion component and D_n^I represents the AWGN component. These components can be evaluated as follows

$$\begin{aligned} D_0^I &= \frac{1}{T_b} \int_0^{T_b} |\alpha_1| w(t) p_k^I(t) \cos(\omega_c t) dt \\ &= \frac{1}{\sqrt{2} T_b} \int_0^{T_b} |\alpha_1| \rho d_{k,j} (p_k^I(t))^2 \cos^2(\omega_c t) dt \\ &= \rho d_{j,k} \frac{1}{\sqrt{2} T_b} \sum_{n=1}^{K} \int_0^{T} |\alpha_1| (p_k^I(t))^2 \cos^2(\omega_c t) dt \\ &= \frac{1}{2\sqrt{2}} |\alpha_1| \rho d_{k,j} \end{aligned} \tag{6.8}$$

is the linear component,

$$D_d^I = \frac{1}{T_b} \int_0^{T_b} d(t) p_k^I(t) \cos(\omega_c t) dt \tag{6.9}$$

represents the nonlinear distortion component, and

$$D_n^I = \frac{1}{T_b} \int_0^{T_b} n(t) p_k^I(t) \cos(\omega_c t) dt \tag{6.10}$$

represents the AWGN component. The components of the Quadrature branch of the receiver can be found in the same way. The bit error probability is a function of the signal-to-total noise ratio (SNR) and the modulation format. The components D_o, D_d and D_n are uncorrelated as proved in the previous section, therefore the probability of bit error of the

k th user can be found from the error probability of a QPSK system as

$$P_e = Q\left(\sqrt{\frac{A^2}{\sigma^2_{D_d^I}+\sigma^2_{D_d^Q}+\sigma^2_{D_n^I}+\sigma^2_{D_n^Q}}}\right) \tag{6.11}$$

where $A = D_0^I + D_0^Q = |\alpha_1|\rho/\sqrt{2}$. The components in the denominator of (6.11) can be evaluated in terms of the PSD of the output signal (see Appendix C):

$$\begin{aligned}\sigma^2_{D_d^I} &= E[(D_d^I)^2] \\ &= \frac{1}{T_b^2}E\int_0^{T_b}\int_0^{T_b} p_k(t)p_k(\lambda)d(t)d(\lambda)\cos(\omega_c t)\cos(\omega_c\lambda)dtd\lambda \\ &= \frac{1}{4K}\int_{-B/2}^{B/2} S_{\tilde{d}\tilde{d}}(f)df \end{aligned} \tag{6.12}$$

and for the AWGN:

$$\begin{aligned}\sigma^2_{D_n^I} &= E[(D_n^I)^2] \\ &= \frac{1}{T_b^2}E\int_0^{T_b}\int_0^{T_b} p_k(t)p_k(\lambda)n(t)n(\lambda)\cos(\omega_c t)\cos(\omega_c\lambda)dtd\lambda \\ &= \frac{N_o}{4T_b}. \end{aligned} \tag{6.13}$$

The linear output power of the k th user can be evaluated as

$$P_l^{(k)} = \frac{|\alpha_1|^2}{2K}\int_{-B/2}^{B/2} S_{\tilde{w}\tilde{w}}(f)df = A^2 = \frac{|\alpha_1|^2\rho^2}{2}. \tag{6.14}$$

Note that the above expressions relate the power of all the components involved in the probability of error expressions to the in-band power measured from the PSD of the CDMA signal. It is more convenient to write the probability of error in terms of the ratio of the Energy per bit E_b to the noise power N_o. This ratio can be evaluated as

$$\frac{E_b}{N_o} = \frac{P_o T_b}{K N_o}.$$

Now, from (6.12) we have

$$A^2 = \frac{P_l}{K} = \frac{P_o - P_d}{K}$$

where $P_o = P_l + P_d$ is the total output power, $P_l = KP_l^{(k)}$ is the total linear power and $P_d = K\sigma_D^2$ where $\sigma_D^2 = \sigma^2_{D_d^I} + \sigma^2_{D_d^Q}$ is the distortion power. Therefore, the signal to noise ratio can be written as:

$$\frac{E_b}{N_o} = \frac{A^2T_b}{N_o} + \frac{\sigma_d^2 T_b}{N_o}$$

and it follows that

$$A^2 = \left[\frac{E_b}{N_o} - \frac{\sigma_d^2 T_b}{N_o}\right] \frac{N_o}{T_b}.$$

The output probability of error due to both the AWGN and nonlinear distortion can then be written in terms of E_b/N_o as:

$$\begin{aligned} P_e &= Q\left(\sqrt{\frac{E_b/N_o - \eta}{(1/2) + \eta}}\right) \\ &= \frac{1}{2}\text{erfc}\left(\sqrt{\frac{E_b/N_o - \eta}{1 + 2\eta}}\right) \end{aligned} \tag{6.15}$$

where

$$\eta = \frac{\sigma_d^2 T_b}{N_o}$$

and Q and erfc are the Q function and the complimentary error function respectively. Note that (6.13) reduces to the probability of error of the system without nonlinear distortion when $\eta = 0$- the case where nonlinear distortion is absent. This formulation is useful since it relates the BER to nonlinear distortion by a simple analytical formula. The parameter η can be evaluated using the simulated output spectrum as discussed in the previous section.

6.3 Conclusion

In this chapter we have developed an analytical analysis for the probability of error in a DS-SS CDMA system in AWGN and the presence of power amplifier nonlinearity. The analytical formulation presented enables the probability of bit error to be related to nonlinear distortion estimated from the output PSD. The output PSD is estimated using signal realizations and the measured AM-AM and AM-PM characteristics. The analysis was based on the assumption that a CDMA signal can be modeled as a Gaussian process which is an acceptable assumption for the forward link. The analysis can be extended to more complicated cases such as including the memory effects of the amplifier and the case of multiple input channels which are left for future work. In Chapter 7 we will verify the validity of the analytical model using simulations.

Chapter 7

Verification

In this chapter we verify all the concepts developed in the previous chapters using simulations and measurements. The verification strategy is illustrated by the block diagram in Fig. 7.1. The verification procedure consists of two parallel paths. The first is the development of the behavioral model parameters using measured amplifier characteristics. The second path is the generation of the complex envelop of the a IS-95 CDMA channel. The resulting signal realizations along with model parameters are then used to develop the output spectrum by which distortion is predicted. The predicted distortion levels are compared to measured valued performed on the modeled amplifier.

This chapter is divided into four sections. The first section deals with the extraction of the behavioral model parameters where we develop the parameters of both the memoryless model and the three-box models using the procedures described in Chapter 4. The resulting behavioral model will then be used in Section (7.2) which deals with the generation of CDMA signal realizations and the computation of the output autocorrelation function and the output PSD. The output PSD will be used to predict distortion levels which will be and verified by measurements. The third section is an investigation of the relationship between analog and digital system distortion where we show by measurements and simulations that this relationship depends on the maximum order of nonlinearity. The last section deal with the verification of the analytical model for system performance by simulations using the transmit/receive system of the IS-95 forward link system.

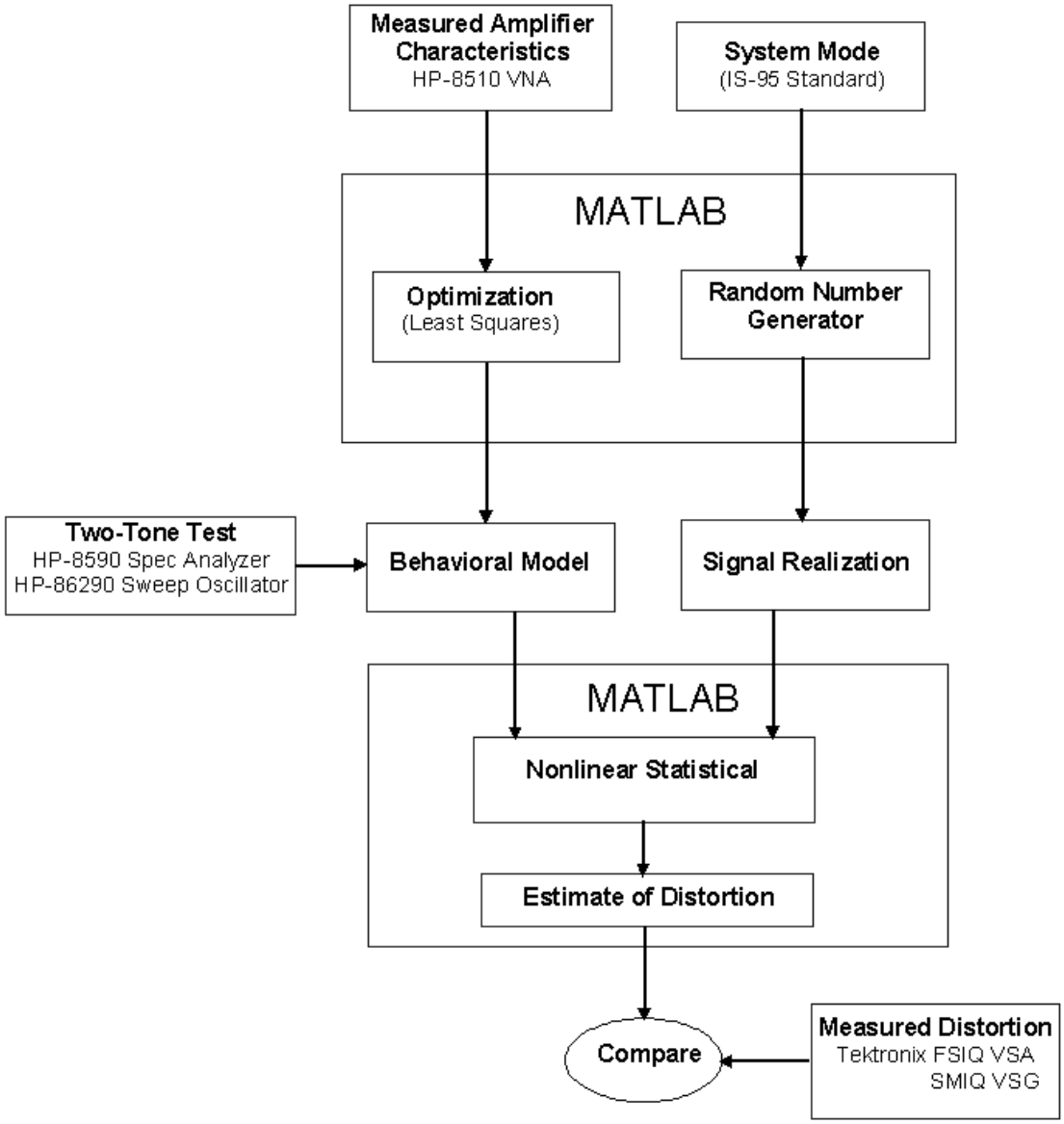

Figure 7.1: Verification Strategy.

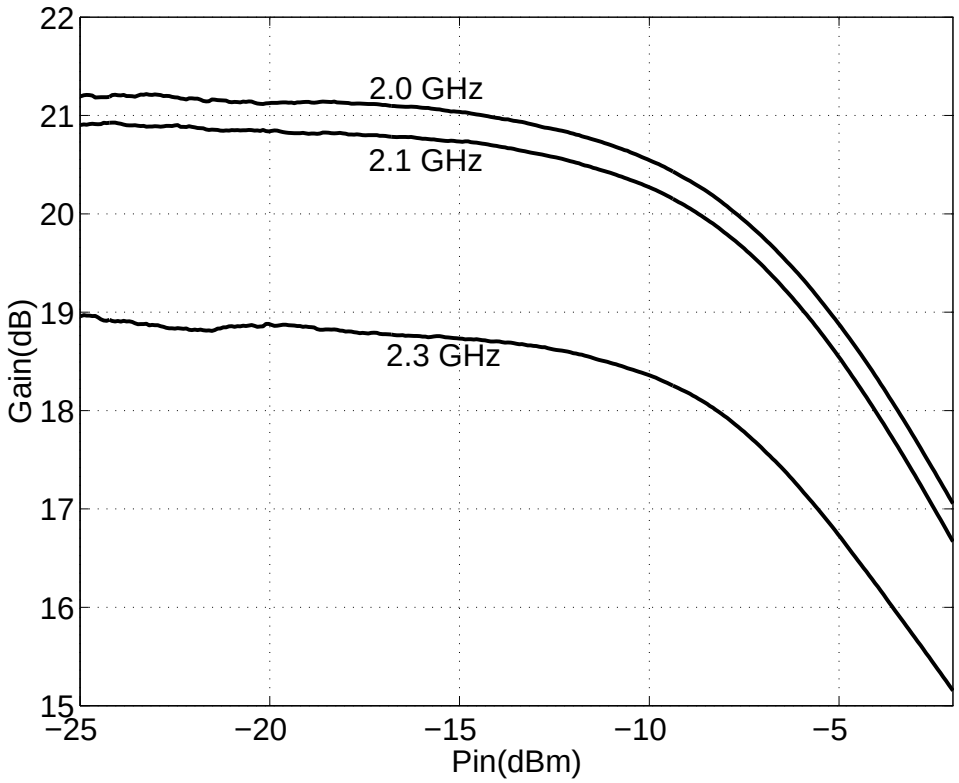

Figure 7.2: Measured AM-AM characteristics of a microwave amplifier at various frequencies

7.1 Behavioral Model

In this section, we first present the characterization of a wideband multichannel amplifier intended to cover the cellular and IMS bands from 2.0 to 2.5 GHz. The amplifier considered is commercially available from AMPLICA and has a gain of 21 dB, an output 1 dB compression point of 11 dBm, and an OIP3 of 18 dBm all at 2.25 GHz which is the middle of the operating band of the amplifier. The amplifier exhibits a similar shape of the AM-AM characteristics (shown in Fig. 7.2) at different frequencies across the band. For this amplifier we extract the parameters of both the memoryless model and the three-box model using the parameter extraction techniques discussed in Chapter 4. The self-similar AM-AM characteristics at various frequencies indicate that the nonlinear reactive (i.e. frequency dependent) effects are insignificant and so the amplifier is a good candidate for the three-box approximation of the Volterra model.

7.1.1 Memoryless Model

The multi-envelope parameter extraction technique discussed in Section 4.3.1 is used to develop the envelope coefficients of the memoryless model. The envelope coefficients $b_{n,k}$ in (2.3) were obtained using a HP 8510 Vector Network Analyzer (VNA) to extract the AM-AM and AM-PM characteristics at $f_1 = 2.1$ GHz of a wideband C-band amplifier. In addition, an external 2.0 GHz signal source injects a second tone at frequency f_2 at various power levels as shown in Fig. 7.3. The AM-AM and AM-PM characteristics at f_1 are determined at each power level of the second source. The power of the VNA signal was swept from -30 dBm to -5 dBm while the power of the second tone was swept manually from -20 dBm to -5 dBm in 0.5 dB steps and hence, 30 sets of measurements were obtained. Table 7.1 lists the 2D-polynomial coefficients of degree $N = 11$, Figs 7.4(a) and 7.4(b) show a 3D plot of the AM-AM and the AM-PM characteristics as a function of the power levels of both signals and Figs 7.5(a) and 7.5(b) show the corresponding polynomial fits. It is worth noting here that this set of coefficients represents the envelope relationship as in (4.39) where it is assumed that the output envelope is related to the input envelopes by that equation. A one-to-one relationship between those coefficients and their instantaneous counterparts cannot be developed in this case. If the instantaneous coefficients are sought, the formulation of the problem can be done as a bivariate case as in [22]. The envelope model in (4.39) was sufficient and comparisons between this model and the bivariate case using simulations showed that they give the same result when the analysis is done at the complex envelope level.

7.1.2 Three Box Multichannel Model

The three-box model parameters were extracted according to the procedure discussed in Section (4.3.2) and using a Vector Network Analyzer (VNA) as follows. The transfer functions $H_{\rm ss}(f)$ and $H_{\rm sat}(f)$ were obtained from S_{21} of the amplifier at low power level (-20 dBm) and at the 1-dB compression point (-8 dBm input power approximately), see Fig. 7.6. The transfer functions of the linear filters, $H_1(f)$ and $H_2(f)$, were computed from the measured filter transfer functions using (4.40) and (4.41) with $f_{\rm ref} = 2.25$ GHz, and are shown in Fig. 7.7. The frequency response of the input filter is seen to have a flat response over the operating bandwidth which verifies the assumption used in Chapter 5 where the input filter

Table 7.1: Envelope behavioral model complex coefficients.

$b_{1,0}$	3.3591-10.7812i
$b_{3,0}$	1.2502+1.2062e2i
$b_{3,1}$	1.4783e1+2.3199e2i
$b_{5,0}$	7.3476e2-5.8665e2i
$b_{5,1}$	-8.5658e2-5.4381e3i
$b_{5,2}$	1.2094e3-1.1498e2i
$b_{7,0}$	-1.6180e4-1.1673e2i
$b_{7,1}$	-9.1893e3+4.6244e4i
$b_{7,2}$	1.3738e4+2.3445e4i
$b_{7,3}$	-9.5786e4-1.5967e5i
$b_{9,0}$	1.2243e5-7.9927e3i
$b_{9,1}$	2.5750e5-1.2319e5i
$b_{9,2}$	-1.1795e5-5.1066e4i
$b_{9,3}$	3.3451e5+8.9860e5i
$b_{9,4}$	2.0552e6+4.4007e6i
$b_{11,0}$	-3.1336e5 +1.1463e5i
$b_{11,1}$	-1.2586e+6-4.9653e4i
$b_{11,2}$	1.1309e5-5.5127e5i
$b_{11,3}$	-6.9983e5-3.8475e6i
$b_{11,4}$	-4.2886e6-8.5872e6i
$b_{11,5}$	-1.5328e7-4.1466e7i

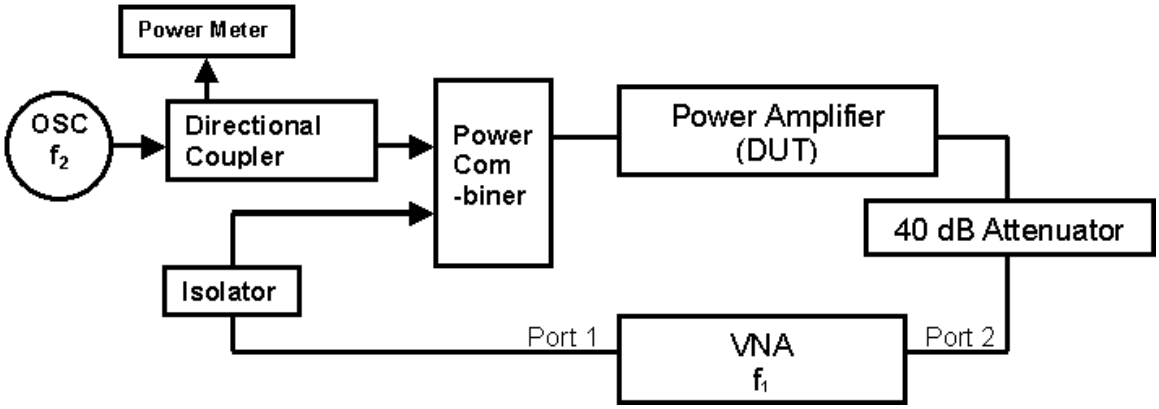

Figure 7.3: AM-AM and AM-PM Measurement setup.

response was assumed constant within each channel's bandwidth, see (5.38). One of the assumptions behind the model extraction procedure is that the phase-frequency response is linear. This response is shown in Fig. 7.8 for the amplifier under test where it seen that it is indeed linear across the band. Finally, the coefficients of the reference static nonlinearity were obtained by measuring the AM-AM and AM-PM characteristics at the reference frequency. A polynomial of order 5 was fitted to the complex data using classical least squares polynomial fitting and a set of envelope coefficients (b_n) obtained. The three-box model combines the frequency dependent characteristics of the linear filters and the static nonlinearity to predict the overall amplifier response. The predicted single-tone response obtained using the three-box model is compared to the measured response in Fig. 7.9 at various power levels and across the band. Thus the three-box model is seen to capture the single-tone behavior of the amplifier and should be entirely satisfactory when used to characterize the multichannel response of the amplifier. The remaining subsections demonstrate that this is so for multi-tone and with multiple digitally modulated signals.

7.1.3 Two Tone Testing with Wide Frequency Separation

In order to investigate the validity of the three-box model for multiple tones, a two-tone test was performed with wide frequency separation. The amplifier response to an input that consists of two equal amplitude tones centered at 2.1 GHz and 2.2 GHz was measured. The frequency separation was chosen so that the asymmetry in the levels of the upper and

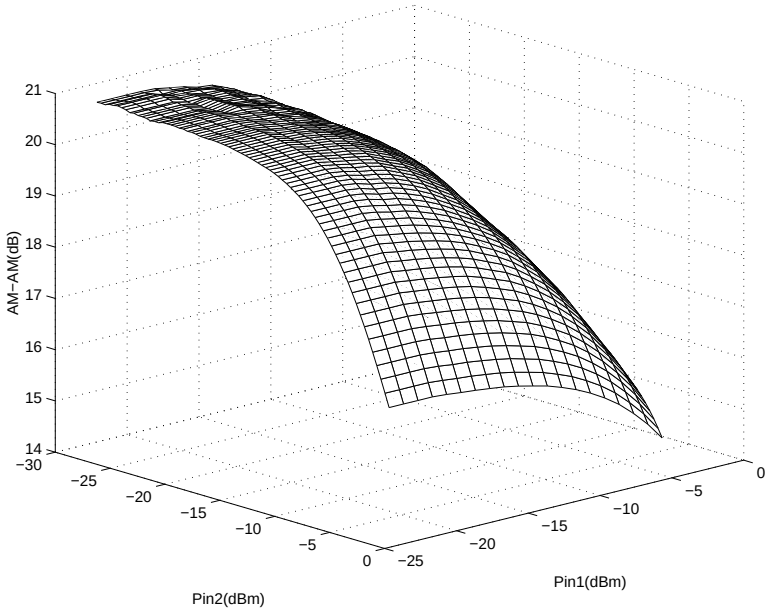

(a)

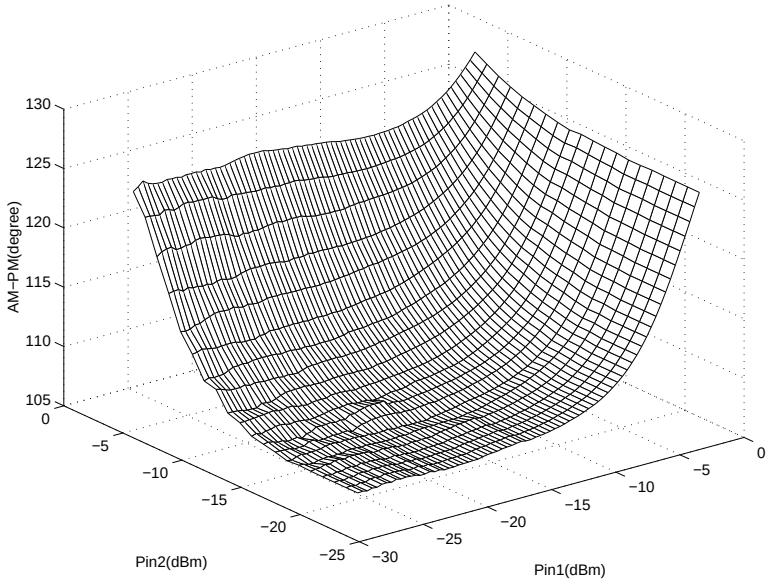

(b)

Figure 7.4: Measure amplifier characteristics as a function of the powers of the two tones, (a): AM-AM and (b): AM-PM.

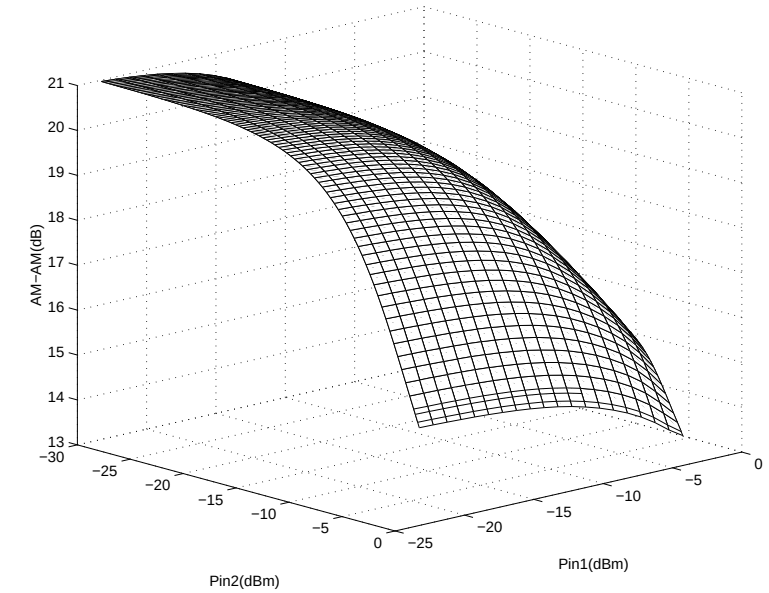

(c)

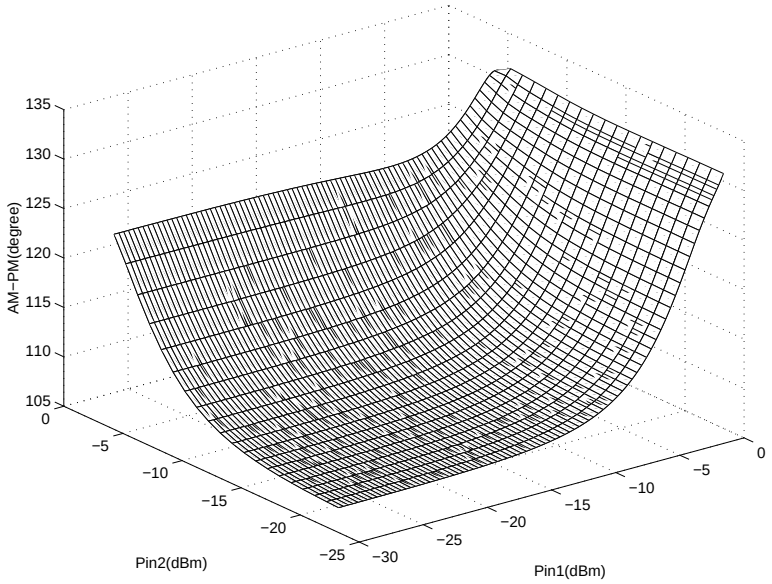

(d)

Figure 7.5: Polynomial fit of amplifier characteristics in Fig. 7.4: (a) AM-AM and (b) AM-PM.

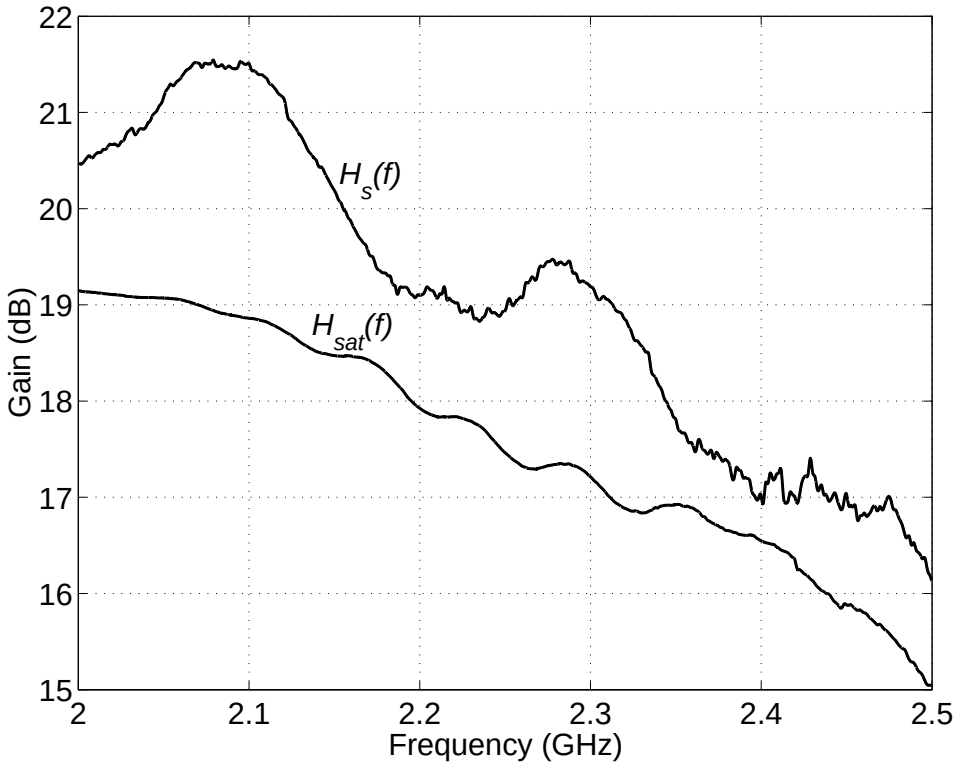

Figure 7.6: Measured small signal and large signal frequency responses $H_{\rm ss}(f)$ and $H_{\rm sat}(f)$.

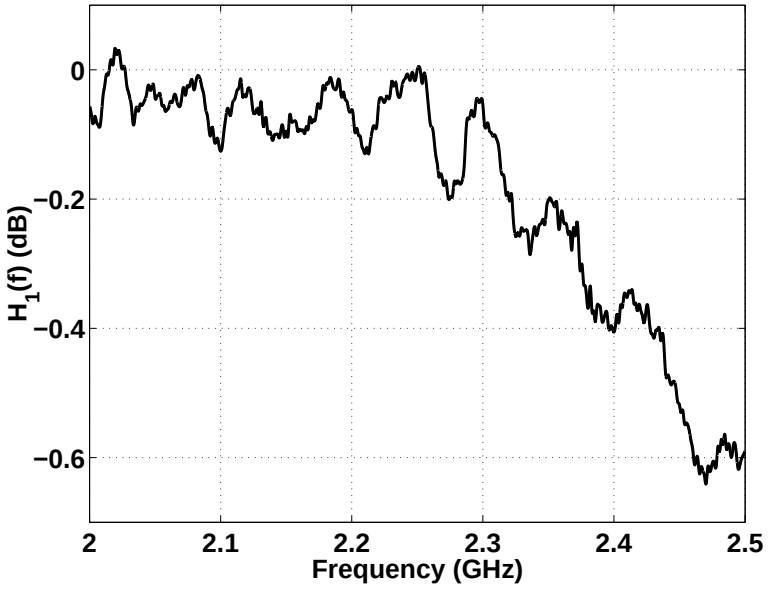

(a)

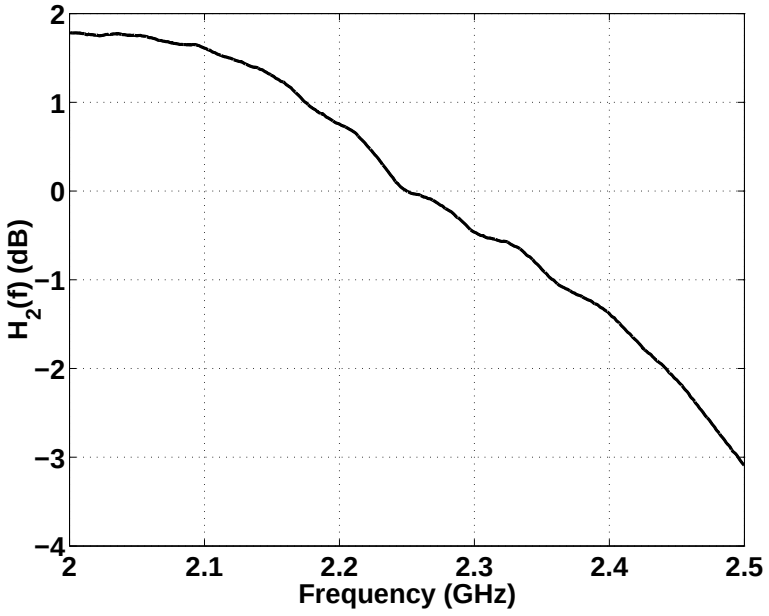

(b)

Figure 7.7: Normalized transfer characteristics of the input filter $H_1(f)$ and the ouput filter $H_2(f)$.

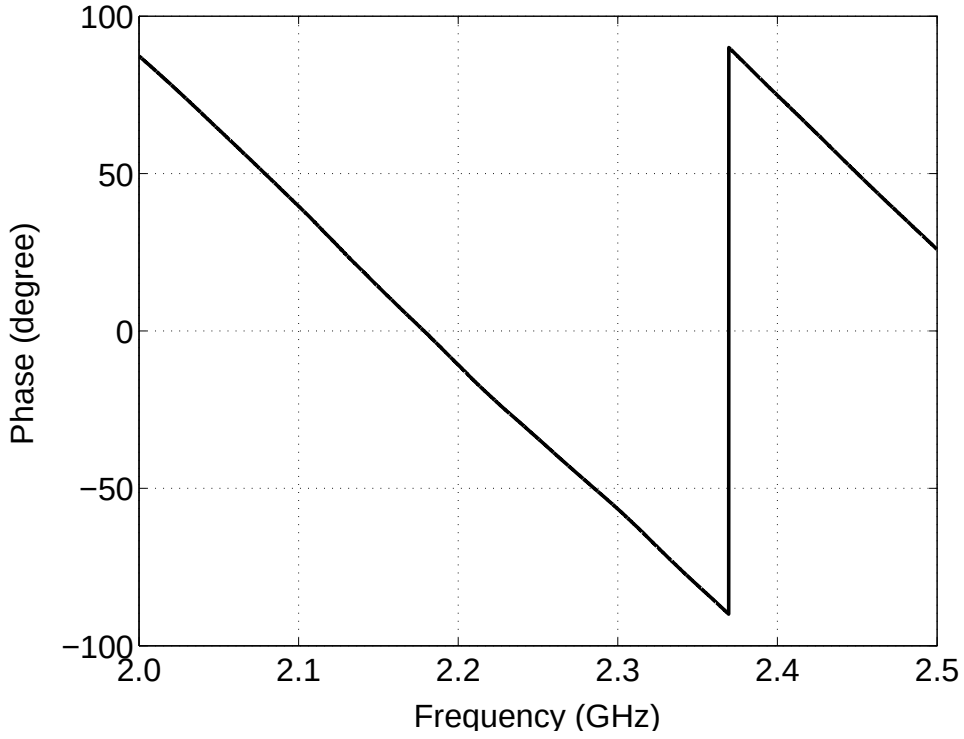

Figure 7.8: Phase response of $H_{\mathrm{ss}}(f)$.

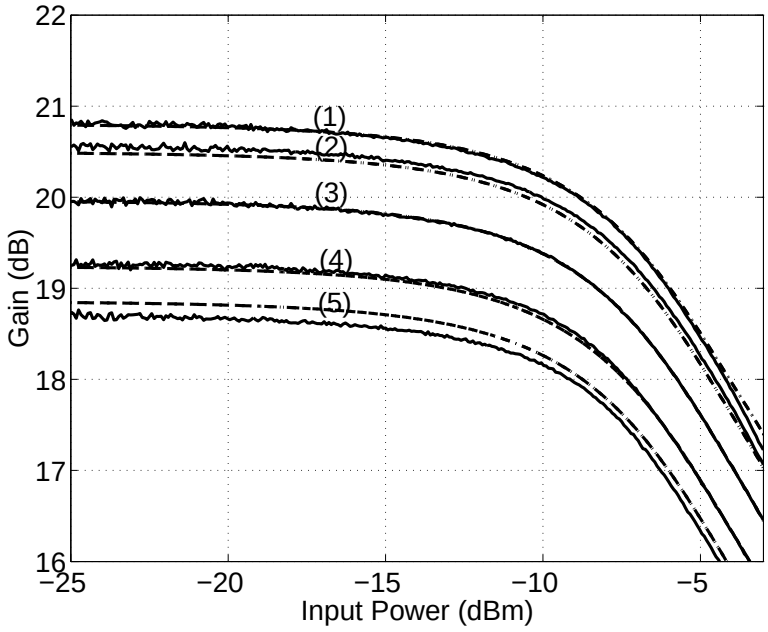

(a)

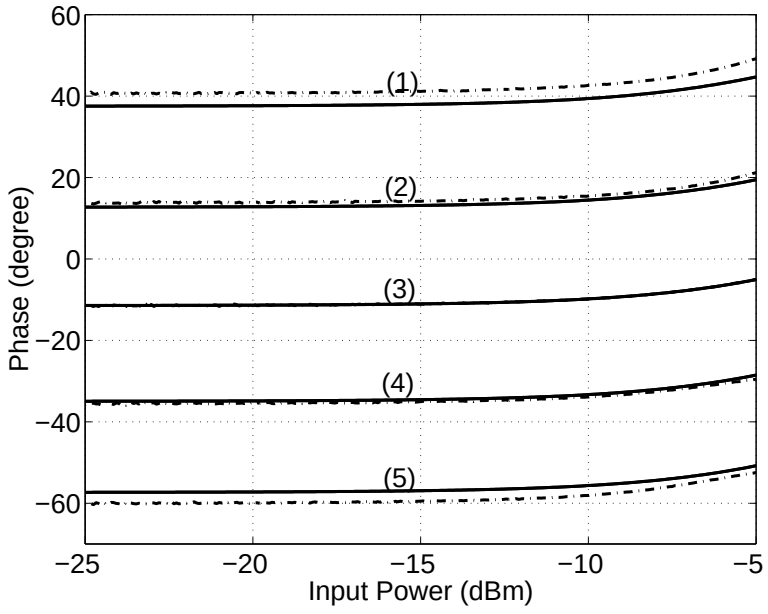

(b)

Figure 7.9: Measured and predicted amplifier characteristics: (a) AM-AM and (b) AM-PM characteristics. Numerals indicate various frequencies: (1) $f_1 = 2.1$ GHz, (2) $f_2 = 2.15$ GHz, (3) $f_3 = 2.2$ GHz, (4) $f_{\text{ref}} = 2.25$ GHz and (5) $f_4 = 2.3$ GHz. The solid lines are measurements and the broken lines are predicted by using the three-box model

lower intermodulation components due to memory effects is evident. Both being less than f_{ref} is a further test of the model. Fig. 7.10 presents the gain characteristics and intermodulation components (IM3) levels predicted by the three-box model and the memoryless model (with the filter responses excluded, $H_1(f) = H_2(f) = 1$). A good agreement between the measured and the simulated values is seen when the three-box model is used. The frequency dependence evident in the measurements is of course not captured by the memoryless model.

The three-box model is capable of predicting the response at various frequencies and signal levels. The asymmetry in the upper and lower intermodulation products is due to the variation of the frequency response of the amplifier with frequency. The figure shows a difference of 2 dB between the two intermodulation components which the model predicts accurately. At high input powers, Fig. 7.10, discrepancies are evident between the measured and calculated responses. These discrepancies are particularly evident above -4 dBm input power corresponding to gain compression of 4 dB and more. The model evidently breaks down at these levels as the power series that captures the nonlinear behavior was fitted using single-tone measurements. While the single tone-measurements captured gain compression at the 4 dB level, the large peak-to-average ratio (PAR) of the two-tone test (PAR=6 dB) results in much larger signal excursions for the same compression level. Thus the power series nonlinear model breaks down and this is exaggerated as power series extrapolate the asymptotic response of the limiting amplifier poorly.

7.1.4 Summary

The model parameters of the memoryless and the three-box behavioral models have been extracted and verified. The memoryless model with its novel parameter extraction technique is capable of modeling the nonlinear behavior of a multichannel amplifier when the frequency separation between input channels is small, i.e. a frequency separation where the amplifier characteristics do not change. The three-box model was shown to capture the behavior of a nonlinear amplifier with self-similar shapes of the AM-AM characteristics at frequencies across the band of interest. The parameters of the memoryless and of the three-box model were extracted using simple VNA measurements, however, more complicated schemes such as two-tone characterization could be used to enhance model accuracy. This concludes the behavioral model part of the verification procedure. In the following sections, the extracted

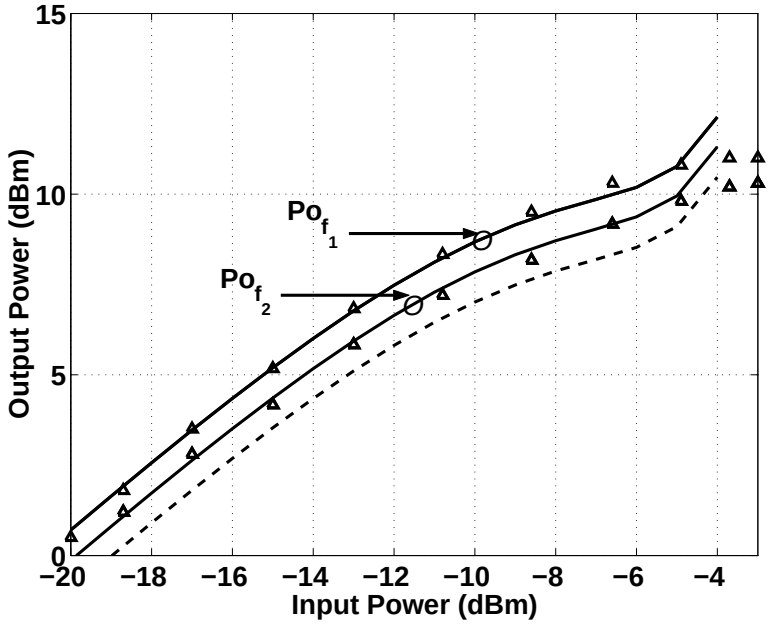

(a)

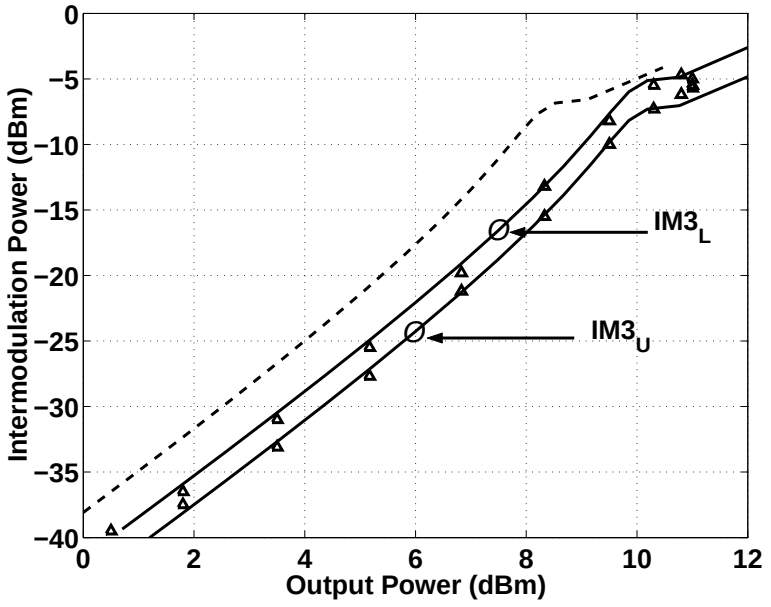

(b)

Figure 7.10: Two-tone test results: (a) output power with $f_1 = 2.1$ GHz and $f_2 = 2.2$ GHz; and (b) upper intermodulation component power level (IM3_U) and lower intermodulation component power level (IM3_L). Solid lines are simulated using the three-box model; broken line are simulated using the memoryless model; and $\triangle$ are measured results.

model parameters will be used to compute the output PSD of the model which is used to predict distortion in a digitally modulated signal environment.

7.2 CDMA Signal Distortion

Nonlinear distortion of digitally modulated signals is apparently fundamentally different from distortion observed with discrete tones. It has been shown in Chapters 3 and 5 that for digitally modulated signals, and in particular those with nonconstant envelope, nonlinearity results in distortion levels that cannot be predicted by traditional discrete tone testing. This gives the nonlinear statistical model developed in this thesis its importance. This is because the statistical approach is capable of relating distortion not only to nonlinear behavior but also to the statistical properties of the input signal and in particular the modulation format and the coding scheme. For multiple input channels, the problem is more sophisticated. First, the nonlinear model needs to be capable of predicting system performance given the variations of the nonlinear behavior with frequency and hence, the development of a behavioral model that includes the memory effects which has been discussed in the previous section. Second, the interaction of multiple channels by nonlinearity gives rise to extra distortion terms and this depends on the statistical contents of the input signals.

In this section, it will be demonstrated that the statistical models developed in Chapter 5 accurately captures distortion of multiple digitally modulated signals. The statistical model uses the behavioral model parameters extracted in Section (7.1) to develop the output spectrum and then the predicted nonlinear behavior, and in particular distortion levels, will be compared to measured values.

7.2.1 Forward Link Signal Generation

The forward link signal realizations were generated according to the IS-95 forward link standard shown in Fig. 5.3. Sixty four random streams each 2^{10}-bits long representing 64 user data streams were generated in MATLAB using a Gaussian random number generator. Each bit streams is then multiplied by one of the 64 Walsh codes generated by a 64×64 Hadamard matrix. The resulting spread data streams are then logically added. The resulting sequence is then modulo-2 added to orthogonal PN codes for the I and Q channels

and then filtered by a 50-tap IS-95 standard wave shaping filter. The resulting signal realization consists of 524,288 samples at a sampling rate of $8B$ where B is the bandwidth of the IS-95 channel and equal to 1.2288 MHz.

7.2.2 Reverse Link Signal Generation

The reverse link signal realizations were generated according to the IS-95 reverse link standard shown in Fig. 5.2. The I and Q random streams each 2^{16}-bit long that represent user data were generated in MATLAB using a Gaussian random number generator. The resulting sequence is then filtered by a 50 tap IS-95 standard wave shaping filter. The resulting signal realization consists of 524288 samples at a sampling rate of $8B$ where B is the bandwidth of the IS-95 channel.

7.2.3 Autocorrelation and Spectrum Estimation

The autocorrelation function of stationary random processes can be obtained from their time averages assuming ergodicity [32]. Therefore, for a single channel system, the autocorrelation function in (5.27) can be evaluated as

$$R_{z_n z_m}(\tau) = \lim_{T\to\infty} \frac{1}{2T} \int_{-T}^{T} z_1^{\frac{(n+1)}{2}} z_1^{*\frac{(n-1)}{2}} z_2^{\frac{(n-1)}{2}} z_2^{*\frac{(n+1)}{2}} dt. \tag{7.1}$$

and for two channel system, the autocorrelation function in (5.30) is evaluated as

$$R_{z_n z_m u_l u_k}(\tau) = \lim_{T\to\infty} \frac{1}{2T} \int_{-T}^{T} z_1^{\frac{(n+1)}{2}-l} z_1^{*\frac{(n-1)}{2}-l} z_2^{\frac{(n-1)}{2}-k} z_2^{*\frac{(n+1)}{2}-k} u_1^l u_1^{*l} u_2^k u_2^{*k} dt. \tag{7.2}$$

The above autocorrelation functions were computed using the signal realizations of both the reverse and forward link in MATLAB using a biased autocorrelation estimator. The output spectrum was computed from the FFT of the computed autocorrelation functions and incorporating the behavioral model parameters (polynomial coefficients and linear filters transfer functions) developed in the previous section. A Hanning window is used to remove spectral leakage. The output spectrum was simulated using both the memoryless and the three-box models. Fig. 7.11 shows simulated output spectrum of a single reverse link CDMA signal and the memoryless model divided into linear and intermodulation components while Fig. 7.12 shows the output spectrum divided into linear, intermodulation and

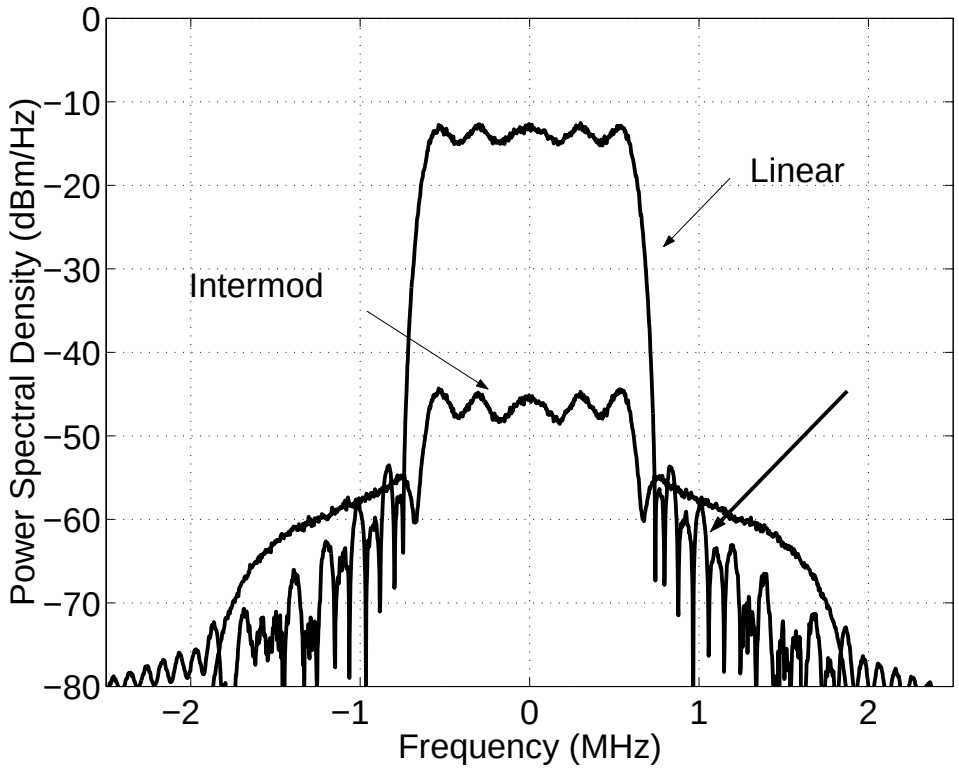

Figure 7.11: Output power spectral density of a nonlinear PA driven by a reverse link IS-95 CDMA signal.

cross-modulation components for a forward link CDMA signal centered at 2.1 GHz assuming that the nonlinear model is excited by the sum of two CDMA channels centered at 2.0 and 2.1 GHz. The output spectrum shows the increase in spectral regrowth and In-Channel distortion over single channel excitation due to cross modulation.

Similar simulations were done for the three-box model. The two channels are centered at 2.0 and 2.1 GHz and the calculated spectrum at the output of the amplifier is shown in Fig. 7.13. At this scale only the carriers of the channels are seen at 2.0 GHz, (a), and 2.1 GHz, (b); and intermodulation components at 1.9 GHz, (c), the lower intermodulation component; and at 2.2 GHz, (d), the upper intermodulation component. This is just the spectrum that would be observed with two tones — unmodulated sine waves — exciting the amplifier. The digitally modulated structure of the channels can be seen in Fig. 7.14 where the components of the spectrum are expanded and the parts of the figure are as indicated in Fig. 7.13. Fig. 7.14 shows the simulated output spectra with the level of the channel at

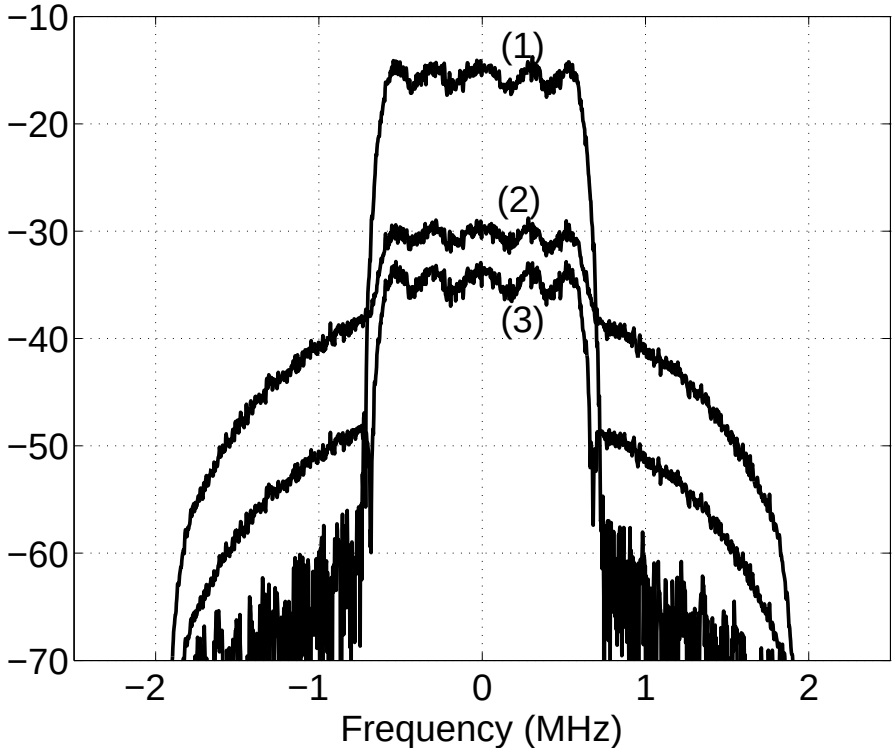

Figure 7.12: Output Spectrum of a nonlinear PA driven by a forward link IS-95 CDMA signal. The spectrum is partitioned into: (1) linear, (2) cross modulation, and (3) intermodulation components.

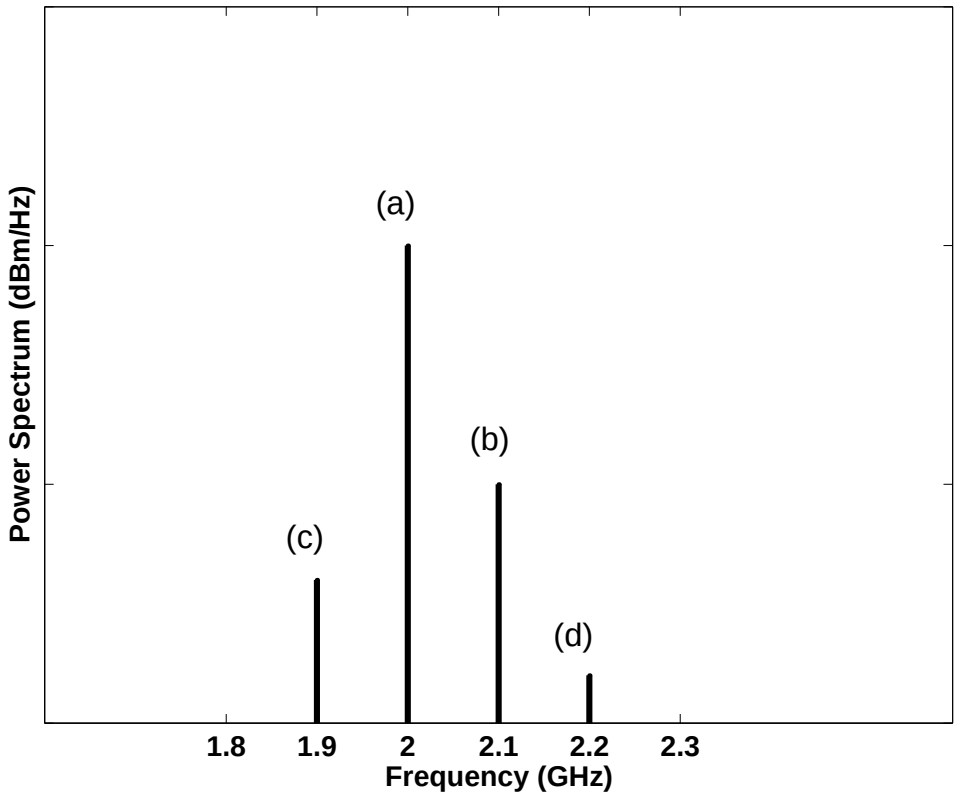

Figure 7.13: Spectrum at the output of the amplifier with two CDMA channels, (a) and (b), applied.

2.1 GHz held constant at −20 dBm and the power of the channel at 2.0 GHz varied from −25 to −5 dBm. The figure shows how the Adjacent Channel Power Ratio (ACPR) at the second carrier increases as the power level of the first carrier is swept. The predictions of the model were verified using ACPR measurements performed on the amplifier. Fig. 7.15 and 7.16 show the intermodulation spectra that result at 2.0 and 2.3 GHz and their corresponding memoryless model output where a discrepancy is seen and this is due to memory effects which the three-box model predicts.

7.2.4 Gaussian Approximation

As shown in the previous section, the output autocorrelation function for a Gaussian input process is given as a function of the first order autocorrelation function. Therefore, in order to find the output spectrum, we need to estimate the input autocorrelation function

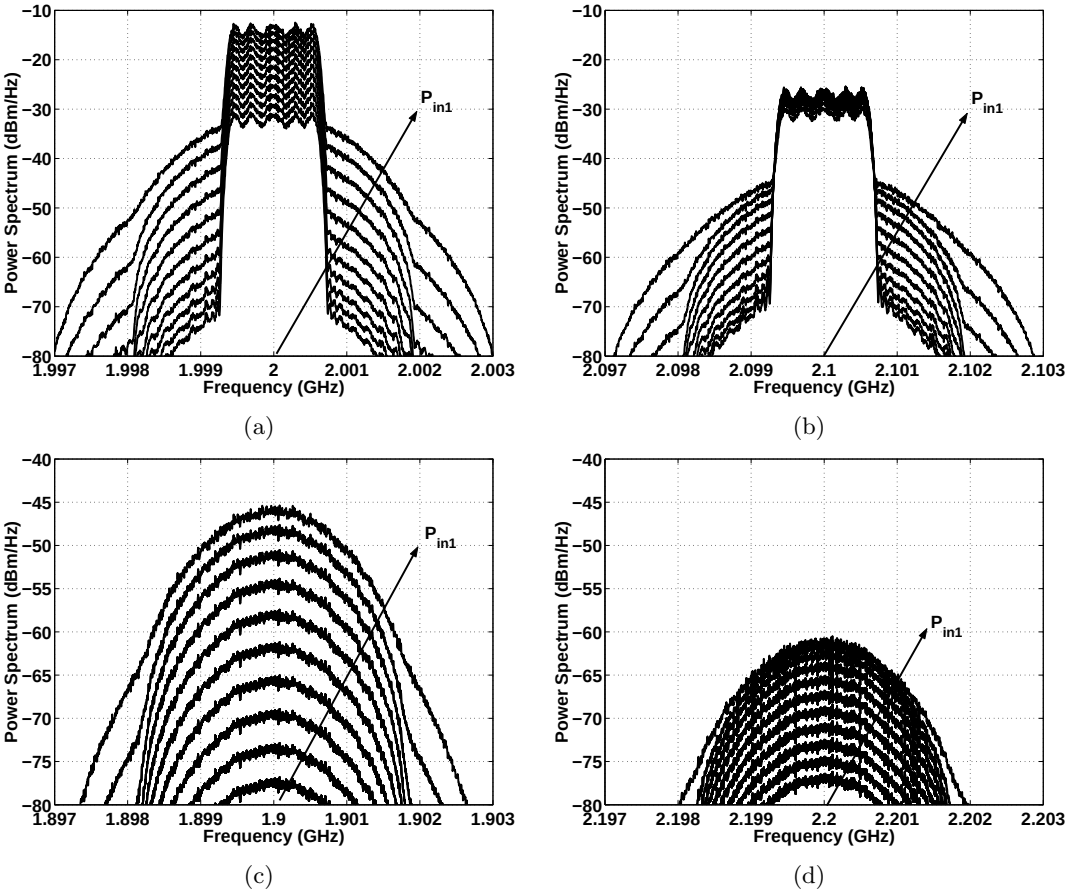

Figure 7.14: Simulated output spectrum: (a) first CDMA channel, (b) second CDMA channel, (c) lower intermodulation component; and (d) upper intermodulation component. Shown are expansions of the corresponding components, (a) through (d), of the broad spectrum shown in Fig. 7.13

.

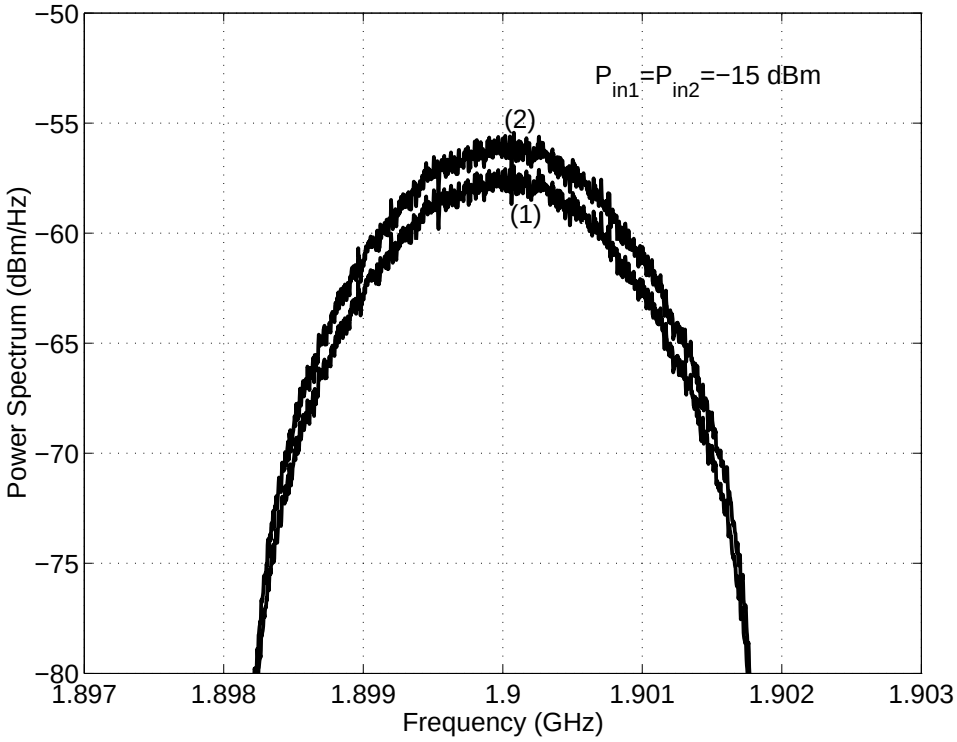

Figure 7.15: Simulated spectrum of the lower intermodulation component with: (1) the memoryless; and (2) the three-box models.

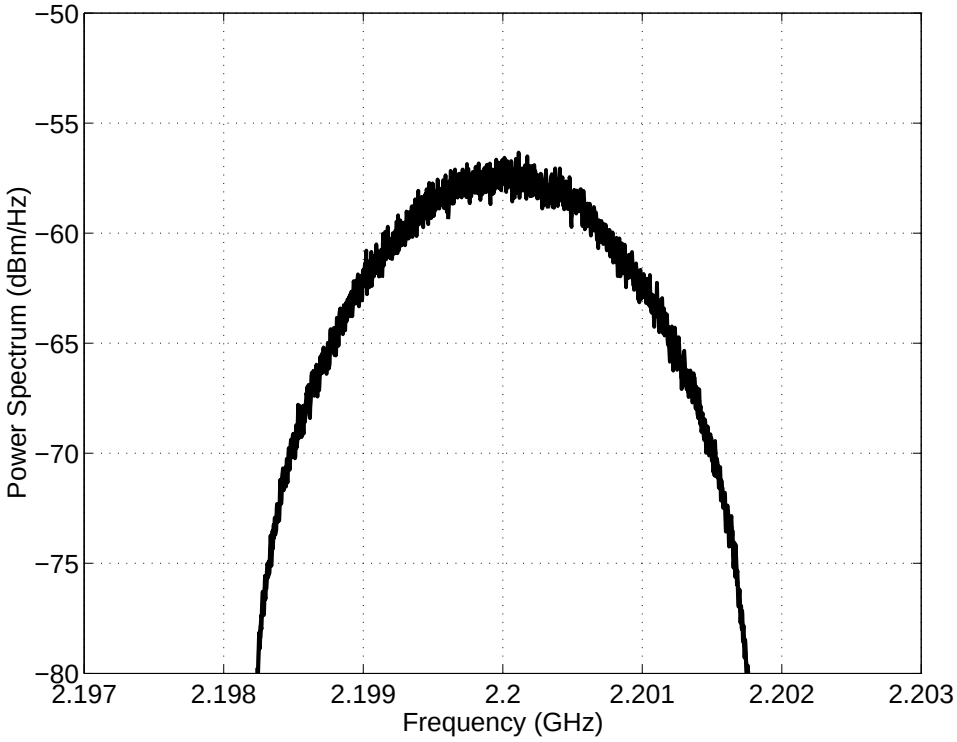

Figure 7.16: Simulated spectrum of the upper intermodulation component with the memoryless and three-box models (the two spectra coincide)

$R_{ww}(\tau)$. This autocorrelation function reduces to a NBGN process when the pulse shaping filter is $h(t) = \text{sinc}(Bt)$ function and therefore

$$R_{\tilde{w}\tilde{w}}(\tau) = \sigma^2_{\tilde{w}}\text{sinc}(B\tau). \tag{7.3}$$

and it follows that

$$S_{\tilde{w}\tilde{w}}(f) = \sigma^2_{\tilde{w}}\text{rect}\left(\frac{f}{2B}\right). \tag{7.4}$$

which is the box shaped spectral density. Figs. 7.17(a) and (b) show the output spectrum computed using signal realization of both the reverse and forward links and from the NBGN assumption for single channel input and using the memoryless model, and Fig. 7.18 shows the simulated ACPR over swept input power. The forward link spectrum is shown for a fully loaded system (K=64) where it is clear that the Gaussian assumption agrees well with actual signal realization. For the reverse link the Gaussian assumption overestimates ACPR by around 6 dB which agrees with the results obtained by [5]. Fig. 7.17 shows the output spectrum computed using signal realization of the forward link and from the NBGN assumption for two channel input where a close agreement is shown. The Gaussian assumption is shown to be reasonably acceptable for the forward link since the transmitted signal consist of a big number of Walsh-coded data sequences which- by central limit theorem, approaches the Gaussian distribution. However, the accuracy of such an assumption decreases if the composite signal is lightly loaded.

7.2.5 Receiver Desensitization

The receiver desensitization problem was also modeled using the generalized statistical analysis of multiple channels in Chapter 5. Fig. 7.20 presents the output spectrum of a single tone when the power amplifier is driven by a single tone and a forward link signal, (Fig. 7.20(a)), and a single tone with a reverse link signal, (Fig. 7.20(b)). The spectrum, developed using (4.4), shows how the spectrum is widened because of the mixing with the modulated CDMA carrier as a result the nonlinear interaction or cross modulation. If the CDMA signal is a reverse link signal, then cross modulation appears as a double hump similar to that predicted in [48] using a circuit level model. On the other hand, if the CDMA signal is a forward link signal, then cross modulation appears close to a triangular shape which is similar to that predicted with the NBGN assumption. This is due to the

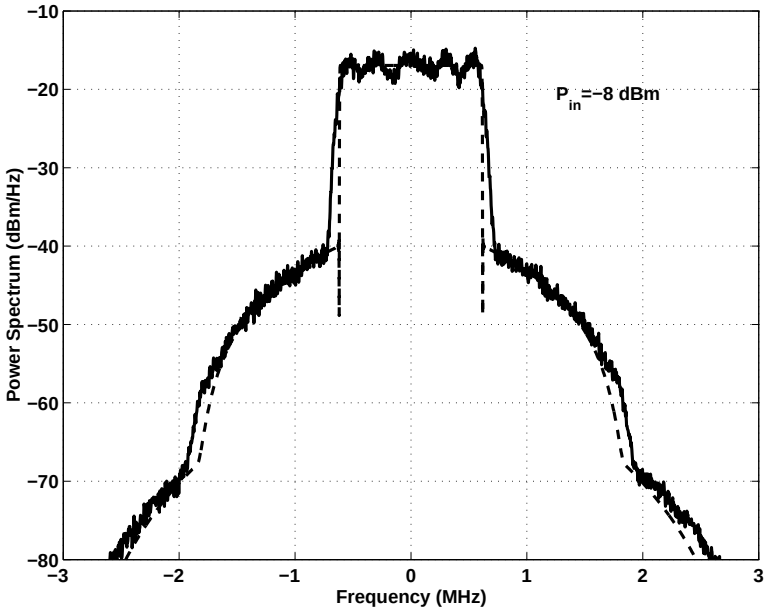

(a)

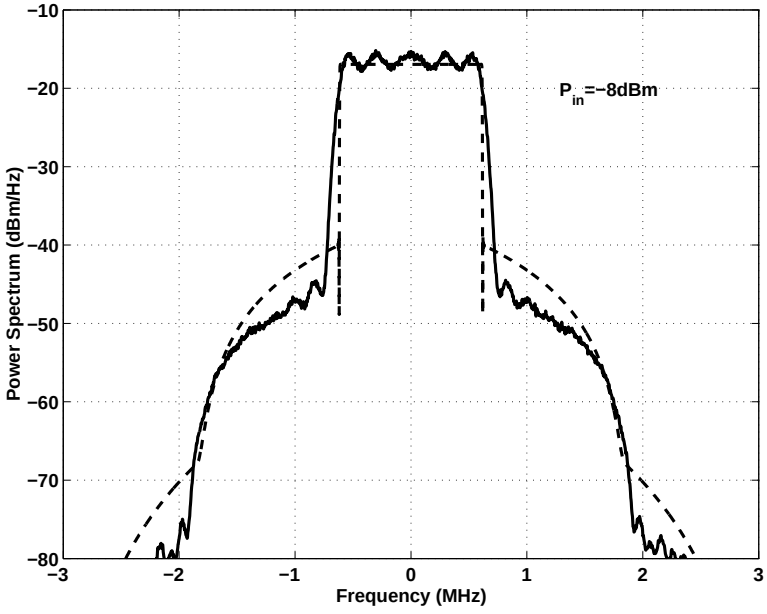

(b)

Figure 7.17: Simulated output spectrum using signal realization (solid) and NBGN model (dashed); (a) forward link and (b) reverse link.

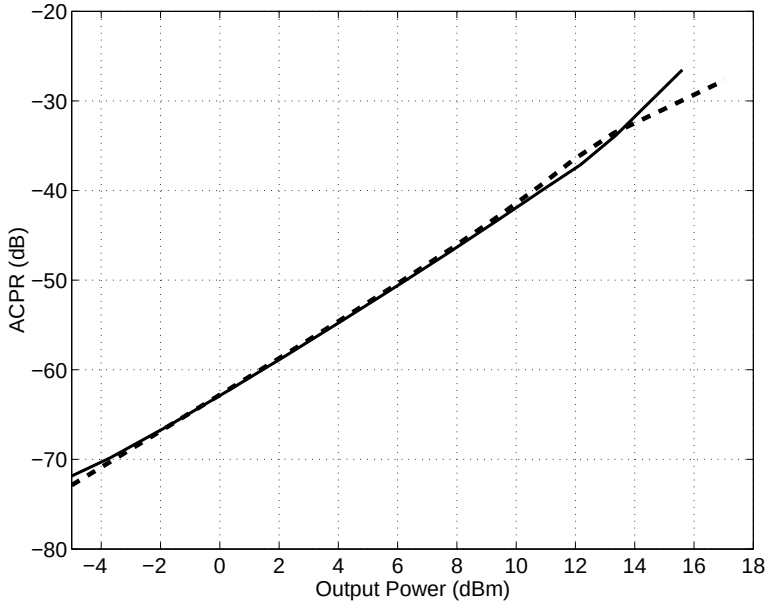

(a)

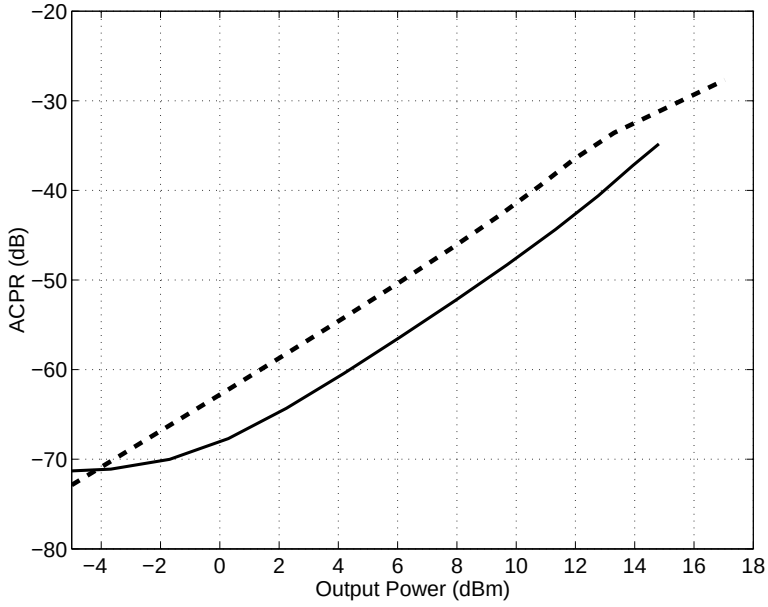

(b)

Figure 7.18: Simulated ACPR versus output power using signal realization (solid) and NBGN model (dashed); (a) forward link and (b) reverse link.

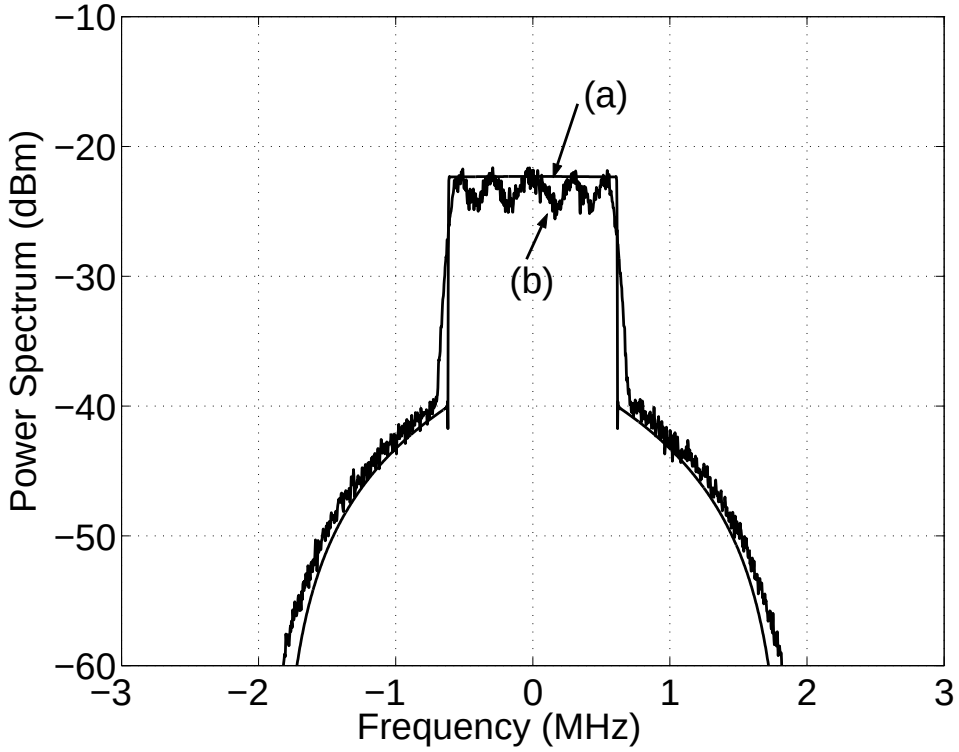

Figure 7.19: Output power spectrum for two-channel input using: (a) Gaussian assumption; and (b) actual signal realization.

fact that the NBGN assumption is better suited to modeling the forward link than the reverse link. Fig. 7.21, shows the cross modulation power in a 30 kHz bandwidth at an offset of 885 kHz from the center frequency of the single tone. The first curve shows cross modulation power as a function of swept input power of the CDMA signal (forward link) in a 25 dBm range ($P_{\text{CDMA}} = -30$ dBm to -5 dBm, $P_{\text{jam}} = -10$ dBm), while the second curve shows the cross modulation power as a function of swept input power of the single tone jammer itself in the same power range ($P_{\text{jam}} = -30$ dBm to -5 dBm, $P_{\text{CDMA}} = -10$ dBm). The two curves show that the jammer power contributes much more strongly to the cross modulation power than the power of the CDMA signal.

7.2.6 Measurements of Distortion

The statistical model was verified experimentally. ACPR and gain compression were predicted from the simulated spectrum as discussed in the previous section. The amplifier whose model was extracted in Section 7.1 was tested with IS-95 forward channel signals using a Vector Signal Generator (VSG) and a Vector Signal Analyzer (VSA). The amplifier was driven by two IS-95 fully loaded forward link channels centered at 2.0 and 2.1 GHz. The ACPR measurements were performed for the signal at 2.1 GHz. Fig. 7.22, shows gain compression and ACPR of the first channel as a function of its output power and the second channel input power. Close agreement with the statistical nonlinear model is shown. Fig. 7.23 shows measured Gain compression and ACPR at the first carrier using the memoryless and the three-box models where it clear that the three-box model predicts ACPR more accurately than the memoryless model.

7.3 Summary

The behavioral model was used to develop a statistical analysis for multiple digitally modulated signals from which the output spectra can be developed. This enables the accurate estimation of intermodulation and cross-modulation distortions which are of great concern in multichannel PA design. It has been shown that the memoryless model with the multi-envelope parameter extraction technique gives good results when the frequency separation between input channels is small enough to have no variations of the AM-AM and AM-PM

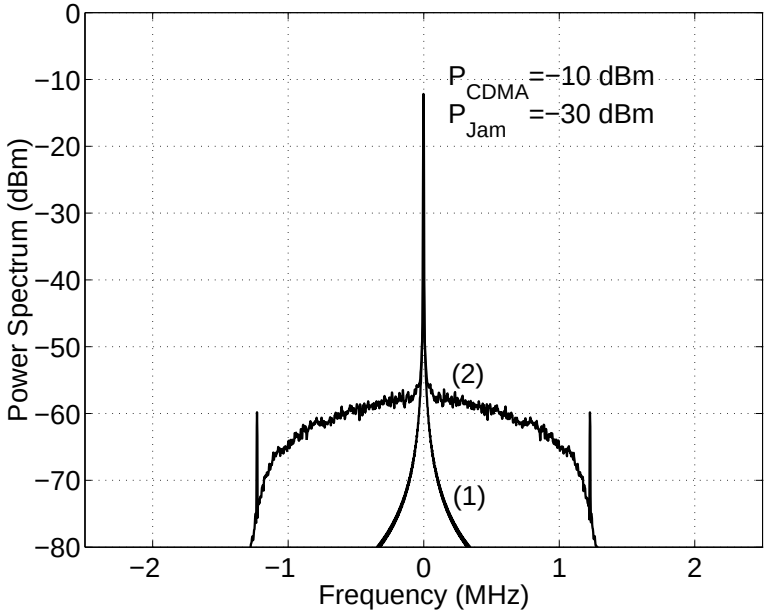

(a)

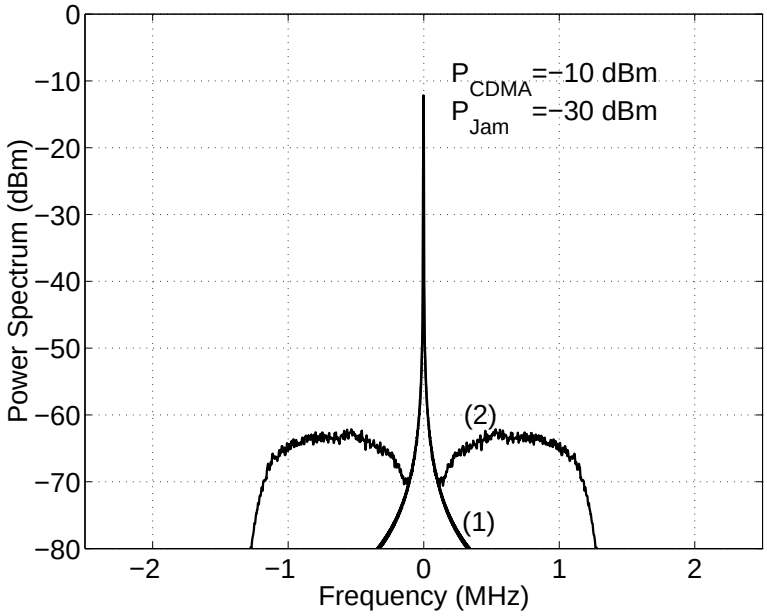

(b)

Figure 7.20: Spectrum of a single tone with: (1) no cross modulation and (2) cross modulation by mixing with a CDMA signal: (a) forward link and (b) reverse link.

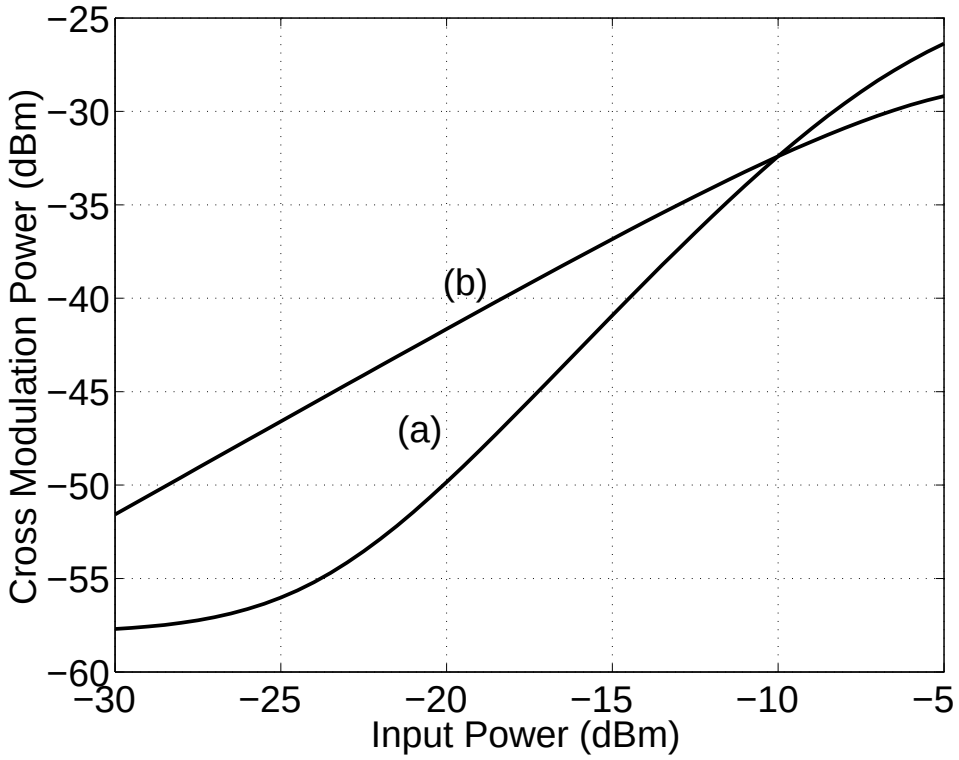

Figure 7.21: Cross modulation power over swept input power: (a) CDMA signal power, and (b) Jammer power.

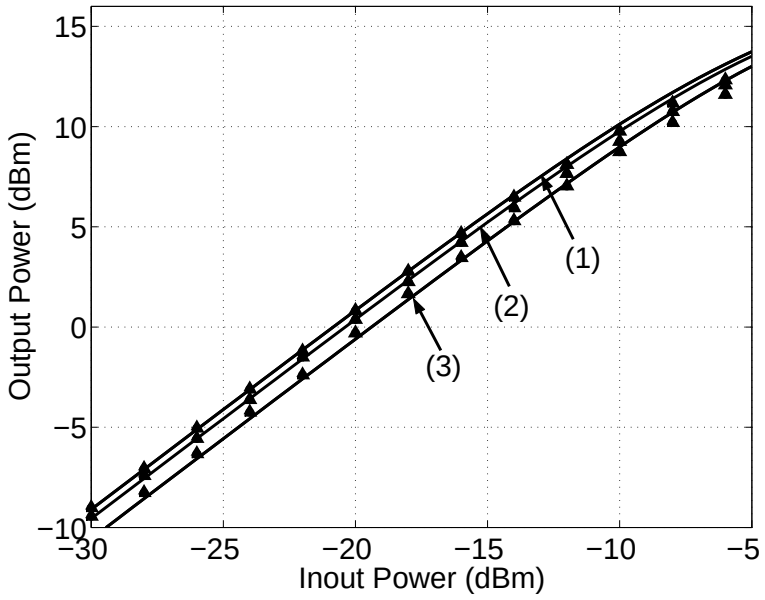

(a)

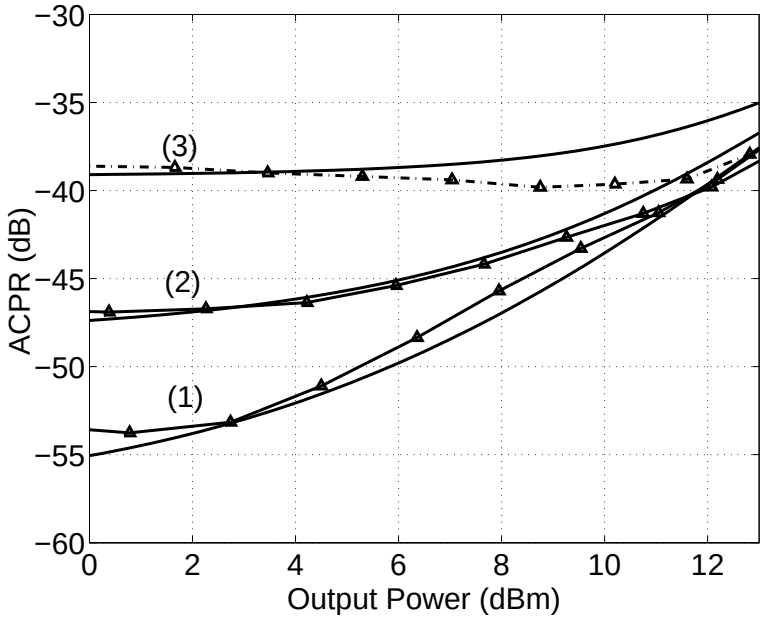

(b)

Figure 7.22: Nonlinear response: (a) Gain compression at the first carrier; and (b) ACPR of the first carrier with second carrier at (1) -20 dBm, (2) -15 dBm and (3) -10 dBm (Solid: simulated, △: measured).

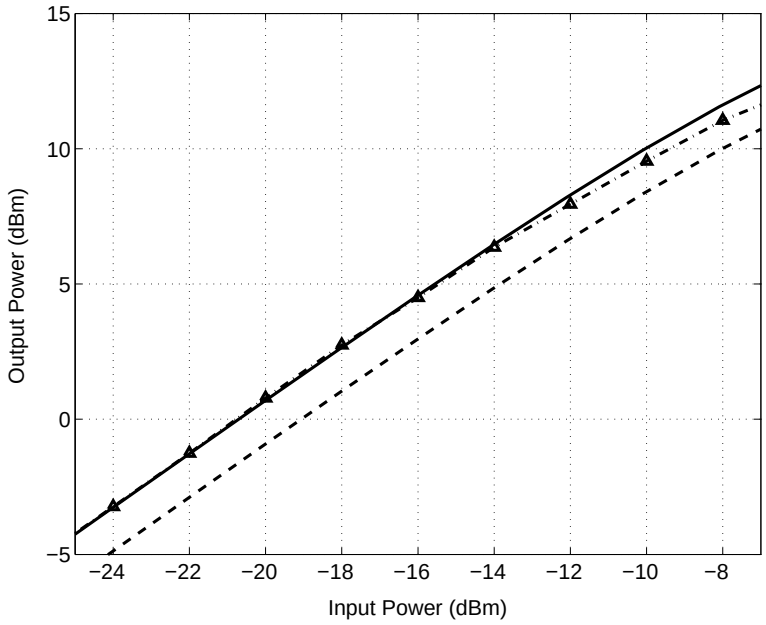

(a)

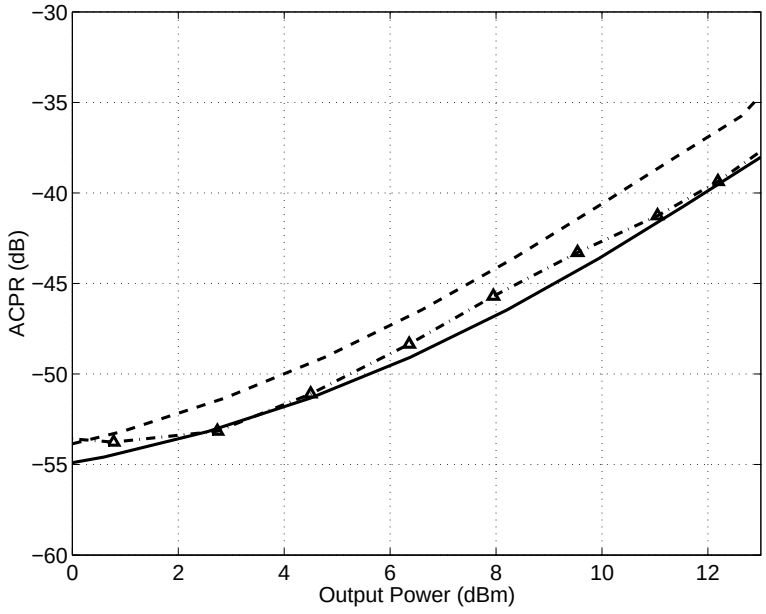

(b)

Figure 7.23: Nonlinear response of the three-box model: (a) Gain compression; and (b) ACPR at the first carrier with the second carrier at -20 dBm, solid line: simulated (three-box), broken line: simulated (memoryless) and •: measured.

characteristics with frequency. Using the three-box model provides better accuracy in the estimation of distortion than does the memoryless model commonly used when only single-tone characterization is available. This is because the three-box model adequately captures the nonlinear response with multiple channels with significant frequency separation of the channels as well as their power levels.

The statistical model shows that intermodulation and cross modulation distortions depend on the statistical properties of the signal which are captured by the autocorrelation function. In a forward link CDMA system, distortion depends on the number of data channels (users) and the selection of Walsh codes involved in the composite signal. This is because the transmitted signal exhibits a PAR that depends on the Walsh codes involved in the composite waveform. It has also been shown that the Gaussian assumption results in a simplified analysis of the autocorrelation function while it gives a good estimate of distortion in the forward link. The analysis that has been presented provides an insight into the design of multichannel amplifiers and CDMA systems.

7.4 Relation between Analog and Digital Signal Distortion

A relationship between IMD of discrete tone signals and SR of digitally modulated signals has long been supposed as they are both due to the same nonlinear processes. A detailed investigation of IMD and SR for various combinations of devices and types of signals (discrete tone and two digitally modulated formats) was previously reported indicating little apparent relationship. This is due to many reasons: first, digitally modulated signal fills the spectrum in a channel and cannot be represented as a collection of discrete tones. Second, the spectral regrowth process results from the third and higher order mixing products not only the third order which means that the correlation between IMR and ACPR becomes lower if the higher order nonlinearities are involved. Thus any simple concepts attempting to relate IMR to ACPR are in effect using third order information to extrapolate to higher order information. Clearly, this is something that can only very approximately be done with the inherent assumption that the magnitudes of the terms decrease with increasing order. Third, while a sinusoid have a Peak to Average Ratio (PAR) of 3 dB, a digital signal experience a higher PAR that ranges from 4.5 dB to 12 dB, which in turns imposes higher linearity requirements for digital signals to prevent compression or clipping of signal

Table 7.2: P_{1dB} and $IIP_3 - P_{1dB}$ for different maximum order of nonlinearity

Order	P_{1dB}	$IIP_3 - P_{1dB}$
3	-5.1	9.6
5	-8.3	12.8
7	-8.4	12.9
13	-8.4	12.9

extremes. Thus, at the peaks of the signals, the nonlinear amplifier is operating at its most extreme nonlinearity. The PAR is a function of the number of code channels transmitted on one carrier frequency, the characteristics of the baseband filter and on the modulation scheme. Therefore, the distortion introduced by the nonlinear process is more dependent on the characteristics of the signal rather than the characteristics of the power amplifier itself, which are usually modeled by two-tone intermodulation test. Generally, it may be assumed that a device that has better IMR could have better ACPR.

In this section we will prove experimentally that this relationship is very weak and it depends on the order of the nonlinear model. The intermodulation and the statistical analyses in chapter 3 were used to simulate distortion in both analog and digital systems. The amplifier considered here is the GaAs MESFET driver amplifier described in [34], where a complex power series of order 13 was fitted to the AM-AM and AM-PM measured data.

7.4.1 Intermodulation Distortion

Fig. 7.24, shows the third-order intermodulation ratio vs. output power for a two-tone input signal around 2 GHz. Initially, the IMR_3 is a third order process depending only on the third order power series term. As the level of input tones increase, the higher order terms of the behavioral model becomes important and the P_{IM3} vs. P_{in} curve does not have a constant slope of 3 as expected. The slope grows above 3 after a certain limit. This is seen with the measured and calculated IMR_3. The measured IMR_{3L} and IMR_{3U} are almost identical. Fig. 7.25 shows the output power vs. input power for different maximum orders of nonlinearity. Table shows the and the difference between and for different maximum orders of nonlinearity. In all the simulations, it can be seen that considering the fifth order term is important in capturing the response up to medium to large power levels. However, little is gained by considering a higher order behavioral model.

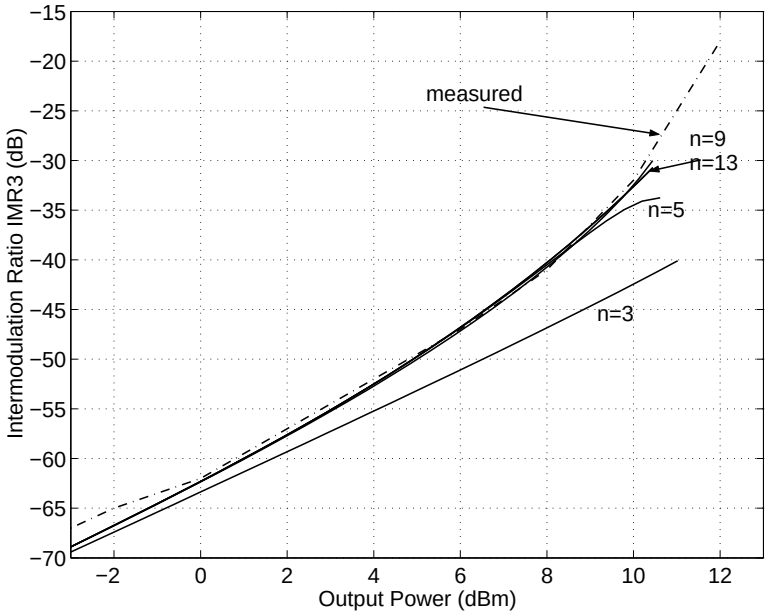

Figure 7.24: Intermodulation Ratio (IMR3) for different maximum order of nonlinearity.

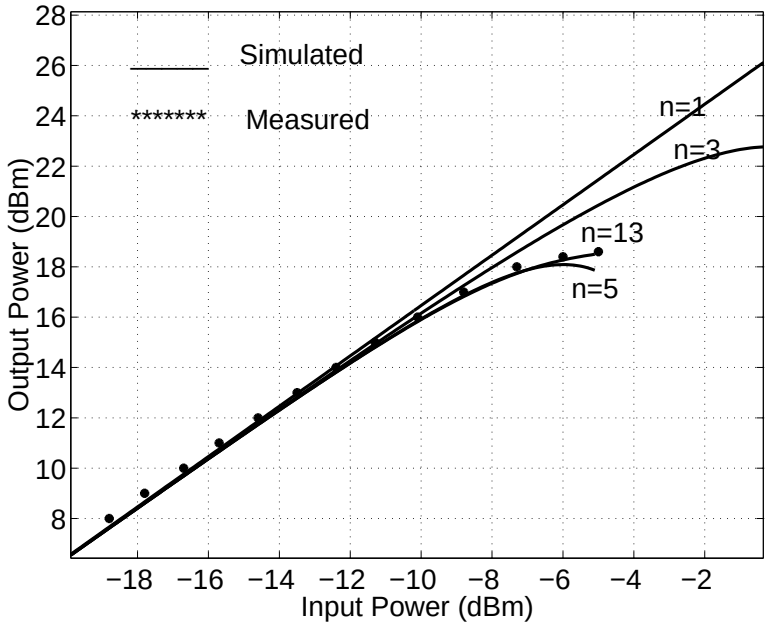

Figure 7.25: 1 dB compression Point with different orders of nonlinearity.

7.4.2 Adjacent Channel Power Ratio

The response of the amplifier considered previously was simulated with a CDMA signal at 900 MHz. The measured and calculated results for ACPR using different maximum orders of the behavioral model are shown in Fig. 7.26. Low order behavioral models, predict the proper trend in the ACPR but the agreement with measurements is good only when very high order (11 th or 13 th) behavioral models are used.

7.4.3 Summary

We have shown that the third order assumption in modeling power amplifiers is not adequate to capture the distortion introduced by the nonlinear behavior and therefore, a relationship between IMR and ACPR cannot be established adequately. The simulations showed that for analog systems, considering fifth order of nonlinearity is enough to give good estimates of IMR while eleventh order is necessary to estimate the ACPR in a digital RF system.

7.5 Probability of Error

The analytical model derived in Chapter 6 was verified by simulations. The forward link signal generated in Section 7.2 was applied to the nonlinear model and then AWGN was added to the distorted signals. The resulting signal was then decoded according to Fig. 6.1. The input power of the signal was swept and the number of erroneous bits were counted at each power level and E_b/N_o. Fig. 7.29 shows the probability of error as a function of signal to noise ratio and at different power levels using the analytical model. The analytical model shows a good agreement with the simulated values.

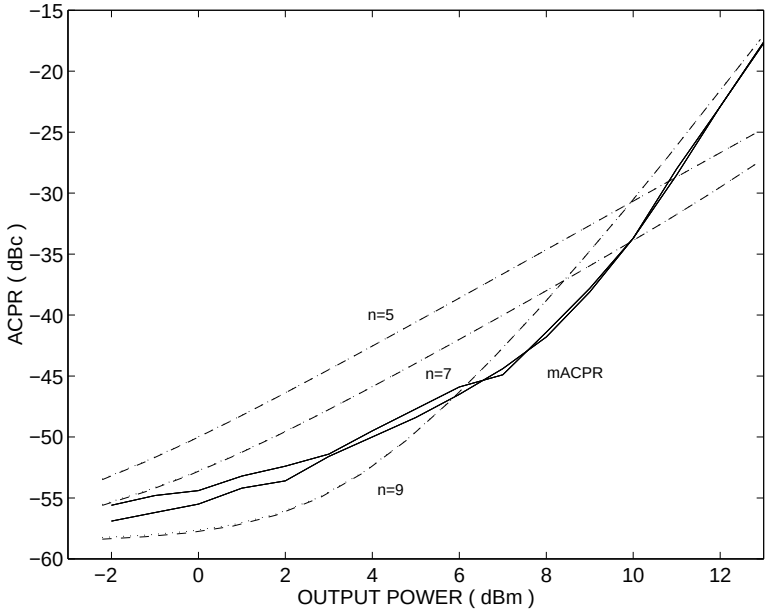

(a)

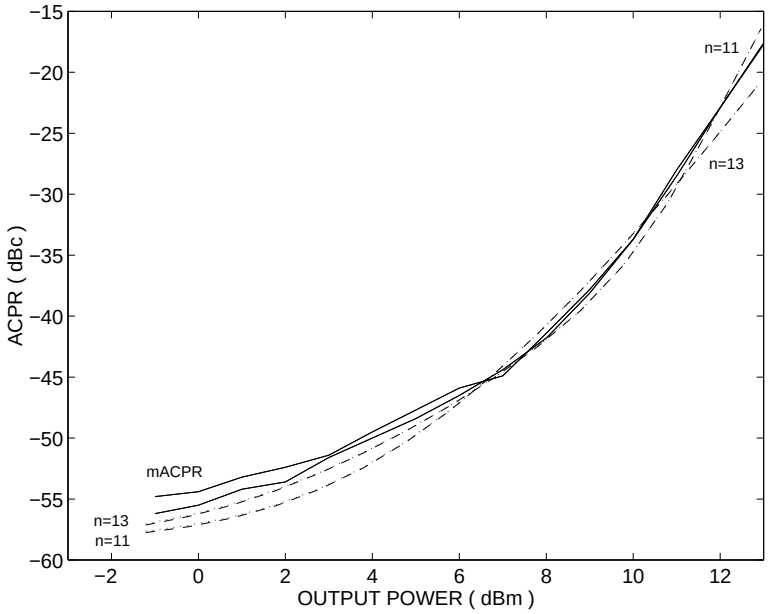

(b)

Figure 7.26: ACPR with different orders of nonlinearity (a) using a maximum order of (3,5,7,9) and; (b) using a maximum order of (11,13); solid: simulated and; dashed: measured.

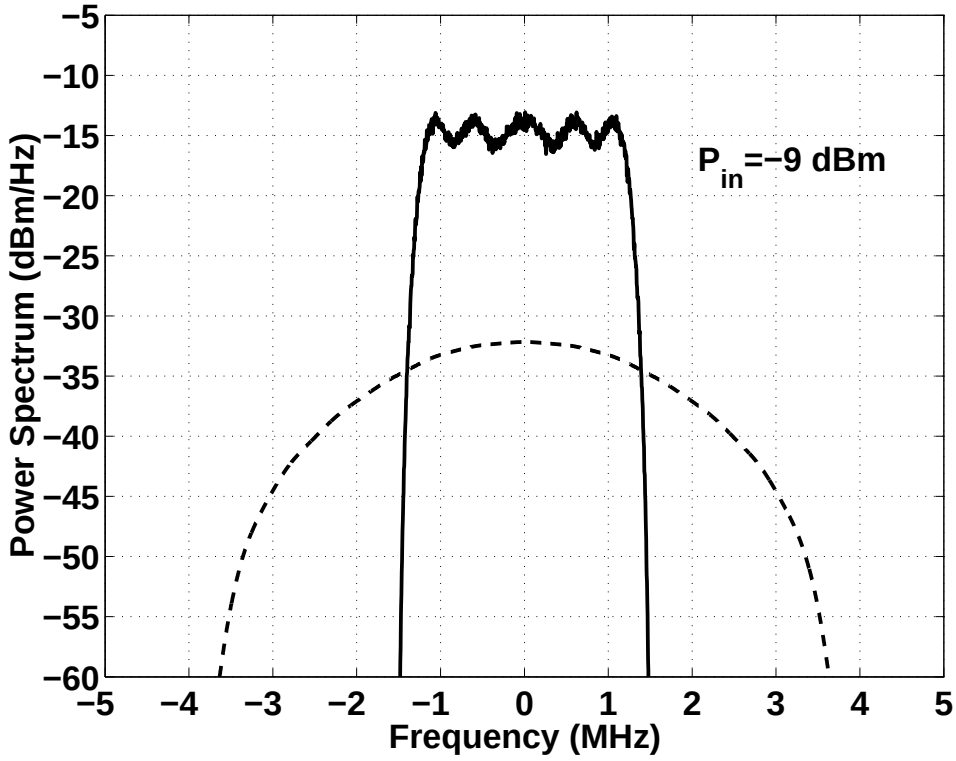

Figure 7.27: Output spectrum partitioned into linear and distortion components.

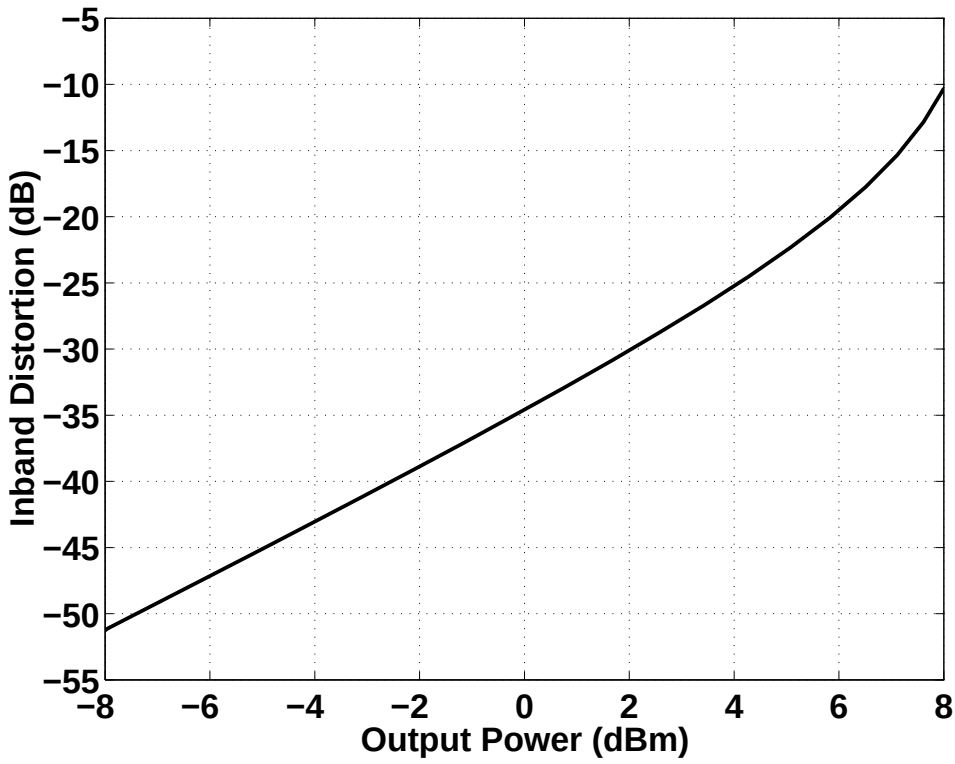

Figure 7.28: In-band distortion as a function of output power.

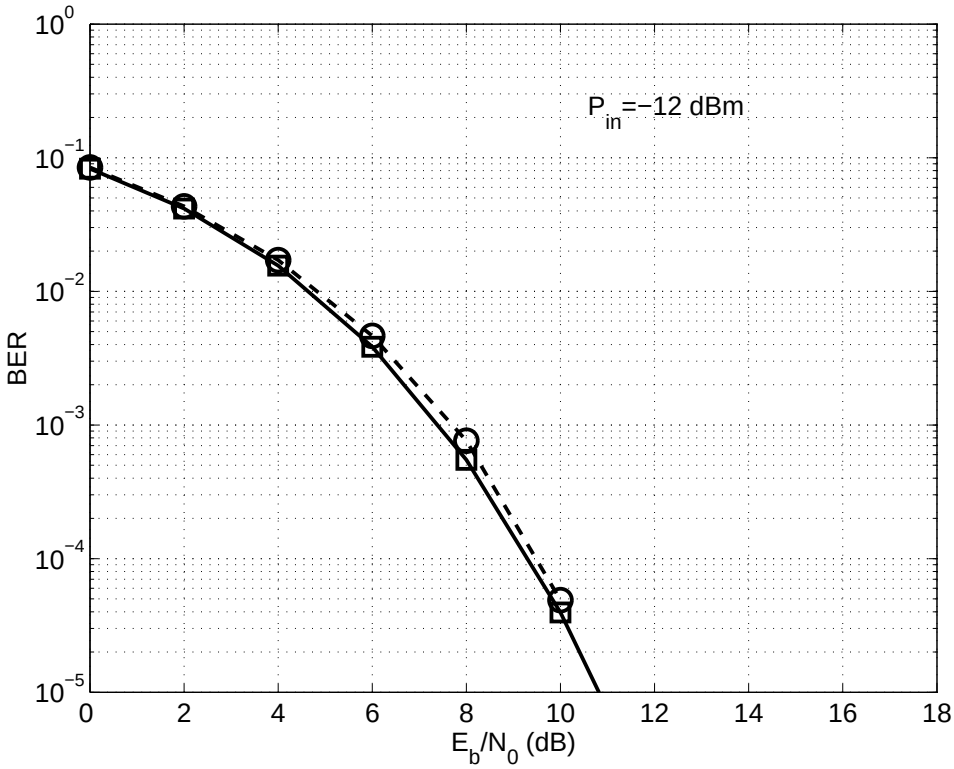

(a)

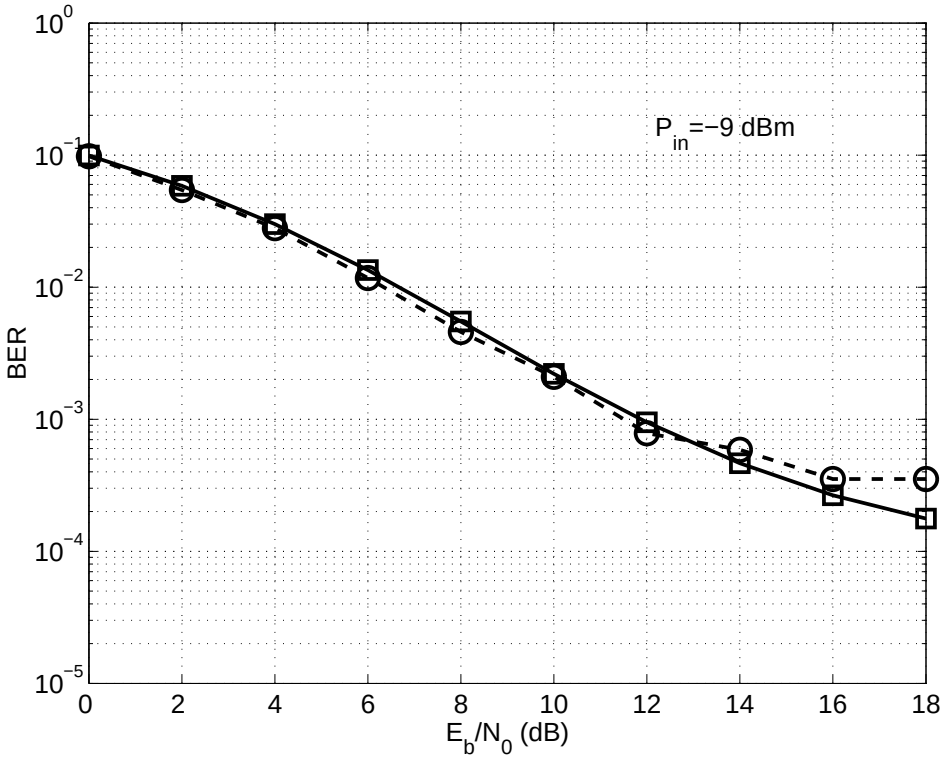

(b)

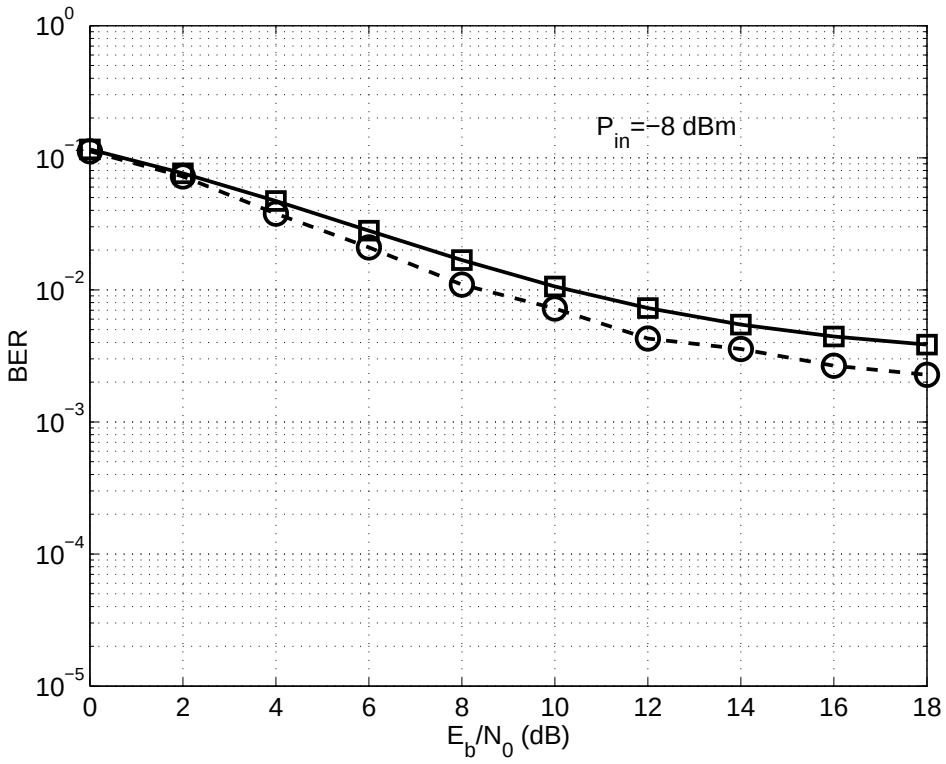

(c)

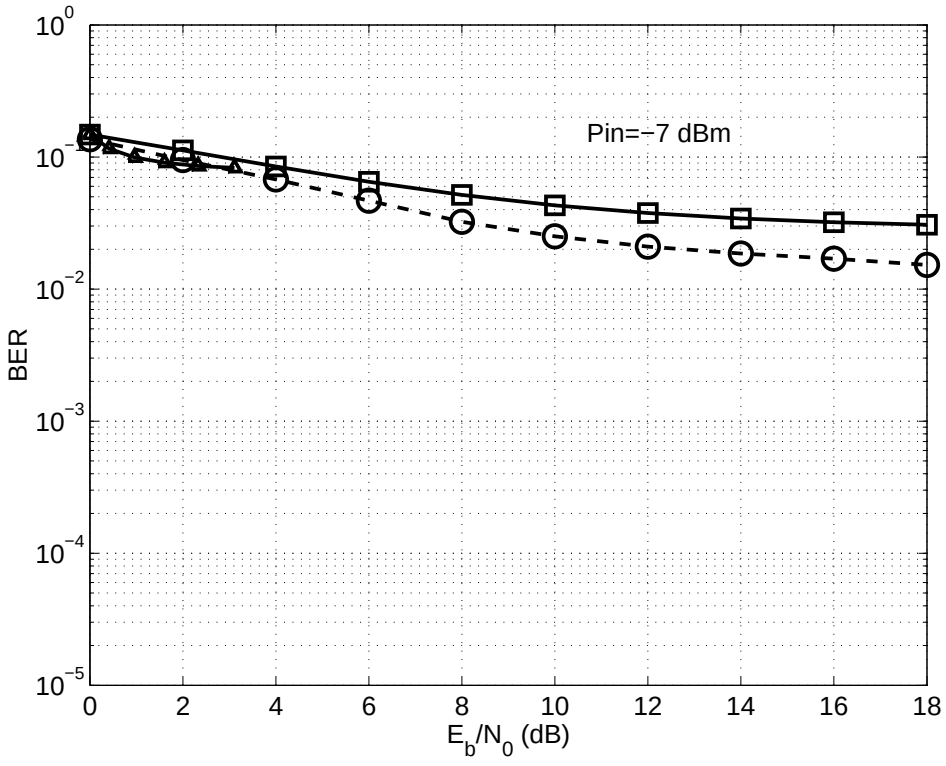

(d)

Figure 7.29: Probability of error at different input power levels: (a) -12 dBm; (b) -9 dBm; (c) -8 dBm; and (d) -7 dBm; △ analytical model and ∘ simulation.

Chapter 8

Conclusions And Future Work

8.1 Conclusions

A generalized statistical analysis for modeling the interaction of multiple channels in a nonlinear amplifier has been introduced and verified. The statistical model shows that intermodulation and cross-modulation distortions depend on the statistical properties of the signal which are captured by the autocorrelation function. In a forward link CDMA system, distortion depends on the number of data channels (users) and the selection of Walsh codes involved in the composite signal. This is because the transmitted signal exhibits a PAR that depends on the Walsh codes involved in the composite waveform. It has also been shown that the Gaussian assumption results in a simplified analysis of the autocorrelation function while it gives a good estimate of distortion in the forward link. The analysis that has been presented provides an insight into the design of multichannel amplifiers and CDMA systems.

The statistical model was coupled with the development and verification of new behavioral modeling techniques for modeling the interaction of multiple digitally modulated signals in a multichannel RF system. The memoryless model with its novel parameter extraction technique captures the behavior of the amplifier when the frequency separation between input channels is small. The three-box approximation of the Volterra model captures the memory effects of a nonlinear power amplifier. In particular, the three-box

model was shown to capture the behavior of a nonlinear amplifier with self-similar shapes of the AM-AM characteristics at frequencies across the band of interest. The parameters of the three-box model were extracted using simple VNA measurements, however, more complicated schemes such as two-tone characterization could be used to enhance model accuracy. It has been shown that using the three-box model provides better accuracy in the estimation of distortion than does the memoryless model commonly used when only single-tone characterization is available. This is because the three-box model adequately captures the nonlinear response with multiple channels with significant frequency separation of the channels as well as their power levels.

In summary this work establishes a methodology for the design of multichannel communication systems by relating distortion introduced by nonlinear devices to the system design with no restrictions on the number of input channels or their frequency separation. In particular we show that a nonlinear RF system can be characterized using simple measurements and so the model can be used with the statistical characterization of multiple digitally modulated signals to determine spectral regrowth, cross-modulation and system bit error rate. Thus the analysis technology presented here can be used to predict system performance prior to fabrication.

8.2 Future Work

8.2.1 Walsh Code Selection

As shown in the Chapter 5, CDMA signals exhibit distortion levels that depends on the statistics of the input signals which is captured by the autocorrelation function. In a forward link Direct Sequence Spread Spectrum (DS-SS) CDMA system, signal statistics can be controlled by the selection of active Walsh codes incorporated in the composite signals.

In a DS-SS system, each CDMA channel supports K users. However, not all users are active at the same time and therefore, a subset of the available Walsh codes are used. Braithwaite [57] studied the effect of Walsh codes on the level of distortion in a multichannel system where he developed a cost function to quantify the effect of Walsh codes on the power variance of the composite signal. The cost function was defined for a third order memoryless

system as:

$$\begin{aligned} J &= E\left[\left|\frac{G(|\tilde{w}|)-G_0}{G_0}\right|^2\right] \\ &= |\bar{b_3}|^2 E\left[|\tilde{w}|^4\right]. \end{aligned} \tag{8.1}$$

This cost function represents, on average, the distortion relative to the linear output and is proportional to the 4 th moment of the input signal. A more realistic parameter is the normalized power variance which is defined as:

$$v_e = \frac{E\left[|\tilde{w}|^4\right]}{E[|\tilde{w}|^2]^2} \tag{8.2}$$

The normalized power variance represents a more realistic figure of merit than the traditional PAR since it is an expected value. Using the forward link signal model the 4 th moment of the signal $\tilde{w}(t)$ can be evaluated as:

$$\begin{aligned} E\left[|\tilde{w}|^4\right] = \quad & \left[3\sigma_w^4 - 2\sum_{i=0}^{K-1}\rho_i^4\right]\overline{f(t)} + 2\sigma_w^4(1-\overline{f(t)}) \\ & +2\sum_{n,m=0}^{K-1} Q_{i,j}^w(n,m)\overline{h^2(t-nT)h^2(t-mT)} \end{aligned} \tag{8.3}$$

where

$$f(t) = \sum_n h^4(t-nT) = \frac{2}{3} + cos(\frac{2\pi t}{T})$$

and the over bar indicates the time average over the bit period:

$$\overline{x(t)} = \int_0^{(K-1)T} x(t)dt$$

Note that the only term that can be controlled in the expression (8.3) is the Q term which is a function of Walsh codes. Agilent [91] Identified the most troublesome combinations of Walsh codes that yield maximum distortion. In [57], Braithwaite studied 6 sets of 9 codes selected from a space of 64 codes as shown in Table (8.1). Fig. (8.1), shows the output spectrum of the signals in Table (8.1) computed using the concepts developed in Chapter 5. The spectral regrowth is shown to be proportional to the cost function computed in [57].

The normalized power variance was adequate to identify the most troublesome combinations of Walsh codes. However, the analysis was done assuming third order nonlinearity which is not adequate to model distortion as shown in Chapter 7. What is really

Table 8.1: Walsh Code sets

Set No.	Active Walsh Codes	v_e
Set 1	$W_0, W_4, W_32, W_8, W_16, W_24, W_40, W_48, W_56$	3.2
Set 2	$W_0, W_1, W_32, W_58, W_59, W_60, W_61, W_62, W_63$	2.45
Set 3	$W_0, W_1, W_32, W_2, W_4, W_8, W_15, W_16, W_51$	2.55
Set 4	$W_0, W_1, W_32, W_2, W_3, W_4, W_5, W_6, W_7$	2.44
Set 5	$W_0, W_1, W_32, W_8, W_9, W_10, W_11, W_12, W_13$	2.48
Set 6	$W_0, W_1, W_32, W_2, W_4, W_8, W_13, W_16, W_18$	2.59

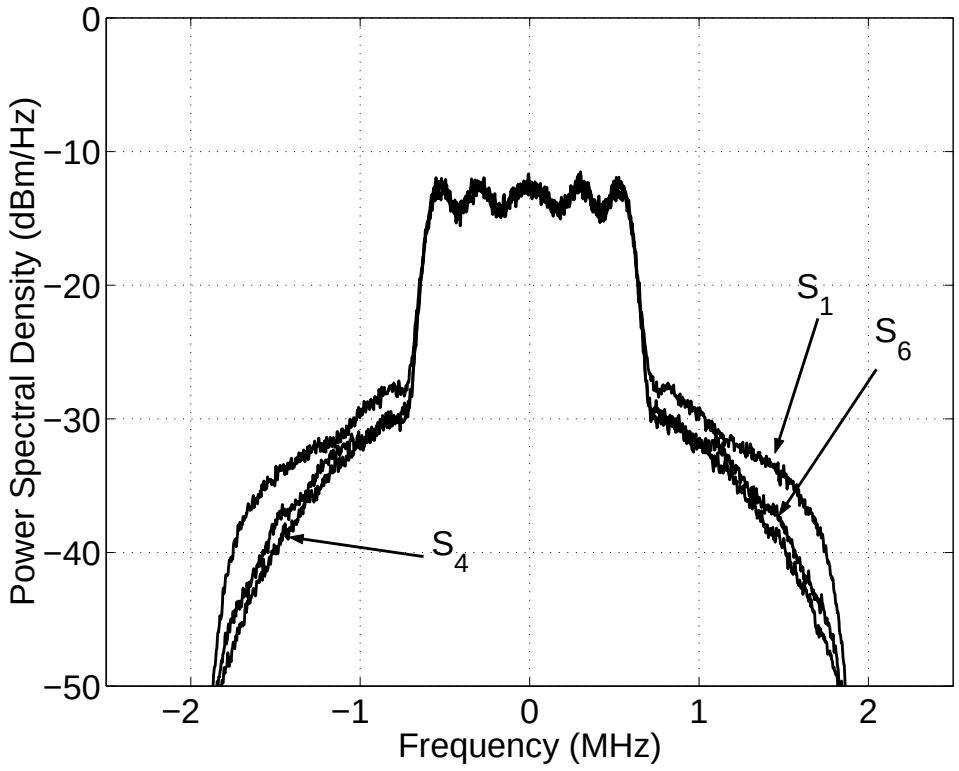

Figure 8.1: Output power spectrum for sets 1, 4 and 6.

needed is the development of an optimization technique for the proper choice of Walsh codes using the autocorrelation function. This can be done by studying the terms that are responsible for nonlinear distortion in the autocorrelation function and hence in the output spectrum. The same procedure can be used with multiple channels where the analysis presented in Chapter 5 could be used as a basis.

8.2.2 Autocorrelation of Arbitrary Number of Input Channels

The autocorrelation analysis of multiple channels was done for two input channels since this case was adequate to understand the problem of the interaction of multiple inputs in a multichannel amplifier. However, the analysis presented in Chapter 4 was general and can be used to develop the autocorrelation function with an arbitrary number of input channels. What is needed is the development of the output envelope at a certain frequency when the input consists of an arbitrary number of channels. This can be done using a technique similar to the Arithmetic Operator Method (AOM) which was developed for discrete tones. Then a formulation of the autocorrelation function can be developed.

8.2.3 Three-Box Model

The autocorrelation analysis using the three-box model in Chapter 5 was done assuming that the input filter frequency response is flat within each input signal bandwidth. This assumption could be removed leading to a more general case where the input filter responses can be incorporated in the output spectrum. Moreover, a single frequency Volterra model could also be used to replace the three-box model leading to wider class of amplifiers that can be modeled.

8.2.4 Bit Error Rate with Multiple Channels

The performance analysis presented in Chapter 6 can be extended to the case of multiple input channels. This can be done by using the Gaussian approximation in the development of the output autocorrelation function as:

$$\begin{aligned} R_{\tilde{y}\tilde{y};\xi_1}(\tau) &= |b_{1,0}|^2 R_{zz}(\tau) + F_1 R_{zz}(\tau) + F_2 R_{uu}^2(\tau) R_{zz}(\tau) + F_3 R_{zz}^3(\tau) \\ &= |b_{1,0}|^2 R_{zz}(\tau) + R_{dd} \end{aligned} \tag{8.4}$$

where

$$\begin{aligned} F_1 &= [4Re[(b_{1,0}b_{3,0}^*]R_{zz}(0) + 2Re[(b_{1,0}b_{3,1}^*]R_{uu}(0) \\ &\quad +4Re[(b_{3,0}b_{3,1}^*]R_{uu}(0)R_{zz}(0) + 4|b_{3,0}|^2R_{zz}(0)^2 + |b_{3,1}|^2(R_{uu}(0)^2] \\ F_2 &= |b_{3,1}|^2 \\ F_3 &= |b_{3,0}|^2 \end{aligned} \tag{8.5}$$

This formulation implies that nonlinear distortion due to the second channels can be treated as a multiplicative noise. A well established theory of performance of communication systems in multiplicative noise [84, 85, 86, 87, 88, 89] can be used to develop an analytical formula for probability of error.

Bibliography

[1] M. Johansson, T. Mattsson, L. Sundstrom, M. Faulkner, "Linearization of multi-carrier power amplifiers," *IEEE 43rd Conf. Veh. Tech.*, May 1993, pp. 684–687.

[2] P. B. Kenington, *High Linearity Amplifier Design*, Artech House Inc., 2000.

[3] Steve C. Cripps, *RF power amplifiers for wireless Communications*, Artech House, 2000.

[4] *Recommended Minimum Performance Standards for Dual Mode Wideband Spread Spectrum Cellular Mobile Stations*, TIA/EIA/IS-98 Interim Standard, July 1996.

[5] V. Aparin and L. E. Larson, "Analysis and reduction of cross-modulation distortion in cdma receivers," *IEEE Trans. Microwave Theory Techn.*, Vol. 51, pp. 1591–1602, May 2003.

[6] K. M. Gharaibeh, K. Gard and M. B. Steer, "Statistical modeling of the interaction of multiple signals in nonlinear RF systems," *IEEE MTT-S Int. Microwave Symp. Digest*, Vol. 1, June 2002, pp. 143–146.

[7] K. M. Gharaibeh and M. B. Steer, "Characterization of cross modulation in multichannel amplifiers using a statistically based behavioral modeling technique," *IEEE Trans. Microwave Theory Techn.*, Dec. 2003.

[8] M. Pawlak, Z. Hasiewicz, "Nonlinear system identification by the Haar multiresolution analysis," *IEEE Transactions on Circuits and Systems*, Vol. 45, pp. 945 -961, Sep. 1998.

[9] P. Crama and J. Schoukens, "Initial estimates of Wiener and Hammerstein systems using multisine excitation" *IEEE Trans. Instrumentation and Measurement*, Vol. 50, pp. 1791–1795, Dec. 2001.

[10] J. Shi and H. H. Sun, "Nonlinear System Identification for Cascaded Block Model: An Application to Electrode Polarization Impedence," *IEEE Trans. Biomedical Engin.*, Vol. 37, pp. 574–587, June 1990.

[11] D.T. Westwick and R.E. Kearney,"Identification of a Hammerstein model of the stretch reflex EMG using separable least squares," *22nd Annual Int. Conf. IEEE Engineering in Medicine and Biology Society*, Vol. 3, July 2000, pp. 1901–1904.

[12] G. B. Stanley, "Wiener kernel estimation for neural systems with natural inputs," *10th Annual Computational Neuroscience Meeting*, Monterey, CA, July 2001, pp.

[13] I. Scott and B. Mulgrew, "Nonlinear system identification and prediction using orthogonal functions," *IEEE Transactions Signal Processing*, Vol. 45, pp. 1842–1853, July 1997.

[14] J. S. Bendat, *Nonlinear System Analysis and Identification*, John Wiley and Sons, NY 1990.

[15] M. Schetzen, "Nonlinear System Modeling based on the Wiener theory," *IEEE*, Vol. 69, Dec. 1981, pp. 1557–1573.

[16] M. Korenberg, "Parallel cascade identification and kernel estimation for nonlinear systems," *Annals of Biomedical Engin.*, Vol. 19, pp. 429–455, 1991.

[17] H. W. Chen, "Modeling and identification of parallel nonlinear systems: structural classification and parameter estimation methods," *IEEE*, Vol. 83, Jan. 1995, pp. 39–66.

[18] S. Boyd, S. and L. "Uniqueness of a basic nonlinear structure," *IEEE Trans. Circuits and Systems*, Vol. 30, Sep. 1983, pp. 648–651.

[19] G. W. Rhyne and M. B. Steer, "Generalized power series analysis of intermodulation distortion in a MESFET amplifier: simulation and experiment," *IEEE Trans. Microwave Theory Techn.*, Vol. 35, pp. 1248–1255, Dec. 1987.

[20] C.-R. Chang, *Computer Aided Analysis of Nonlinear Analog Microwave Circuits using Frequency Domain Spectral Balance*, Ph.D. Dissertation, Electrical and Computer Engineeering Department, North Carolina State University, Raleigh, NC, 1990.

[21] G. W. Rhyne, *Nonlinear Analysis of Microwave Circuits*, Ph.D. Dissertation, Electrical and Computer Engineeering Department, North Carolina State University, Raleigh, NC, 1988.

[22] P. J. Lunsford, II, The frequency domain behavioral modleing and simulation of nonlinear analoge circuits and systems, Ph.D. dissertation, North Carolina State University, Raleigh, NC, 1993.

[23] C. P. Silva, A. A. Moulthrop and M. S. Muha, "Polyspectral techniques for nonlinear system modeling and distortion compensation," *IEEE Int. Vacuum Electronics Conf., IVEC 2002*, April 2002, pp. 314–315.

[24] M. Maqusi, "Characterization of nonlinear distortion in HRC multiplexed cable television systems," *IEEE Trans. Circuits and Systems*, Vol. 32, pp. 605–609, June 1985.

[25] H. Ku, M. D. McKinley and J. S. Kenney, "Quantifying memory effects in RF power amplifiers ," *IEEE Trans. Microwave Theory Techn.*, Vol. 50, pp. 2843–2849, Dec. 2002.

[26] J. Shi and H. H. Sun,"Nonlineaar System Identification Via Parallel Cascaded Structure," *Proceedings Int. Conf. IEEE Engin. Medicine Biology*, Nov. 1990, pp. 1897–1898.

[27] H. W. Chen, L. D. Jacobson, J. P. Gaska and D. A. Pollen, "Structural classification of multi-input biological nonlinear systems," *IEEE Conf. Systems, Man and Cybernetics*, Vol. 3, Nov. 1989, pp. 903–908.

[28] C. -R. Chang, M. B. Steer, "Frequency-domain nonlinear microwave circuit simulation using the arithmetic operator method," *IEEE Trans. Microwave Theory Techn.*, Vol. 38, pp. 1139–1143, Aug. 1990.

[29] K. Kashyap, T. Wada, M. Katayama, T. Yamazato and A. Ogawa, "The performance of CDMA system using p/4-shift QPSK and p/2-shift BPSK with the nonlinearity of HPA,"*IEEE Int. Symp. Personal, Indoor and Mobile Radio Comm.,PIMRC 96*, Vol. 2, Oct. 1996, pp. 492–496.

[30] D. W. Bennett, P. B. Kenington and R. J. Wilkinson, "Distortion effects of multicarrier envelope limiting," *IEE Proc. Comm.*, Vol. 144, Oct. 1997, pp. 349–356.

[31] M. Jeruchim, P. Balaban and S. Shanmugan, *Simulation of Communication Systems*, Kluwer Academic/Plenum Publishers, 2000.

[32] K. Gard, H. Gutierrez, M. B. Steer, "Characterization of spectral regrowth in microwave amplifiers based on the nonlinear transformation of a complex Gaussian process," *IEEE Trans. Microwave Theory Techn.*, Vol. 47, pp. 1059–1069, July 1999.

[33] H. Gutierrez, K. Gard and M. B. Steer, "Nonlinear Gain Compression in Microwave amplifiers using generalized power series analysis and transformation of input statistics," *IEEE Trans. Microwave Theory Techn.*, Vol. 48, pp. 1774–1777, Oct. 2000.

[34] K. Gard, H. Gutierrez, M. B. Steer, "Autocorrelation analysis of distortion generated from bandpass nonlinear circuits,", *IEEE Conf. Custom Integrated Circuits*, May 2001, pp. 345–348.

[35] K.Gard, L. E. Larson and M. B. Steer, "Generalized autocorrelation analysis of spectral regrowth from bandpass nonlinear circuits," *2001 IEEE MTT-S Int. Microwave Symp. Digest*, May 2001, pp. 9–12.

[36] A. Papoulis, *Probability, random variables, and stochastic processes*, McGraw Hill, 1991.

[37] J. Sevy, "The Effect of Multiple CW and FM Signals Passed Through a Hard Limiter or TWT," *IEEE Trans. Comm.*, Vol. 14, pp. 568–578, Oct 1966.

[38] R. Kirlin, "Performance of polarity correlators or limiters with pseudorandom additive input noise," *IEEE Trans. Information Theory*, Vol. 23, pp. 265–267, Mar. 1977.

[39] J. Jones, "Hard-limiting of two signals in random noise," *IEEE Trans. Information Theory*, Vol. 9, pp. 34–42, Jan. 1963.

[40] J. Max, "Envelope Fluctuations in the Output of a Bandpass Limiter," *IEEE Trans. Comm.*, Vol. 18, pp. 597–605, Oct. 1970

[41] B. F. McGuffin, "The effect of bandpass limiting on a signal in wideband noise," *IEEE Military Comm. Conf.*, Vol.1, Oct. 1992, pp. 206–210.

[42] H. Baer, "Interference effects of hard limiting in PN spread-spectrum systems," *IEEE Trans. Comm.*, Vol. 30, pp. 1010–1017, May 1982.

[43] J. Roberts, E. Tsui, D. Watson, "Signal-to-noise ratio evaluations for nonlinear amplifiers," *IEEE Trans. Comm.*, Vol. 27, pp. 197–201, Jan. 1979.

[44] R. Price, "A useful theorem for nonlinear devices having Gaussian inputs," *IEEE Transactions on Information Theory*, Vol. 4, pp. 69–72, June 1958.

[45] *Mobile Station-Base Station Compatibility Standard for Dual-Mode Wideband Spread-Spectrum Cellular Systems*, TIA/EIA Standard IS-95, 1993.

[46] R. Gross, D. Veeneman, "SNR and spectral properties for a clipped DMT ADSL signal," *IEEE Conf. Comm.*, Vol.2, May 1994, pp. 843–847.

[47] R. Gross, D. Veeneman, "Clipping distortion in DMT ADSL systems," *Electron. Lett.* , Volume: 29, Nov. 1993, pp. 2080–2081.

[48] V.Aparin, "Analysis of CDMA signal spectral regrowth and waveform quality," *IEEE Trans. Microwave Theory Techn.*, Vol. 49, pp. 2306–2314, Dec. 2001.

[49] J. W. Graham and L. Ehrmen, *Nonlinear System Modeling and Analysis with Application to Communication Receivers*, Rome Air Developement Center, Rome, N.Y., June 1973.

[50] M. S. Muha, C. J. Clark, A. A. Moulthrop and C. P. Silva, "Validation of power amplifier nonlinear block models," *IEEE MTT-S Int. Microwave. Symp. Digest*, Vol. 2, June 1999, pp. 759–762.

[51] C. P. Silva, C. J. Clark, A. A. Moulthrop and M. S. Muha, "Optimal-filter approach for nonlinear power amplifier modeling and equalization," *IEEE MTT-S Int. Microwave Symp. Digest*, Vol. 1 , June 2000, pp. 437–440.

[52] C. P. Silva, A. A. Moulthrop, M. S. Muha and C. J. Clark, "Application of polyspectral techniques to nonlinear modeling and compensation," *IEEE MTT-S Int. Microwave Symp. Digest*, Vol. 1, May 2001, pp. 13–16.

[53] J. S. Kenney and A. Leke, "Design considerations for multicarier CDMA base station power amplifiers," *Microwave J.*, Vol. 42, pp. 76–7, 79–80, 82, 84, 86, Feb. 1999.

[54] T. Wang and T. Brazil, "Using Volterra mapping based behavioral models to evaluate ACI and cross modulation in CDMA communication systems," *High Frequency Postgraduate Student Colloquium*, Dublin, Ireland, Sep., 2000, pp. 102–108.

[55] B. K. Ko, D. B. Cheon, S. W. Kim, J. S. Ko, J. K. Kim, B. H. Park "A nightmare for CDMA RF receiver: the cross modulation," *IEEE Asia Pacific Conference on ASICs*, Aug. 1999, pp. 400–402.

[56] T. S. Rappaport, *Wireless Communications: Principles and Practice*, Prentice Hall, 1996.

[57] R. N. Braithwaite, Using Walsh code selection to reduce the power variance of band-limited forward-link CDMA waveforms," *IEEE Selected Areas in Communications*, Vol. 18, pp. 2260–2269, Nov 2000.

[58] R. N. Braithwaite, "Nonlinear amplification of CDMA waveforms: An analysis of power amplifier gain errors and spectral regrowth," *Proc. IEEE Veh. Technol. Conf.*, May 1998, pp. 2160-2166.

[59] R. N. Braithwaite, "Exploiting data and code interactions to reduce the power variance for CDMA sequences," *IEEE Selected Areas in Communications*, Vol. 19, June 2001, pp. 1061–1069.

[60] W. Qiang, M. Testa and R. Larkin, "Linear RF power amplifier design for CDMA signals," *IEEE MTT-S Int. Microwave Symp. Digest*, Vol. 2, June 1996, pp. 851–854.

[61] G. T. Zhou, "Analysis of spectral regrowth of weakly nonlinear power amplifiers," *IEEE Conf. Acoustics, Speech, and Signal Processing*, Vol. 5, June 2000, pp. 2737–2740.

[62] C. Liu, H. Xiao, Q. Wu and F. Li, "Linear RF power amplifier design for TDMA signals: A spectrum analysis approach," *Proc. IEEE Int. Acoustics, Speech, and Signal Processing*, Vol. 4, May 2001, pp. 2665–2668.

[63] V. K. Lau, "Average of peak-to-average ratio (PAR) of IS95 and CDMA2000 systems-single carrier *IEEE Comm. Lett.*," Vol. 5, pp. 160–162, April 2001.

[64] L. Thibault and T. L. Minh, "Performance evaluation of COFDM for digital audio broadcasting," *IEEE Trans. Parametric Study Broadcasting*, Vol. 43, pp. 64–75, March 1997.

[65] E. Bogenfeld, R. Valentin, K. Metzer and W. S. Greff, "Influence of nonlinear HPA on trellis-Coded OFDM for terrestrial broadcasting of digital HDTV," *IEEE Global Telecomm. Conf.*, Vol. 3, Nov. 1993, pp. 1433–1438.

[66] Y. Guo and J. R. Cavallaro, "Post-compensation of RF non-linearity in mobile OFDM systems by estimation of memory-less polynomial," *IEEE Symp. Circuits and Systems*, Vol. 1, May 2002, pp. 217–220.

[67] R. Dinis and A. Gusmao, "Performance evaluation of a multicarrier modulation technique allowing strongly nonlinear amplification," *IEEE Conf. Comm.*, Vol. 2, June 1998, pp. 791–796.

[68] J. H. Jong and W. E. Stark, "Performance analysis of coded multicarrier spread-spectrum systems in the presence of multipath fading and nonlinearities," *IEEE Trans. Comm.*, Vol.49, pp. 168–79, Jan. 2001.

[69] A. R. Bahai, M. Singh, A. J. Goldsmith, B. R. Saltzberg, "A new approach for evaluating clipping distortion in multicarrier systems," *IEEE Selec. Areas Comm.*, Vol. 20, pp. 1037–1046, June 2002.

[70] D. Dardari, V. Tralli and A. Vaccari, "A theoretical characterization of nonlinear distortion effects in OFDM systems," *IEEE Trans. Comm.*, Vol. 48, pp. 1755–1764, Oct. 2000.

[71] A. A. Saleh, "Frequency-independent and frequency-dependent nonlinear models of TWT amplifiers" *IEEE Trans. Comm.* Vol., Nov. 1981, pp. 1715–1720.

[72] A. Akinniyi and J. Long, "Statistical characterization of intermodulation products in a multicarrier LPA design," *IEEE Veh. Tech. Conf.*, Vol. 1, May 1993, pp. 688–691.

[73] P. Banelli, "Theoretical analysis and performance of OFDM signals in nonlinear fading channels," *IEEE Trans. Wireless Comm.*, Vol. 2, pp. 284–293, March 2003.

[74] P. Banelli and S. Cacopardi, "Theoretical analysis and performance of OFDM signals in nonlinear AWGN channels," *IEEE Trans. Comm.*, Vol. 48, pp. 430–441, March 2000.

[75] A. Conti, D. Dardari and V. Tralli, "An analytical framework for CDMA systems with a nonlinear amplifier and AWGN," *IEEE Trans. Comm.*, Vol. 50, p.1110–1120, July 2002.

[76] A. Conti, D. Dardari and V. Tralli, "On the performance of CDMA systems with nonlinear amplifier and AWGN," *IEEE Symp. Spread Spectrum Tech. and App.*, Vol. 1, Sep. 2000, pp. 197–202.

[77] L. Rugini, P. Banelli and S. Cacopardi, "Performance analysis of the decorrelating multiuser detector for nonlinear amplified DS-CDMA signals," *IEEE Conf. Comm.*, Vol. 3, April 2002, pp. 1466–1470.

[78] E. H. Dinan, B. Jabbari, "Spreading codes for direct sequence CDMA and wideband CDMA cellular networks," *IEEE Comm. Magazine*, Vol. 36, pp. 48–54, Sep. 1998.

[79] L. Staphorst, M. Jamil and L. P. Linde, "Performance of a synchronous balanced QPSK CDMA system using complex spreading sequences in AWGN," *IEEE AFRICON* Vol. 1, Sep. 1999, pp. 215–220.

[80] J. Cheng and N. C. Beaulieu, "Accurate DS-CDMA bit-error probability calculation in Rayleigh fading," *IEEE Trans. Wireless Comm.*, Vol. 1, pp. 3–15, Jan. 2002.

[81] V. Sorokine and S. Younis, "Analysis of performance measures of forward CDMA link with non-linear devices in the signal path," *IEEE Global Telecomm. Conf.*, Vol. 6, Nov. 1998, pp. 3302–3307.

[82] P. C. Li and E. Geraniotis, "Performance analysis of synchronous M-PSK CDMA multi-tier systems with a nonlinear amplifier," *IEEE Symp. Comp. and Comm.*, July 1997, pp. 275–279.

[83] V. J. Garg, K. Smolik and J. Wilkers, *Applications of CDMA in Wireless/Personal Communications*, Prentice Hall, 1996.

[84] D. Harres, "Nonlinear processing of Manchester data corrupted by multiplicative noise," *IEEE Conf. Comm.*, Vol. 2, June 1998, pp. 683–687.

[85] M. Coulon, J. Y. Tourneret and A. Swami, "Detection of multiplicative noise in stationary random processes using second and higher order statistics," *IEEE Trans. Sig. Proc.*, Vol. 48, pp. 2566–2575, Sep. 2000.

[86] A. Swami, "Multiplicative noise models: parameter estimation using cumulants," *Workshop on Spectrum Estimation and Modeling*, Oct. 1990, pp. 212–216.

[87] M. Frey and D. Andescavage "An analytic theory for power law detection of bursty targets in multiplicative noise," *IEEE Trans. Sig. Proc.*, Vol. 46, pp. 2837-2841, Oct. 1998.

[88] M. Ghogho, A. Nandi and B. Garei, "Locally optimum detectors for deterministic signals in multiplicative noise," *IEEE Conf. Acoustics, Speech, and Signal Processing*, Vol. 4, May 1998, pp. 2137–2140.

[89] I. Song and T. S. Uhm, "Multiplicative noise model and composite signal detection," *IEE Proc. Radar and Signal Processing*, Vol. 138 pp. 531–538, Dec. 1991.

[90] H. Ku, M. D. McKinley and J. S. Kenney, "Extraction of accurate behavioral models for power amplifiers with memory effects using two-tone measurements," *IEEE MTT-S Int. Microwave Symp. Digest*, Vol. 1, June 2002, pp. 139–142.

[91] *HP ESG-D series signal generators, dual arbitrary waveform generator and multi-channelCDMApersonality*, Users and Programming Guide, HP Part no. E4400-90148, Mar. 1998.

[92] V. Aparin, B Butler and P. Draxler, "Cross Modulation In CDMA Receivers," *IEEE MTT-S Int. Microwave Symp. Digest*, June 2000, pp.

[93] C. Liu, H. Xiao, Q. Wu and F. Li, "Spectrum design of RF power amplifier for wireless communication systems," *IEEE Trans. Consumer Electronics*, Vol. 48, pp. 72–80, Feb. 2002.

[94] T. S. Goh and R.D. Pollard,"ACPR prediction of CDMA systems through statistical behavioural modelling of power amplifiers with memory," *Int. Conf. Comm. Sys.*, Vol. 2, Nov. 2002, pp. 1189–1193.

Other Useful References Not Cited in the Text

[95] K. M. Gharaibeh and M. B. Steer, "Statistical modeling of cross modulation in multichannel power amplifiers using a new behavioral modeling technique," *IEEE MTT-S International Microwave Symp. Digest*, June 2003, pp 343–346.

[96] J. C. Pedro and N. B. Carvalho, "On the use of multi-tone techniques for assessing RF components' intermodulation distortion," *IEEE Trans. Microwave Theory Techn.*, Vol. 47, pp. 2393–2402, Dec. 1999.

[97] S. J. Yi, S. Nam, S H. Oh and J. H. Han, "Prediction of a CDMA output spectrum based on intermodulation products of two-tone test," *IEEE Trans. Microwave Theory Techn.*, Vol. 49, pp. 938–946, May 2001.

[98] J. C. Pedro and N. B. Carvalho, "On the use of multi-tone techniques for assessing RF components' intermodulation distortion," *IEEE Trans. Microwave Theory Techn.*, Vol. 47, pp. 2393–2402, Dec. 1999.

[99] K. M. Gharaibeh, K. Gard, H. Gutierrez and M. B. Steer, "The importance of nonlinear order in modeling intermodulation distortion and spectral regrowth," *IEEE Radio and Wireless Conf. (RAWCON)*, Aug. 2002, pp. 161–164.

[100] J. F. Sevic, M. B. Steer and A. M. Pavio, "Nonlinear analysis methods for the simulation of digital wireless communication systems," *Int. J. of Microwave and Millimeter-wave Computer Aided Engin.*, Vol. 6, May 1996, pp. 197–216.

[101] J. F. Sevic and M. B. Steer, "Analysis of GaAs MESFET spectrum regeneration driven by a DQPSK modulated source," *IEEE MTT-S Int. Microwave Symp. Digest*, Vol. 3, June, 1995, pp. 1375–1378.

[102] P. Z. Peebles, *Probability, random variables, and random signal principles*, McGraw Hill, 2001.

[103] J. G. Proakis, *Digital communications*, McGraw-Hill, 2001.

[104] G. R. Cooper and C. D. McGillem, *Modern communications and spread spectrum*, McGraw-Hill, 1986.

[105] M. Schetzen, *The Volterra and Wiener theories of nonlinear systems*, J. Wiley, 1980.

[106] R. Haber and L. Keviczky, *Nonlinear system identification: input-output modeling approach*, Kluwer Academic Publishers, 1999.

[107] J. S. Bendat and A. G. Piersol, *Engineering applications of correlation and spectral analysis*, J. Wiley, 1993.

[108] N. Rozario and A. Papoulis, "Some results in the application of polyspectra to certain nonlinear communication systems," *IEEE Signal Processing Workshop on Higher-Order Statistics*, June 1993, pp. 37–41.

[109] G. W. Rhyne and M. B. Steer, "A New Frequency domain approach to the analysis of nonlinear microwave circuits," *IEEE MTT-S Int. Microwave Symp. Digest*, Vol. 85, Jun 1985, pp. 401–404.

[110] P. J. Lunsford and M. B. Steer, "The relationship between bivariate Volterra analysis and power series analysis with application to behavioral modeling of microwave circuits, *Int. J. of Microwave and Millimeter-wave Computer Aided Engin.*, vol. 1, pp. 253–262, 1991.

[111] G. W. Rhyne, M. B. Steer and B. D. Bates, "Frequency-domain nonlinear circuit analysis using generalized power series," *IEEE Transactions on Microwave Theory Techn.*, Vol. 36, pp. 379–387, Feb. 1988.

[112] P. Crama and Y. Rolain, "Broad-band measurement and identification of a Wiener-Hammerstein model for an RF amplifier," *ARFTG Conf. Digest*, Dec. 2002, pp. 49–57.

[113] J. S. Lee and L. E. Miller, "Analysis of peak-to-average power ratio for IS-95 and third generation CDMA forward link waveforms," *IEEE Trans. on Veh. Tech.*, Vol. 50, pp. 1004–1013, July 2001.

[114] O. Vaananen, J. Vankka, T. Viero and K. Halonen, "Reducing the crest factor of a CDMA downlink signal by adding unused channelization codes," *IEEE Comm. Lett.*, Vol. 6, pp. 443–445, Oct. 2002.

[115] S. -W. Chen, W. Panton and R. Gilmore, "Effects of nonlinear distortion on CDMA communication systems," *IEEE Trans. Microwave Theory Techn.*, Vol. 44, pp. 2743 –2750, Dec. 1996.

[116] P. Jain, "Limiting of signals in random noise," *IEEE Trans. Inf. Theory*, Vol. 18, pp. 332–340, May 1972.

[117] G. Karam and H. Sari, "Analysis of predistortion, equalization, and ISI cancellation techniques in digital radio systems with nonlinear transmit amplifiers," *IEEE Transactions Comm.*, Vol. 37, pp. 1245–1253, Dec. 1989.

[118] T. S. Chu, "Intermodulation in CDMA," *IEEE Int. Symp. Personal, Indoor and Mobile Radio Communications*, Vol.2, Sep. 1994, pp. 595–600.

[119] D. Anderson and P. Wintz, "Analysis of a spread-spectrum multiple-access system with a hard limiter," *IEEE Trans. Comm.*, Vol. 17, pp. 285–290, April 1969.

[120] G. Jacovitti and A. Neri, "Estimation of the autocorrelation function of complex Gaussian stationary processes by amplitude clipped signals," *IEEE Trans. Inf. Theory*, Vol. 40, pp. 239–245, Jan. 1994.

[121] J. Keilson, N. Mermin and P. Bello, "A theorem on cross correlation between noisy channels," *IEEE Trans. Inf. Theory*, Vol. 5, pp. 77–79, June 1959.

[122] M. Pursley, D. Sarwate and W. Stark, "Error probability for direct-sequence spread-spectrum multiple-access communications–Part I: Upper and lower bounds," *IEEE Trans. Comm.*, Vol. 30, pp. 975–984, May 1982.

[123] E. Geraniotis and M. Pursley, "Error probability for direct-sequence spread-spectrum multiple-access communications–Part II: Approximations," *IEEE Trans. Comm.*, Vol. 30, pp. 985–995, May 1982.

[124] C. -R. Chang and M. B. Steer, "Frequency-domain nonlinear microwave circuit simulation using the arithmetic operator method," *IEEE Trans. Microwave Theory Techn.*, Vol. 38, pp. 1139–1143, Aug. 1990.

[125] J. K. Cavers, "The effect of data modulation format on intermodulation power in nonlinear amplifiers," *Vehicular Tech. Conf.*, Vol. 1, June 1994, pp. 489–493.

[126] D. Divsalar and M. Simon, "The power spectral density of digital modulations transmitted over nonlinear channels," *IEEE Trans. Comm.*, Vol. 30, pp. 142–151, Jan 1982.

[127] E. L. Pinto and J. C. Brandao, "On the efficient use of computer simulated digital signals to evaluate performance parameters," *IEEE J. Selec. Areas Comm.*, Vol. 6, pp. 52–57, Jan. 1988.

[128] F. D. Neeser and J. L. Massey, "Proper complex random processes with applications to information theory," *IEEE Trans. Inf. Theory*, Vol. 39, pp. 1293–1302, July 1993.

[129] N. Blachman, "The uncorrelated output components of a nonlinearity," *IEEE Trans. Inf. Theory*, Vol. 14, pp. 250–255, March 1968.

[130] T. Maseng, "On the Characterization of a Bandpass Nonlinearity by Two-Tone Measurements," *IEEE Trans. Comm.* Communications, Vol. 26, pp. 746–754, Jun 1978.

[131] F. H. Raab, P. Asbeck, S. Cripps, P. B. Kenington, Z. B. Popovic, N. Pothecary, J. F. Sevic and N. O. Sokal, "Power amplifiers and transmitters for RF and microwave," *IEEE Trans. Microwave Theory Techn.*, Vol. 50, pp. 814–826, March 2002.

[132] C. Fager, J. C Pedro, N. B. deCarvalho and H. Zirath, "Prediction of IMD in LDMOS transistor amplifiers using a new large-signal model," *IEEE Trans. Microwave Theory Techn.*, Vol. 50, pp. 2834–2842, Dec. 2002.

[133] N. B. Carvalho and J. C. Pedro, "Multi-tone intermodulation distortion performance of 3rd order microwave circuits," *IEEE MTT-S Int. Microwave Symp. Digest*, Vol. 2, June 1999, pp. 763–766.

[134] J. C. Pedro and N. B. Carvalho, "On the use of multitone techniques for assessing RF components' intermodulation distortion," *IEEE Trans. Microwave Theory and Techn.*, Vol. 47, pp. 2393–2402, Dec. 1999.

[135] H. Lai and Y. Bar-Ness, "A new predistorter design for nonlinear power amplifiers using the minimum distortion power polynomial model (MDP-PM)," *IEEE Veh. Tech. Conf.*, Vol. 4, Oct. 2001, pp. 2216–2220.

[136] D. M. Goebel, R. R. Liou, W. L. Menninger, Z. Xiaoling and E. A. Adler, "Development of linear traveling wave tubes for telecommunications applications," *IEEE Trans. Electron Devices*, Vol. 48, pp.: 74–81, Jan. 2001.

[137] E. Biglieri, S. Barberis and M. Catena, "Analysis and compensation of nonlinearities in digital transmission systems," *IEEE J. Selec. Areas Comm.*, Vol. 6, pp. 42–51, Jan. 1988.

[138] A. Bernardini and S. De Fina, "Analysis of different optimization criteria for IF predistortion in digital radio links with nonlinear amplifiers," *IEEE Trans. Comm.*, Vol. 45, pp. 421–428, April 1997.

Appendix A

2-D Polynomial Fitting

To formulate the problem, let $G_{i,j}$ where $1 \leq i \leq I$ and $1 \leq j \leq J$ be the data points obtained from single tone measurements (this represent the measured S_{21} parameter which represents the amplifier gain). The indexes i and j indicate the data point measured at the i th power step of the signal $\tilde{w}_1(t)$ and the j th power step of the signal $\tilde{w}_2(t)$. The number of data points is $I \times J$ and can be obtained by sweeping the input power of the signal $\tilde{w}_1(t)$ in I power steps and sweeping the power of $\tilde{w}_2(t)$ in J power steps. Therefore, the problem leads to a linear system optimization and the coefficients can be obtained using the method of least squares. Let $\tilde{w}_1(t) = z$ and $\tilde{w}_2(t) = u$, then by forming a set of equations,

the least squares problem reduces to solving a system of linear equations of the form

$$\begin{pmatrix} G_{1,1} \\ G_{2,1} \\ \vdots \\ G_{I,1} \\ G_{1,2} \\ G_{2,2} \\ \vdots \\ G_{I,2} \\ \vdots \\ G_{1,J} \\ G_{2,J} \\ \vdots \\ G_{I,J} \end{pmatrix} = \begin{pmatrix} 1 & z_1^2 & u_1^2 & z_1^4 & z_1^2u_1^2 & u_1^4 & z_1^6 & \dots & u_1^{N-1} \\ 1 & z_2^2 & u_1^2 & z_2^4 & z_2^2u_1^2 & u_1^4 & z_2^6 & \dots & u_1^{N-1} \\ \vdots & \vdots & \vdots & \vdots & \vdots & \vdots & \vdots & \dots & \vdots \\ 1 & z_I^2 & u_1^2 & z_I^4 & z_I^2u_1^2 & u_1^4 & z_I^6 & \dots & u_1^{N-1} \\ 1 & z_1^2 & u_2^2 & z_1^4 & z_1^2u_2^2 & u_2^4 & z_1^6 & \dots & u_2^{N-1} \\ \vdots & \vdots & \vdots & \vdots & \vdots & \vdots & \vdots & \dots & \vdots \\ 1 & z_I^2 & u_2^2 & z_I^4 & z_I^2u_2^2 & u_2^4 & z_I^6 & \dots & u_2^{N-1} \\ \vdots & \vdots & \vdots & \vdots & \vdots & \vdots & \vdots & \dots & \vdots \\ 1 & z_1^2 & u_J^2 & z_1^4 & z_1^2u_J^2 & u_J^4 & z_1^6 & \dots & u_J^{N-1} \\ \vdots & \vdots & \vdots & \vdots & \vdots & \vdots & \vdots & \dots & \vdots \\ \vdots & \vdots & \vdots & \vdots & \vdots & \vdots & \vdots & \dots & \vdots \\ 1 & z_J^2 & u_J^2 & z_I^4 & z_I^2u_J^2 & u_J^4 & z_I^6 & \dots & u_J^{N-1} \end{pmatrix} \begin{pmatrix} b_{1,0} \\ b_{3,0} \\ b_{3,1} \\ b_{5,0} \\ b_{5,1} \\ b_{5,2} \\ \vdots \\ \vdots \\ \vdots \\ \vdots \\ \vdots \\ b_{N,\frac{N-1}{2}} \end{pmatrix}$$

or in matrix notation:

$$\mathbf{G} = \mathbf{A}\mathbf{b} \tag{A.1}$$

where the matrix $\mathbf{A}$ is a Vandermonde matrix. The least squares solution yields the coefficients $b_{n,k}$ which can then be obtained as

$$\mathbf{b} = [\mathbf{A}^T\mathbf{A}]^{-1}(\mathbf{A}^T\mathbf{G}) \tag{A.2}$$

The number of coefficients is equal to $((N+1)(N+3)/8)$.

Appendix B

Properties of Gaussian Random Processes

In order to evaluate (5.50), we start by evaluating the following correlation functions:

$$\begin{aligned} E[\tilde{w}_1\tilde{w}_2^*] &= R_{\tilde{w}\tilde{w}}(\tau) \\ E[\tilde{w}_1^*\tilde{w}_2] &= R_{\tilde{w}\tilde{w}}(\tau) \\ E[\tilde{w}_1\tilde{w}_1^*] &= E[\tilde{w}_2\tilde{w}_2^*] = R_{\tilde{w}\tilde{w}}(0) \\ E[\tilde{w}_1\tilde{w}_2] &= E[\tilde{w}_2\tilde{w}_2] = 0 \end{aligned} \tag{B.1}$$

then using (5.49), we evaluate each term in (5.50):

$$\begin{aligned} &E[\tilde{w}_1\tilde{w}_2^*] = R_{\tilde{w}\tilde{w}}(\tau) \\ &E[\tilde{w}_1\tilde{w}_2^{*^2}\tilde{w}_2] = 2R_{\tilde{w}\tilde{w}}(0)R_{zz}(\tau) \\ &E[\tilde{w}_1^2\tilde{w}_1^*\tilde{w}_2^*] = 2R_{\tilde{w}\tilde{w}}(0)R_{\tilde{w}\tilde{w}}(\tau) \\ &E[\tilde{w}_1^2\tilde{w}_1^*\tilde{w}_2^{*^2}\tilde{w}_2] = 2R_{\tilde{w}\tilde{w}}^3(\tau) + 4R_{\tilde{w}\tilde{w}}(0)^2R_{\tilde{w}\tilde{w}}(\tau) \\ &E[\tilde{w}_1^2\tilde{w}_1^*\tilde{w}_2^*] = 2R_{\tilde{w}\tilde{w}}(0)R_{\tilde{w}\tilde{w}}(\tau) \\ &E[\tilde{w}_1\tilde{w}_2\tilde{w}_2^{*^2}] = 2R_{\tilde{w}\tilde{w}}(0)R_{\tilde{w}\tilde{w}}(\tau) \end{aligned} \tag{B.2}$$

Similarly for (5.52):

$$
\begin{aligned}
E[r_1 r_2^*] &= E[r_1^* r_2] = R_{rr}(\tau) \\
E[r_1 r_1^*] &= E[r_2 r_2^*] = R_{rr}(0) \\
E[r_1 r_2] &= E[r_2 r_2] = 0 \\
E[s_1 s_2^*] &= E[s_1^* s_2] = R_{ss}(\tau) \\
E[s_1 s_1^*] &= E[s_2 s_2^*] = R_{ss}(0) \\
E[s_1 s_1] &= E[s_2 s_2] = 0 \\
E[r_1 s_2^*] &= E[s_1 r_2^*] = 0 \\
E[r_1 s_2] &= E[s_1 r_2] = 0.
\end{aligned} \tag{B.3}
$$

If the two processes are Gaussian then the property (5.49) applies. Therefore, using (B.3) we evaluate each term in (5.52):

$$
\begin{aligned}
E[r_1 r_2^{*^2} r_2] &= 2R_{rr}(0)R_{rr}(\tau) \\
E[r_1^2 r_1^* r_2^*] &= 2R_{rr}(0)R_{rr}(\tau) \\
E[r_1^2 r_1^* r_2^{*^2} r_2] &= 2R_{rr}^3(\tau) + 4R_{rr}(0)^2 R_{rr}(\tau) \\
E[r_1^2 r_1^* r_2^*] &= 2R_{rr}(0)R_{rr}(\tau) \\
E[r_1 r_2 r_2^{*^2}] &= 2R_{rr}(0)R_{rr}(\tau) \\
E[s_1 s_1^* s_2 s_2^*] &= R_{ss}(0)^2 + R_{ss}(\tau)^2.
\end{aligned}
$$

Collecting the power like terms,the expression in (5.52) follows directly.

Appendix C

Derivation of Probability of Error

Equation (6.8) follows by evaluate the following integral:

$$\begin{aligned}&\int_0^{T_b} p_k(t-nT)p_k(t-nT)dt\\ &=\sum_{n=1}^{K}\int_0^{T} p_k(t-nT)p_k(t-nT)dt = KT = T_b\end{aligned}$$

The variance in (6.13) is evaluated as follows:

$$\begin{aligned}\sigma^2_{D_d^I} &= E[(D_d^I)^2]\\ &= \frac{1}{T_b^2}E\int_0^{T_b}\int_0^{T_b} p^I(t)p^I(\lambda)d(t)d(\lambda)\cos(\omega_c t)\cos(\omega_c\lambda)dtd\lambda\\ &= \frac{K}{T_b^2}\int_0^{T}\int_0^{T} p^I(t)p^I(\lambda)E[d(t)d(\lambda)]\cos(\omega_c t)\cos(\omega_c\lambda)dtd\lambda\\ &= \frac{K}{2T_b^2}\int_0^{T}\int_0^{T} R_{pp}(t-\lambda)R_{dd}(t-\lambda)[\cos(\omega_c(t-\lambda))+\cos(\omega_c(t+\lambda))]dtd\lambda\\ &= \frac{K}{2T_b^2}\int_0^{T} R_{pp}(\tau)R_{dd}(\tau)\cos(\omega_c\tau)d\tau\\ &= \frac{K}{2T_b^2}\int_0^{T} R_{pp}(\tau)R_{\tilde{d}\tilde{d}}(\tau)d\tau\\ &= \frac{K}{4T_b^2}\int_{-\infty}^{\infty} |P(0)|^2 S_{\tilde{d}\tilde{d}}(f)df\\ &= \frac{KT^2}{4T_b^2}\int_{-B/2}^{B/2} S_{\tilde{d}\tilde{d}}(f)df\end{aligned}$$

$$= \frac{1}{4K}\int_{-B/2}^{B/2} S_{\tilde{d}\tilde{d}}(f)df.$$

and for the AWGN in (6.12):

$$\begin{aligned}
\sigma_n^2 &= E[I_n^2] \\
&= \frac{1}{T_b^2}E\int_0^{T_b}\int_0^{T_b} p(t)p(\lambda)n(t)n(\lambda)\cos(\omega_c t)\cos(\omega_c\lambda)dtd\lambda \\
&= \frac{1}{2T_b^2}\int_0^{T_b}\int_0^{T_b} p(t)p(\lambda)E[n(t)n(\lambda)][\cos(\omega_c(t-\lambda)) + \cos(\omega_c(t+\lambda))]dtd\lambda \\
&= \frac{1}{2T_b^2}\int_0^{T_b}\int_0^{T_b} R_{pp}(t-\lambda)R_{nn}(t-\lambda)\cos(\omega_c(t-\lambda))dtd\lambda \\
&= \frac{1}{2T_b^2}\int_0^{T_b} R_{pp}(\tau)R_{nn}(\tau)\cos(\omega_c\tau)dtd\lambda \\
&= \frac{K}{2T_b^2}\int_0^{T} R_{pp}(\tau)\frac{N_0}{2}\delta(\tau)dtd\lambda \\
&= \frac{KN_0}{4T_b^2}\int_{-B/2}^{B/2}|P(0)|^2df \\
&= \frac{KN_0}{4T_b^2}\frac{1}{B} \\
&= \frac{KN_0}{4T_b^2}T \\
&= \frac{N_0}{4T_b}.
\end{aligned}$$

where $|P(0)|^2 = \frac{1}{B^2} = T^2$.

Appendix D

MATLAB CODE

The MATLAB code which was used in the simulations of CDMA signal spectrum and the estimation of system BER is listed below.

- *cd_cd_analytic_3box.m*: Sweeps the power of input signals and plots the output spectrum and estimates ACPR.
- *cd_cd_Analytic_IMD_3box.m*: Sweeps the power of input signals and computes the spectrum of the intermodulation components.
- *intermod_3box.m*: Sweeps the power of two discrete tones and computes the intermodulation power.
- *spectrum_file_gen_cross.m*: Computes the autocorrelation and the spectrum file which is used in the ACPR sweep file *cd_cd_analytic_3box.m*.
- *spectrum_file_gen_IMD.m*: Computes the autocorrelation and the spectrum file of the intermodulation components which is used in *cd_cd_analytic_IMD*$_3$*box.m*.
- *ber_swp.m*: Generates estimates of BER of an IS-95 system with amplifier nonlinearities using simulations and the analytical model (*biterrorrate_gauss*).
- *biterrorrate_gauss.m*: Generates estimates of BER for IS-95 system using an analytical model.

D.1 Output Spectrum and ACPR Simulation

```
% cd_cd_analytic_3box.m
% This file plots the output spectrum and ACPR vs output power of
% a two-channel input using the two-channel autocorrelation technique
% and the three box behavioral model.
% This file reads in a spectrum file containing all spectral terms,
% a file containing complex power series coefficients and behavioral
% model filter responses. The input power is swept and the output
% power spectrum is calculated.

clear all, close all
% Set ACPR measurement variables in MHz
acpr_offset=.885; acpr_bw=.03; cdma_bw=1.2288;

%load spectrum file
load mxgen50_cross_S64_S64_5.mat

%Create frequency vector
len=size(S,2); m=len/2; delf=8*1.2288/len; x=-(m):(m-1); f=delf*x;

% Load measured filter responses
load H1_tst load H2_tst

lenh=length(H2); m=lenh/2; x=-(m):(m-1); fh=delf*x;

% N is the order of the behavioral model
N=13;

% Choose the reference characteristics.
f_ref=2250; fn1=2000; fn2=2100;

% load the reference polynomial coefficients
switch f_ref
    case 2050
    load b_ref_2tone_205.mat
case 2100
    load b_ref_2tone_210.mat
    case 2150
    load b_ref_2tone_215.mat
case 2200
    load b_ref_2tone_220.mat
    case 2250
    load b_ref_2tone_225.mat
end
```

```
% Convert the envelop coefficients to instantaneous coefficients
coin=b; n=1:length(coin); a=zeros(1,12); a(n)=b(n);

c(1)=a(1); c(3)=(4/3)*a(2); c(5)=(8/5)*a(3); c(7)=(35/64)*a(4);
c(9)=(128/63)*a(5); c(11)=(512/231)*a(6); c(13)=a(7); c(15)=a(8);
c(17)=a(9); c(19)=a(10); c(21)=a(11); c(23)=a(12);

f1=fn1-2250; f2=fn2-2250; fr=f_ref-2250; bw1=find(fh>f1-delf*len/2
& fh<f1+delf*len/2); bw2=find(fh>f2-delf*len/2 &
fh<f2+delf*len/2); df=find(fh>fr-2*delf & fh<fr+2*delf);

% Compute the model filter responses
J21=abs(H2(bw1))./abs(mean(H2(df)));
J22=abs(H2(bw2))./abs(mean(H2(df)));
J11=mean(abs(H1(bw1)))./abs(mean(H1(df)));
J12=mean(abs(H1(bw2)))./abs(mean(H1(df)));

%%%%%%%%%%%%%%%%%%%%%%%%%%%%%%%%%%%%%%%%%%%%%%%%%%%%%%%%%%%%%%%%%%%%%%%%%%%
% Set the input powers of the two channels
Pin1=-30:2:-0; Pin2=-20:5:-20 for j=1:length(Pin1)
    for w=1:length(Pin2)
        ps2=sqrt(10^((Pin2(w))/10));
        ps1=sqrt(10^((Pin1(j))/10));
        h3=0;
        h2=0;
        h1=0;
        h=0;
        for n=1:2:N
            for m=1:2:N
                for l=0:(n-1)/2
                    for k=0:(m-1)/2
                        n1=((n+1)/2)-l;
                        m1=((m+1)/2)-k;
                        h=h+1;
                        A=factorial(n)*factorial(m)/(factorial(l) ...
                            *factorial(l)*factorial(k)*factorial(k) ...
                            *factorial((n+1-2*l)/2)* ...
                            factorial((n-1-2*l)/2)* ...
                            factorial((m-1-2*k)/2)* ...
                            factorial((m+1-2*k)/2));
                        B=c(n)*conj(c(m))*A/2^(n+m-2);
                        C1=((J11.*ps1).^(n+m-2*l-2*k)).* ...
                        ((J12*ps2).^(2*l+2*k))*B;
                        % total spectrum of the three box model
```

```
                        Sz1(h,:)=C1.*S(h,:);
                        C=((ps1).^(n+m-2*l-2*k)).*((ps2).^(2*l+2*k))*B;
                        % total spectrum of the memoryless model
                        Sz(h,:)=C.*S(h,:);
                    end
                end
            end
        end
        % Output Spectrum of the memoryless model
        Szt=sum(Sz,1);
        % Output Spectrum of the three-box model
        Szt1=sum(Sz1,1).*(J21).^2;
        Po(j,:)=10*log10(Szt/.05);
        Po1(j,:)=10*log10((Szt1)/.05);
        offset=(round(length(Szt)/2)-round(.5*cdma_bw/delf))...
        :(round(length(Szt)/2)+round(.5*cdma_bw/delf));
        acp_offset_low=find(f>=(-acpr_offset-acpr_bw/2)
        & f<=(-acpr_offset+acpr_bw/2));
        acp_offset_hi=find(f>=(acpr_offset-acpr_bw/2)
        & f<=(acpr_offset+acpr_bw/2));
        Pzchan(w,j)=10*log10(sum(abs((Szt(offset)/(50*.001)))));
        Pz_acp_low=10*log10(sum(abs((Szt(acp_offset_low))))/(50*.001));
        Pz_acp_hi=10*log10(sum(abs((Szt(acp_offset_hi))))/(50*.001));
        Z_ACP_LO(w,j)=Pzchan(w,j)-Pz_acp_low;
        Z_ACP_HI(w,j)=Pzchan(w,j)-Pz_acp_hi;
        Pzchan1(w,j)=10*log10(sum(abs((Szt1(offset)/(50*.001)))));
        Pz_acp_low1=10*log10(sum(abs((Szt1(acp_offset_low))))/(50*.001));
        Pz_acp_hi1=10*log10(sum(abs((Szt1(acp_offset_hi))))/(50*.001));
        Z_ACP_LO1(w,j)=Pzchan1(w,j)-Pz_acp_low1;
        Z_ACP_HI1(w,j)=Pzchan1(w,j)-Pz_acp_hi1;
    end
end
%%%%%%%%%%%%%%%%%%%%%%%%%%%%%%%%%%%%%%%%%%%%%%%%%%%%%%%%%%%%%%%%%%%%%%%%%%%%

% Plot Gain compression of the first carrier
figure plot(P_in1,Pzchan1,'k-',P_in1,Pzchan,'r-') axis([-25 -5 -5
16])

% Plot ACPR vs Output Power of the first carrier
figure plot(Pzchan1,-Z_ACP_HI1,'b-',Pzchan,-Z_ACP_HI,'r-') axis([0
13 -60 -30])

% Plot the output Spectrum of the first carrier
figure plot((f+fn1)/1000,Po1,'b') axis([(-3+fn1)/1000 (3+fn1)/1000
```

```
-80 -10])

% Plot the output Spectrum of the first carrier
figure plot((f+fn2)/1000,Po2,'b') axis([(-3+fn2)/1000 (3+fn2)/1000
-80 -10])
```

D.2 Output Spectrum of Intermodulation Components

```
% cd_cd_Analytic_IMD_3box.m
% This file plots the output spectrum of the intermodulation
% components using the two-channel autocorrelation technique and
% the three box behavioral model. This file reads in a spectrum
% file containing all spectral terms, a file containing complex
% power series coefficients and behavioral model
% filter responses. The input power is swept and the output
% power spectrum is calculated.

clear all, close all
% Set ACPR measurement variables in MHz
acpr_offset=.885; acpr_bw=.03; cdma_bw=1.2288;

%%%%%%%%%%%%%%%%%%%%%%%%%%%%%%%%%%%%%%%%%%%%%%%%%%%%%%%%%%%%%%%%%%%%%%%%%%%%
%load the behavioral model measured filter responses
load H1_tst.txt
load H2_tst.txt

lenh=length(H2); m=lenh/2; x=-(m):(m-1); fh=delf*x;
%%%%%%%%%%%%%%%%%%%%%%%%%%%%%%%%%%%%%%%%%%%%%%%%%%%%%%%%%%%%%%%%%%%%%%%%%%%%
% N is the order of the behavioral model
N=13;

% Choose the reference characteristics.
f_ref=2250;

% Choose the input carrier frequencies of the input channels
fn1=2000; fn2=2100; fn3=2*fn1-fn2; fn4=2*fn2-fn1;

% load the reference polynomial coefficients
switch f_ref case 2100
    load b_ref_2tone_210.mat
    case 2150
    load b_ref_2tone_215.mat
case 2200
```

```
    load b_ref_2tone_220.mat
    case 2250
    load b_ref_2tone_225.mat
    case 2300
    load b_ref_2tone_230.mat
end


% Convert the envelop coefficients to instantaneous coefficients
coin=b; n=1:length(coin); a=zeros(1,12); a(n)=b(n);

c(1)=a(1); c(3)=(4/3)*a(2); c(5)=(8/5)*a(3); c(7)=(35/64)*a(4);
c(9)=(128/63)*a(5); c(11)=(512/231)*a(6); c(13)=a(7); c(15)=a(8);
c(17)=a(9); c(19)=a(10); c(21)=a(11); c(23)=a(12);

fl=2*fn1-fn2; fu=2*fn2-fn1;

f1=fn1-2250; f2=fn2-2250; fr=f_ref-2250; fL=fl-2250; fU=fu-2250;

bw1=find(fh>f1-delf*len/2 & fh<f1+delf*len/2);
bw2=find(fh>f2-delf*len/2 & fh<f2+delf*len/2);

bwL=find(fh>fL-delf*len/2 & fh<fL+delf*len/2);
bwU=find(fh>fU-delf*len/2 & fh<fU+delf*len/2);

df=find(fh>fr-2*delf & fh<fr+2*delf);

% Compute the model filter responses
J2L=abs(H2(bwL))./abs(mean(H2(df)));
J2U=abs(H2(bwU))./abs(mean(H2(df)));

J11=abs(H1(bw1))./abs(mean(H1(df)));
J12=abs(H1(bw2))./abs(mean(H1(df)));

%%%%%%%%%%%%%%%%%%%%%%%%%%%%%%%%%%%%%%%%%%%%%%%%%%%%%%%%%%%%%%%%%%%%%%%%%%%%

% load Spectrum file of the Upper and Lower Intermodulation Components
load mxgen80_IMDL_test.mat; SL=S;
load mxgen80_IMDU_test.mat;
SU=S;

% Create frequency vector
len=size(S,2); m=len/2; delf=8*1.2288/len; x=-(m):(m-1); f=delf*x;
```

```
% Set the input powers of the two channels
Pin1=-15:2:-15; Pin2=-15:5:-15;

for w=1:length(Pin1)
    ps2=sqrt(10^((Pin2)/10));
    ps1=sqrt(10^((Pin1(w))/10));
    h=0;
    h1=0;
    for n=3:2:N
        for m=3:2:N
            for l=0:(n-3)/2
                for k=0:(m-3)/2
                    h=h+1;
                    A=factorial(n)*factorial(m)/(factorial(l)...
                    *factorial(l+1)*factorial(k)* ...
                    factorial(k+1)*factorial((n+1-2*l)/2) ...
                    *factorial((n-3-2*l)/2)* ...
                    factorial((m-3-2*k)/2)*factorial((m+1-2*k)/2));
                    B=c(n)*conj(c(m))*A/(2^(n+m-2));
                    C=((ps1).^(n+m-2*l-2*k-2)).*((ps2).^(2*l+2*k+2))*B;
                    SzL(h,:)=C.*SL(h,:);       % total spectrum
                    C1=((J11.*ps1).^(n+m-2*l-2*k-2)). ...
                    *((J12.*ps2).^(2*l+2*k+2))*B;
                    SzL1(h,:)=C1.*SL(h,:);       % total spectrum
                    clear A B C C1
                    h1=h1+1;
                    A=factorial(n)*factorial(m)/(factorial(l)* ...
                    factorial(l+1)*factorial(k)* ...
                    factorial(k+1)*factorial((n+1-2*l)/2)* ...
                    factorial((n-3-2*l)/2)* ...
                    factorial((m-3-2*k)/2)*factorial((m+1-2*k)/2));
                    B=c(n)*conj(c(m))*A/(2^(n+m-2));
                    C=((ps1).^(2*l+2*k+2)).*((ps2).^(n+m-2*l-2*k-2))*B;
                    SzU(h1,:)=C.*SU(h1,:);       % total spectrum
                    C1=((J11.*ps1).^(2*l+2*k+2)).* ...
                    ((J12.*ps2).^(n+m-2*l-2*k-2))*B;
                    SzU1(h1,:)=C1.*SU(h1,:);       % total spectrum
                end
            end
        end
    end
    % SztU1 is the composite output spectrum of IM3U
    % with the filters included
    SztU1=sum(SzU1,1);
```

```
    PoU1(w,:)=10*log10((J2U.^2).*SztU1/.05);
    % SztU is the composite output spectrum of IM3U
    % with the filters excluded
    SztU=sum(SzU,1);
    PoU=10*log10(SztU/.05);      % total
    % SztU1 is the composite output spectrum of IM3L
    % with the filters included
    SztL1=sum(SzL1,1);
    PoL1(w,:)=10*log10((J2L.^2).*SztL1/.05);
    % SztU is the composite output spectrum of IM3L
    % with the filters excluded
    SztL=sum(SzL,1);
    PoL=10*log10(SztL/.05);

    figure(1)
    plot((f+fn3)/1000,PoL,'b',(f+fn3)/1000,PoL1,'r')
    axis([(fn3-3)/1000 (fn3+3)/1000 -80 -20])
    hold on

    figure(2)
    plot((f+fn4)/1000,PoU,'b',(f+fn4)/1000,PoU1,'r')
    axis([(fn4-3)/1000 (fn4+3)/1000 -80 -20])
    hold on
end
```

D.3 Two-Tone Simulation Using the Three-Box Model

```
% intermod_3box.m
% This file computes the intermodulation distortion of
% a nonlinear power amplifier described by the three box model
% or by the memoryless model.
% The file plots the intermodulation distortion power IM3
% vs output power.


clear all

%load the behavioral model measured filter responses
% and compute model filter responses
load DD_F90.txt H2=(DD_F90(:,1)+j*DD_F90(:,2)); H2=interp(H2,32);
f=2000:500/length(H2):2500-500/length(H2); H_2=abs(H2);
```

```
load DD_F200.txt HH=DD_F200(:,1)+j*DD_F200(:,2);
H_1=interp(HH,32); H1=H_1./H2;

% N is the order of the behavioral model
N=13;

% Choose the reference characteristics.
f_ref=2250;

% Choose the input carrier frequencies of the input channels
f1=2100; f2=2200; f3=2*f1-f2; f4=2*f2-f1;


switch f_ref case 2100
    load b_ref_2tone_210.mat
    case 2150
    load b_ref_2tone_215.mat
case 2200
    load b_ref_2tone_220.mat
    case 2250
    load b_ref_2tone_225.mat
end


% Convert the envelop coefficients to instantaneous coefficients
coin=b; n=1:length(coin); a=zeros(1,12); a(n)=b(n);

c(1)=a(1); c(3)=(4/3)*a(2); c(5)=(8/5)*a(3); c(7)=(35/64)*a(4);
c(9)=(128/63)*a(5); c(11)=(512/231)*a(6); c(13)=a(7); c(15)=a(8);
c(17)=a(9); c(19)=a(10); c(21)=a(11); c(23)=a(12);




df=1;

fs_ref=find(f>f_ref-df & f<f_ref+df); Si=(mean(H1(fs_ref)));
So=(mean(H2(fs_ref)));

fs1=find(f>f1-df & f<f1+df); S1i=(mean(H1(fs1)))/Si;
S1o=(mean(H2(fs1)))/So;

fs2=find(f>f2-df & f<f2+df); S2i=(mean(H1(fs2)))/Si;
```

```
S2o=(mean(H2(fs2)))/So;

fs3=find(f>f3-df & f<f3+df); S3i=(mean(H1(fs3)))/Si;
S3o=(mean(H2(fs3)))/So;

fs4=find(f>f4-df & f<f4+df); S4i=(mean(H1(fs4)))/Si;
S4o=(mean(H2(fs4)))/So;


%%%%%%%%%%%%%%%%%%%%%%%%%%%%%%%%%%%%%%%%%%%%%%%%%%%%%%%%%%%%%%%%%%%%%%%%%%%%
% Set the input powers of the two channels
Pin=-20:1:-4; for p=1:length(Pin)
    ps=sqrt(.1*10^(Pin(p)/10));
    u1=ps*S1i;
    u2=ps*S2i;
    y1=0;
    y1m=0;
    for n=1:2:N
        for k=0:(n-1)/2
            M=factorial(n)/(factorial(k)*factorial(((n-1)/2)-k) ...
                *factorial(((n+1)/2)-k)*factorial(k));
            y1=y1+M*(c(n)/2^(n-1))*abs(u2)^(2*k)*abs(u1)^(n-2*k);
            y1m=y1m+M*(c(n)/2^(n-1))*abs(ps)^(2*k)*abs(ps)^(n-2*k);
        end
    end
    Vo1(p)=y1*S1o;
    Vo1_mem(p)=y1m;
    y1=0;
    y1m=0;
    for n=1:2:N
        for k=0:(n-1)/2
            M=factorial(n)/(factorial(k)*factorial(((n-1)/2)-k) ...
                *factorial(((n+1)/2)-k)*factorial(k));
            y1=y1+M*(c(n)/2^(n-1))*abs(u1)^(2*k)*abs(u2)^(n-2*k);
            y1m=y1m+M*(c(n)/2^(n-1))*abs(ps)^(2*k)*abs(ps)^(n-2*k);
        end
    end
    Vo2(p)=y1*S2o;
    Vo2_mem(p)=y1m;


   Im=0;
   Im_m=0;
   for n=3:2:N
```

```
        for k=0:(n-3)/2
            M=factorial(n)/(factorial(k+1)*factorial(((n-3)/2)-k) ...
                *factorial(((n+1)/2)-k)*factorial(k));
            Im=Im+M*(c(n)/2^(n-1))*abs(u2)^(2*k+1)*abs(u1)^(n-1-2*k);
            Im_m=Im_m+M*(c(n)/2^(n-1))*abs(ps)^(2*k+1)*abs(ps)^(n-1-2*k);
        end
    end
    Im3L(p)=Im*S3o;
    Im3L_mem(p)=Im_m;

    Im=0;
    Im_m=0;
    for n=3:2:N
        for k=0:(n-3)/2
            M=factorial(n)/(factorial(k+1)*factorial(((n-3)/2)-k) ...
                *factorial(((n+1)/2)-k)*factorial(k));
            Im=Im+M*(c(n)/2^(n-1))*abs(u1)^(2*k+1)*abs(u2)^(n-1-2*k);
            Im_m=Im_m+M*(c(n)/2^(n-1))*abs(ps)^(2*k+1)*abs(ps)^(n-1-2*k);
        end
    end
    Im3U(p)=Im*S4o;
    Im3U_mem(p)=Im_m;
end

Po1=10*log10(abs(Vo1).^2/.1); Po2=10*log10(abs(Vo2).^2/.1);
Imod3L=10*log10(abs(Im3L).^2/.1);
Imod3U=10*log10(abs(Im3U).^2/.1);

Po1_mem=10*log10(abs(Vo1_mem).^2/.1);
Po2_mem=10*log10(abs(Vo2_mem).^2/.1);
Imod3L_mem=10*log10(abs(Im3L_mem).^2/.1);
Imod3U_mem=10*log10(abs(Im3U_mem).^2/.1);


figure plot(Pin,Po1,'b-',Pin,Po1_mem,'ro-') axis([-20 -3 0 15])

figure plot(Po1,Imod3L,'-',Po1_mem,Imod3L_mem,'ro-') hold on
plot(Po1,Imod3U,'-',Po1_mem,Imod3U_mem,'ro-') axis([0 14 -40 0])
```

D.4 Output Autocorrelation and Spectrum Generation

```
% spectrum_file_gen_cross.m
% This file generates all spectral terms necessary for
```

```
% calculating output spectrum of a two-channel input.
% An input time domain waveform file is read in then all
% autocorrelation terms are calculated. The spectral terms
% are then calculated from the FFT of the autocorrelation terms.


clear all

% load cdma signal realization
load cdma_for80_1.mat z=CDMA_0; load cdma_for80_2.mat u=CDMA_0;
cz=conj(z); cu=conj(u);

N=13;

% Set the width of autocorrelation window length
y=2^11;

% Compute the autocorrelation estimate
A=[]; for n=1:2:N
    for m=1:2:N
        for l=0:(n-1)/2
            for k=0:(m-1)/2
                A=[A;((n+1)/2)-l ((n-1)/2)-l ((m-1)/2)-k ...
                ((m+1)/2)-k l l k k];
            end
        end
    end
end

for k=1:size(A,1);
    r(k,:)=xcorr((z.^A(k,1)).*(cz.^A(k,2)).*(u.*cu).^A(k,5), ...
    conj((z.^A(k,3)).*(cz.^A(k,4)).*(u.*cu).^A(k,7)),y,'biased');
end

% Compute the nth order odd power spectrums
% Hanning window is used to suppress FFT spectral leakage
len=size(r,2); for k=1:size(A,1);
    S(k,:)=fftshift(fft(hanning(len)'.*r(k,:)/len));
end

save mxgen80_cross_S64_S64_5t S
```

D.5 Output Autocorrelation and Spectrum Generation of Intermodulation Components

```
% spectrum_file_gen_IMD.m
% This file generates all spectral terms necessary for
% calculating output spectrum of intermodulation components
% of a two-channel input. An input time domain waveform file
% is read in then all autocorrelation terms are calculated.
% The spectral terms are then calculated from the FFT of the
% autocorrelation terms.

clear all

% load cdma signal realization
load cdma_for80_1.mat z=CDMA_0; load cdma_for80_2.mat u=CDMA_0;
cz=conj(z); cu=conj(u);

N=13;

% Set the width of autocorrelation window length
y=2^11;

% Compute the autocorrelation estimate
 A=[];
for n=3:2:N
    for m=3:2:N
        for n1=0:(n-3)/2
            for m1=0:(m-3)/2
                A=[A; ((n+1)/2)-n1 ((n-3)/2)-n1 n1 n1+1 ...
                ((m-3)/2)-m1 ((m+1)/2)-m1 m1+1 m1];
            end
        end
    end
end

for k=1:size(A,1);
    r(k,:)=xcorr((z.^A(k,1)).*(cz.^A(k,2)).*(u.^A(k,3)).* ...
        (cu.^A(k,4)),conj((z.^A(k,5)).*(cz.^A(k,6)).* ...
        (u.^A(k,7)).*(cu.^A(k,8))),y,'biased');
end

% Compute the nth order odd power spectrums
% Hanning window is used to suppress FFT spectral leakage
```

```
len=size(r,2); for k=1:size(A,1);
    S(k,:)=fftshift(fft(hanning(len)'.*r(k,:)/len));
end

save mxgen80_IMDL_test S;

%%%%%%%%%%%%%%%%%%%%%%%%%%%%%%%%%%%%%%%%%%%%%%%%%%%%%%%%%%%%%%%%%%%%%%%%%%%%%%%
clear all

% load cdma signal realization
load cdma_for80_1.mat z=CDMA_0; load cdma_for80_2.mat u=CDMA_0;
cz=conj(z); cu=conj(u);

N=13;

% Set the width of autocorrelation window length
y=2^11;

 A=[];
for n=3:2:N
    for m=3:2:N
        for n1=0:(n-3)/2
            for m1=0:(m-3)/2
                A=[A;  n1 n1+1 ((n+1)/2)-n1 ((n-3)/2)-n1  ...
                m1+1 m1 ((m-3)/2)-m1 ((m+1)/2)-m1 ];
            end
        end
    end
end

for k=1:size(A,1);
r(k,:)=xcorr((z.^A(k,1)).*(cz.^A(k,2)).*(u.^A(k,3)).* ...
        (cu.^A(k,4)),conj((z.^A(k,5)).* ...
        (cz.^A(k,6)).*(u.^A(k,7)).*(cu.^A(k,8))),y,'biased');
end

len=size(r,2); for k=1:size(A,1);
S(k,:)=fftshift(fft(hanning(len)'.*r(k,:)/len)); etime(clock,t0);
t0=clock; end

save mxgen80_IMDU_test  S;
```

D.6 BER Simulations

```
% ber_swp.m
% This file generates estimates of BER of an IS-95 system
% with amplifier nonlinearities using simulations (biterrorrate)
% and an analytical model (biterrorrate_gauss). The input power
% is swept between -25 and -5 dBm and the signal to noise ratio (EbN0)
% between 0 and 20 dB. The number of data bits is n=2^10 bits
% and the detection is done for one of the users indicated by (user).

clear all




% select user
user=1;
% select length of input bit stream
n=2^10;
% sweep over signal to noise ratio
EbN0=0:2:20;
% sweep over input power
Pin=-20:1:-5;


for p=1:length(Pin)
    tic
    B1=zeros(length(EbN0),1);
    for k=1:63
        [B]=biterrorrate(n(p),Pin(p),EbN0,user);
        B1=B1+B;
        k
    end
    p
    BER(:,p)=B1/(n(p)-1)/k;
    toc
end
%
semilogy(EbN0,BER,'ro-') hold on
BERg=biterrorrate_gauss(Pin,EbN0); semilogy(EbN0,BERg,'b^-')
axis([0 18 10^-5 1])
```

D.7 BER Analytical Model

```
% biterrorrate_gauss.m
% This file generates estimates of BER for IS-95 system using
% an analytical model. The output spectrum is estimated using
% signal realization and the Gaussian assumption. After the spectrum
% is generated, the output linear and distortion powers are estimated
% and the BER is calculated using an analytical formula.



function
[BERg,Pout,Pinband,So,So1,Sd,f]=biterrorrate_gauss(Ping,EbN0dB)

% Set ACPR measurement variables in MHz
acpr_offset=.885; acpr_bw=.03; cdma_bw=1.2288;

% Power series coefficients
b1=abs(9.88479315674680+2.05300921111804i);
b3=-(3/4)*abs(82.34935858936478+50.23356880169632i); cb1=conj(b1);
cb3=conj(b3);

% load autocorrelation function estimate
load rx_100_64user.mat p=max(rx1); rx1=transpose(rx1)/p;

% creat a frequency vector
len=length(rx1); m=len/2; delf=1.2288*4/len; x=-(m):(m-1);
f=delf*x;


for w=1:length(EbN0dB) % sweep over signal to noise ratio
    for k=1:length(Ping) % sweep over input power
        ps=sqrt(.1*(10^((Ping(k))/10)));
        rz=ps^2*rx1;
        r1z=rz;
        r3z=(rz.^2).*conj(rz);
        r5z=(rz.^3).*conj(rz).^2;
        % Compute the nth order odd power spectrums
        % Hanning window is used to surprises FFT spectral leakage
        Sz1=fftshift(fft(hanning(len).*r1z/len));
        Sz33=fftshift(fft(hanning(len).*r3z/len));
        Sz55=fftshift(fft(hanning(len).*r5z/len));
        %
        f1=abs(b1)^2;
        f11=4*real(b1*cb3)*ps^2+4*abs(b3)^2*ps^4;
```

```
        f2=2*abs(b3)^2;
        f3=0;
        %
        Szt1=f11*Sz1+f1*Sz1; % total output spectrum
        Szt=(f1+f11)*Sz1+f2*Sz33+f3*Sz55; % linear output spectrum
        Sdt=f2*Sz33+f3*Sz55; % output distortion spectrum
        %
        %
        offset=find(f>=-1.2288/2 & f<+1.2288/2);
        %
        K=64;
        T=K/1.2288e6;
        sigd(k)=(1/K)*sum(abs(Sdt(offset)))/2;
        EbN0=(10^((EbN0dB(w))/10));
        Po(k)=sum(abs(Szt1(offset)))/K/2;
        EbN0=(10^((EbN0dB(w))/10));
        N0=T*Po(k)/(EbN0)/2;
        eta=sigd(k)*T/N0;
        Num=EbN0-eta;
        Den=1+2*eta;
        SERg(w,k)=erfc(sqrt(Num/Den));
        BERg(w,k)=.5*SERg(w,k);
    end
end
```